ENHANCED THERMAL CONDUCTIVITY UO_2-BEO NUCLEAR FUEL: NEUTRONIC PERFORMANCE STUDIES AND ECONOMIC ANALYSES

A Thesis

by

JOSHUA RYAN SMITH

Submitted to the Office of Graduate Studies of
Texas A&M University
in partial fulfillment of the requirements for the degree of

MASTER OF SCIENCE

Approved by:

Co-Chairs of Committee,	Jean C. Ragusa
	Sean M. McDeavitt
Committee Member,	Sunil Khatri
Head of Department,	Yassin Hassan

December 2012

Major Subject: Nuclear Engineering

ABSTRACT

The objective of this work was to continue the evaluation of the high thermal conductivity UO_2-BeO (UBO) nuclear fuel. Current ceramic UO_2 fuel offers many fuel performance benefits, but it has a low thermal conductivity. This results in high operating fuel temperatures, but this is a well-excepted performance compromise. Addition of Beryllium oxide to the fuel structure has been shown to increase the fuel thermal conductivity and provide positive neutronic benefits.

Pellet heat conduction studies were performed at different linear heat generation rates (LHGR). At an average LHGR of 163.4 W/cm, UBO 10vol% fuel showed a decrease of 74 and 166 °C in the effective and centerline temperature, respectively. Similarly at a peak LHGR of 590 W/cm, UBO 10vol% fuel showed a decrease of 219 and 493 °C, respectively. A drawback to UBO fuel is the lower eutectic melting point. At 590 W/cm and beginning of cycle, the melting margin for UO_2 and UBO 10vol% is 411 and 254 °C, respectively.

Comparisons of fuel types were performed using 2D infinite lattice and 3D equilibrium core neutronic simulations. A 2D lattice analysis showed that an increased UBO fuel enrichment is necessary to maintain an equivalent cycle length as UO_2 fuel. Using a mass equivalent ^{235}U basis and the linear reactivity model for an 18-month cycle, UBO 5vol% and 10vol% fuel showed a cycle increase of 1.9 and 3.3 days, respectively. Similarly, the 3D core simulation showed a cycle increase of 2.2 and 3.3 days, respectively. However, the maximum 3D burnup was increased by 3707 and 7624 MWd/t, respectively, which may cause selective UBO placement.

An economic analysis of UBO fuel compared the increased cycle length to the extra fuel costs associated with UBO fuel. The 18-month break-even fuel cost occurred at 4.03 and 8.15 days for the UBO 5vol% and 10vol% fuel, respectively. Since the computed cycle length was shorter than the break-even fuel cost, this resulted in a -12,365 and -25,712 $/reload-assembly penalty, respectively.

ACKNOWLEDGEMENTS

Thanks to my mom and dad for their support during all my educational endeavors. Also thanks to my advisor, Dr. Jean Ragusa, for his guidance and answering my many questions. I would also like to acknowledge my committee members for their contributions, Dr. Sean McDeavitt and Dr. Sunil Khatri. Lastly thanks to IBC Advanced Alloys and Jim Malone for support of this research.

NOMENCLATURE

A	Area (cm^2)
h	Heat Transfer Coefficient (W/m^2-K)
k	Thermal Conductivity (W/m-K)
m	Mass (kg)
M	Molar Mass (g/mol)
N	Atom Density (atoms/cm-barn)
N_a	Avogadro's Number (mol^{-1})
q'''	Volumetric Heat Generation Rate (W/cm^3)
LHGR	Linear Heat Generation Rate (W/cm)
T	Temperature (K)
wf	Weight Fraction
vf	Volume Fraction
ρ	Density (g/cm^3)
pd	Power Density (MW/MTU)
Q	Thermal Power (MWth)
NPV	Net Present Value ($)
LFC	Levelized Fuel Cost ($/MWh)
γ	Fraction of Heat Generated in Fuel

LIST OF ABBREVIATIONS

AO	Axial Offset
BOC	Beginning of Cycle
BOL	Beginning of Life
BU	Burnup
ECO	Enhanced Conductivity Oxide
EOC	End of Cycle
EFPD	Effective Full Power Days
LRM	Linear Reactivity Model
PPF	Power Peaking Factor
PWR	Pressurized Water Reactor
UBO	UO_2+BeO Fuel Mixture

TABLE OF CONTENTS

LIST OF FIGURES

LIST OF TABLES

1 INTRODUCTION

1.1 Background and Literature Review

Uranium-oxide is the most prominent fuel used in Light Water Reactors today. The desirable properties UO_2 fuels include: good compatibility with water and cladding, relatively high density, low thermal expansion, easy fabrication, and a high melting temperature. However, because UO_2 is a ceramic fuel, its thermal conductivity is much lower compared to that of metallic fuels. The thermal conductivity of UO_2 is temperature-dependent and varies from 4 to 3 W/m-K for temperatures between 500 and 900 °C [1]. This low thermal conductivity causes large temperature gradients across the fuel pellet, resulting in relatively poor fuel performance. Despite the lower thermal conductivity, the beneficial properties of UO_2 provide a well-accepted fuel performance compromise.

Fuel performance is negatively affected by increased pellet temperatures. Higher temperature increases the rate at which fuel swelling, fission gas release, pellet-cladding interaction, pellet cracking, and fuel restructuring occurs. These undesirable properties limit the maximum fuel rod burnup. Lowering the fuel temperature using a high conductivity material like Beryllium can result in many fuel performance gains. Beryllium-doped UO_2 oxide can provide thermal conductivity improvements and its addition to standard UO_2 fuel is studied in this M.S. thesis.

1.1.1 Early Study

An early study of Beryllium-oxide (BeO) mixed with UO_2 was performed in 1996. UBO (UO_2+BeO) pellets were fabricated to evaluate the changes in fuel thermal conductivity. Two BeO precipitate distributions were tested. The first distribution was a continuous BeO precipitate along the grain boundary while the second distribution contained a fine, spherical BeO precipitate evenly distributed in the fuel microstructure [2]. Using a laser flash method to evaluate the thermal conductivity, increased conductivity was observed with increasing BeO content. For a continuous BeO addition at 1.2 wt% BeO (4.2 vol%) and 1100 K, the thermal conductivity was 25% higher than a conventional UO_2 pellet while the dispersed BeO type showed a 10% improvement [2].

1.1.2 Purdue University Study

Recent work on the development of UBO fuel was performed in 2006 by researchers at the School of Nuclear Engineering at Purdue University. UBO pellets were produced using both a green granule process and a slug-bisque process at 10 vol% BeO. Experimental results indicate the green granule method of preparation provided the largest increase in UBO conductivity [3]. At low and high temperatures, the UBO conductivity was increased 56% and 33% compared to standard UO_2 conductivity, respectively [4]. Work performed at Purdue University focused primarily the fabrication of UBO pellets and measurements of the thermal conductivity. An extensive review of the material work and processing methods is found in Purdue University publications [3], [4].

1.1.3 AREVA Study

1.1.3.1 Description

In 2007 a comparative fuel performance and neutronic study was performed at AREVA. The fuel rod performance of the UBO fuel was calculated using the COPERNIC code developed by AREVA. COPERNIC can provide fuel performance results such as: fuel and cladding temperature, clad stresses and strains, internal fuel rod pressures, cladding crud predictions, and centerline fuel melting [5]. In addition, COPERNIC can model

different operational transients. These transients can cause high axial power peaking that could lead to a reactor shutdown.

Fuel performance studies were based on a Babcock & Wilcox reactor using a 15 x 15 assembly design. A fuel rod diameter of 10.5664 mm was used [5]. The fuel performance was analyzed for three cycles using COPERNIC. Different ECO (enhanced conductivity fuel), or UBO, fuel types were considered using varying BeO addition and thermal conductivity. For example, the ECO-4/10 study used a 4 vol% BeO addition with a 10% increase in thermal conductivity. The ECO-10/50 used a 10 vol% BeO addition with a 50% increase in thermal conductivity. All studies were performed assuming all UO_2 fuel rods were directly replaced with ECO fuel.

Two important input parameters were modified in COPERNIC. It is assumed the same amount of power is generated in both the ECO and standard UO_2 fuel. However the ECO fuels contain less UO_2. For example, a standard fuel contains 95.9 vol% UO_2 while the ECO-4/x contains 91.9 vol% UO_2 [5]. Therefore the ECO-4/x has a power 95.9/91.9 = 1.0435 times the standard fuel [5]. The additional power affects the fission gas production in COPERNIC and therefore the fission gas release multiplier was modified by 1/1.0435 = 0.9583 to correctly adjust the model [5]. In addition, the linear power was adjusted for the ECO fuels. The fraction of heat generated in the fuel was adjusted by 97.3%/1.0435 = 93.24% while the remaining 2.7% of the heat was assumed to be directly deposited in the coolant [5].

1.1.3.2 Fuel Temperature

Fuel temperature is decreased due to the increased thermal conductivity. The ECO-4/5, ECO-4/10, and ECO-10/50 showed a 15, 33, and 122 °C decrease in fuel temperature compared to the standard fuel, respectively [5]. The increased conductivity also revealed benefits for the centerline fuel temperature during transients. A transient was performed for the ECO-4/x fuels at mid-cycle. After the transient the ECO-4/5 showed a decrease of 18 °C compared to the ECO-4/0 whereas the difference for the standard fuel was over 60 °C [5].

1.1.3.3 Fuel Performance

Results from COPERNIC showed an increased EOL burnup of 2.8 and 7.2 GWd/t compared to standard fuel for the ECO-4/x and ECO-10/50, respectively [5]. The increased burnup was a result of the reduced UO_2 loading and the equivalent energy requirement. COPERNIC results also indicated better fuel performance due to reduced fission gas release and fuel rod internal pressure. At EOL, a standard UO_2 fuel would have a fission gas release of approximately 19.6% [5]. Studies for ECO-4/0 and ECO-4/5 fuel type showed a fission gas release reduction of 1.7% and 4.0% compared to the standard fuel [5]. The ECO-10/50 showed a reduction of 6.0% compared to the standard fuel [5]. Similarly, the internal fuel rod pressures at EOL were reduced by 0.5, 2.0, and 9.1 MPa for the ECO-4/0, ECO-4/5, and ECO-10/50, respectively [5]. Standard fuel has approximately an internal rod pressure of approximately 16 MPa at EOL [5]. These results demonstrate that a significant increase in fuel performance is possible with the enhanced conductivity fuels.

1.1.3.4 LOCA Analysis

A LOCA analysis is complicated and is a function of cycle depletion. The severity of the LOCA event depends on when the transient occurs during the cycle. Results from the COPERNIC study are for the maximum local linear heat generation rate. At BOL and EOL, the ECO-4/10 fuel showed an increase of 4.9 and 3.2 kW/m, respectively. Similarly, the ECO-10/50 fuel showed an increase of 23.5 and 14.8 kW/m, respectively [5]. Standard fuel is approximately 55 and 37 kW/m at BOL and EOL, respectively [5].

1.1.3.5 Neutronics

The neutronic effect of ECO fuels depends on many parameters such as number of reload assemblies, assembly zoning enrichment, and cycle length. Neutronic calculations were performed using CASMO-3. An equilibrium cycle was determined with a core completely converted to the ECO fuel type. There was neither mixing of the UO_2 and ECO pins within the assembly itself nor mixing of ECO assemblies and non-ECO assemblies. Additional calculations were performed using SCALE 5.0 to model the

depletion of BeO. CASMO-3 uses coarse energy groups and will not deplete the Beryllium. Results from SCALE showed a slight depletion of Beryllium. Over three cycles, only 0.15% of the initial Beryllium was depleted [5].

Two reload types were considered: a 60 and a 56 reload assembly basis. The enrichment of standard UO_2 fuel for the two reload types were 4.027 and 4.227 wt%, respectively [5]. In order to have an equivalent k_{inf} at end-of-cycle, the ECO fuel needed an increased enrichment of 0.0073 wt% [5]. The benefit of reduced fuel temperature, (n,2n) reaction in Beryllium, and moderating properties of BeO were assumed to offset the reduced uranium loading. However, as later studied in this M.S. thesis, a much higher enrichment was necessary for the UBO fuel to meet or exceed the standard UO_2 cycle length. Section 5 and 6 describe the increased enrichment requirements.

1.1.3.6 Economics

Economic calculations were performed assuming an enrichment cost of $110/SWU and uranium feed cost of $53.5/kg U [5]. The total uranium loading for the 60 reload assembly cycle was 27,820 and 27,290 kg for the UO_2 and ECO fuel, respectively [5]. Considering the 0.0073 wt% enrichment increase and the 530 kg total uranium loading decrease, the ECO fuel showed a net savings of $501,000 per reload ($8350/assembly) [5]. Results for the 56 assembly reload exhibit a similar economic savings. As later studied in this M.S. thesis, the economic analysis results indicate an economic penalty due to the much higher enrichment requirements.

1.2 Current UBO Fuel Development at TAMU

Phase 1 of the UBO fuel concept was developed between 2005 and 2008 at Purdue University. The goal was to fabricate lab-scale UBO fuel pellets and characterize the thermal conductivity. Phase 2 began in 2008 with a research collaboration between Purdue, Texas A&M, and IBC Advanced Alloys. Following a meeting with Westinghouse in late 2009, efforts were shifted from fuel fabrication to nuclear simulations to better assess neutronic performance of UBO fuel. At the conclusion of Phase 2, 2D neutronic studies were completed and BeO powder arrived at TAMU.

1.2.1 Naramore Study

Work performed by Naramore at Texas A&M focused on assessing neutronic performance of the UBO fuel and presenting an overview of fabrication methods. Neutronic studies were performed using the computer code DRAGON. A 1/8 geometry of a 17x17 assembly was simulated in an infinite lattice medium. Nominal PWR conditions were assumed for the thermal-hydraulic analysis.

Cycle analysis was accomplished using the Linear Reactivity Model. Both a three and four batch reload strategy was considered. An initial cycle analysis was performed with a direct addition of BeO to the fuel. However, it was determined that the cycle length was shorter for the UBO fuel due to the decreased uranium loading. To compensate, the cycle analysis for UBO fuel was performed on a mass equivalent ^{235}U basis. Section 5.1.2 explains the mass equivalence concept in detail.

Using a mass equivalence basis, a 10vol% addition of BeO had a cycle increase of approximately 19 days over the standard UO_2 fuel for both the three and four batch strategies [6]. At end of cycle (EOC), the UBO 10vol% fuel showed an increased burnup between 4,000-5,000 MWd/tHM for the three and four batch strategies [6]. At beginning of cycle (BOC), the UBO 10vol% fuel showed an increased reactivity between 2800-2900 pcm for the three and four batch strategies [6]. It was concluded that the batch strategy used weakly affects the cycle results.

Fabrication of the UBO fuel pellets is a multi-stage process. Initially the uranium dioxide power is pre-compacted using a punch and die system. Next a mortar and pestle is used to ground the pellet into smaller granules. Specific sized granules are filtered out using sieves. These steps are required so that a thin layer of BeO power covers the UO_2 granules [6]. The UO_2 granules are processed using a ball mill system to create consistent and spherical granules.

At this stage, the BeO powder can be processed using a green granule or slug-bisque method. Since the green granule method provides a greater thermal conductivity, only this processing method was used. After the BeO powder is introduced, the self-milling is

continued for approximately 30 minutes to complete the mixing [6]. Following the mixing, a final compaction is performed. The last step is to place the pellet in a ceramic vessel to be sintered at a high temperature of 1600 °C [6].

Three important neutronic gains were originally identified by using Beryllium in the fuel [6]. First a lower fuel temperature results in positive Doppler reactivity gains. Second better thermalization provided by the Beryllium results in a positive spectral effect. Lastly, the (n,2n) reaction in the Beryllium cross section can provide a small boost in reactivity. However, as later studied in this M.S. thesis, the dominant neutronic gains are due to changes in the fuel volume. Section 5 provides a detailed neutronic study identifying the main reactivity contributors.

1.2.2 Continuing Work

Phase 3 of the UBO development extends from 2011-2013. Two research thrusts were formed at TAMU. One group was dedicated to furthering UBO fuel fabrication methods at the TAMU fuel cycle laboratory. The second group focused on extending neutronic studies to a 3D full core analysis. Research presented in this M.S. thesis represents the conclusion of the Phase 3 neutronic studies and economic analyses.

1.3 Beryllium Cross Section

One neutronic benefit of UBO fuel is the favorable cross section of ^{9}Be. Beryllium has been used in nuclear reactors as a reflector because of its moderating properties. Neutron interactions with ^{9}Be are dominated by elastic scattering. Figure 1.1 displays the dominant cross section for ^{9}Be in the thermal and intermediate energy ranges.

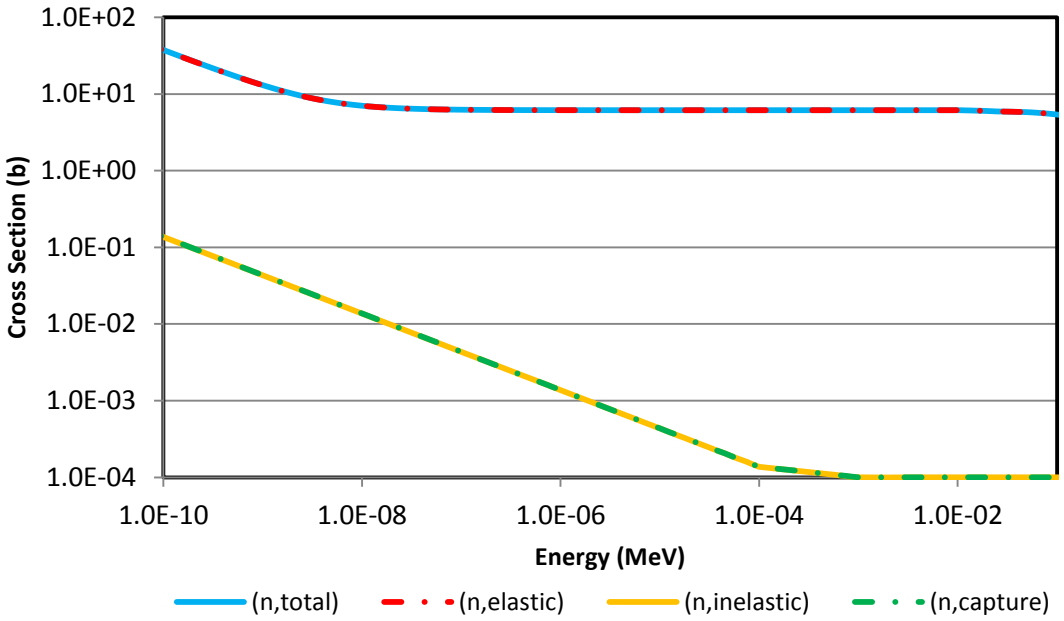

Figure 1.1 Principal cross sections for ^{9}Be in the thermal and intermediate energy range [7].

The total cross section for ^{9}Be is almost entirely due to elastic scattering in the thermal and intermediate energy ranges. An inelastic cross section with a 1/v behavior in the thermal range is present, but contributes little to the total cross section. The majority of the inelastic scattering is due to the neutron capture reaction. The ^{9}Be cross sections in the fast energy range are shown in Figure 1.2.

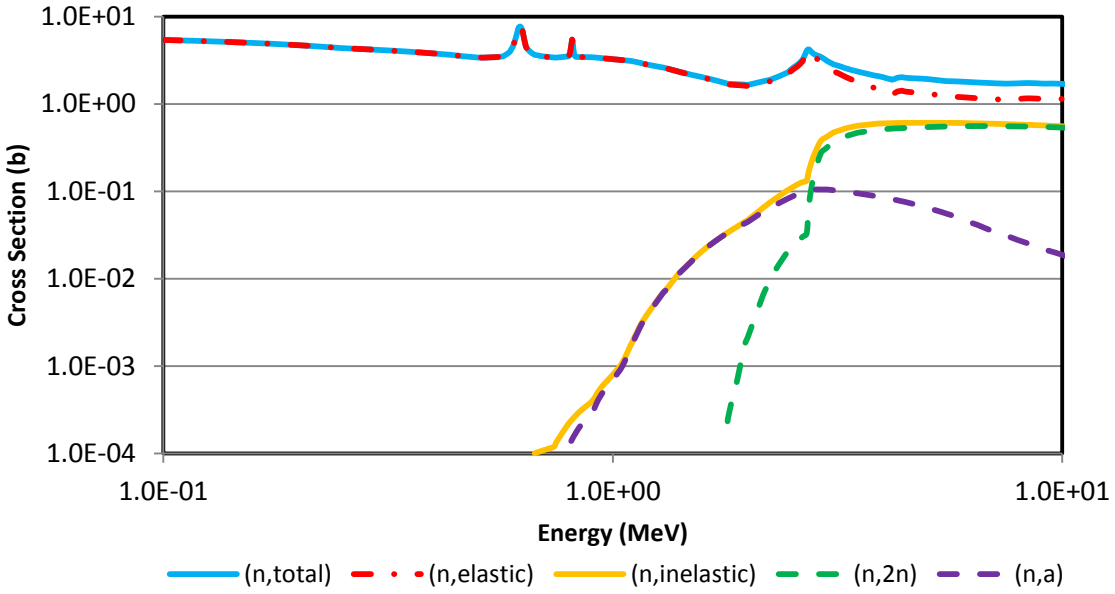

Figure 1.2 Principal cross sections for ^{9}Be in the fast energy range [7].

Elastic scattering is also the dominant cross section in the fast energy range. Inelastic scattering makes a small contribution to the total cross section between 1 and 10 MeV. The inelastic scattering is principally due to a (n,2n) reaction and a (n,α) reaction. However, the (n,2n) reaction has a negligible effect on reactivity. Since a neutron interaction with ^{9}Be primarily results in an elastic scatter and little absorption, ^{9}Be has excellent moderating properties.

1.4 Eutectic Melting UBO Fuel

One concern for UBO fuel is the lower melting point due to a eutectic formation with UO_2 and BeO. A phase diagram for UBO fuel is shown in Figure 1.3. The melting point for fresh UO_2 and UBO fuels is approximately 2800 °C and 2150 °C, respectively [8]. Therefore UBO fuel has a loss of 650 °C in fuel melting margin. However, some of the fuel melt margin is regained due to the lower centerline temperature of UBO fuels. The amount of margin lost is dependent on the volume fraction of BeO added.

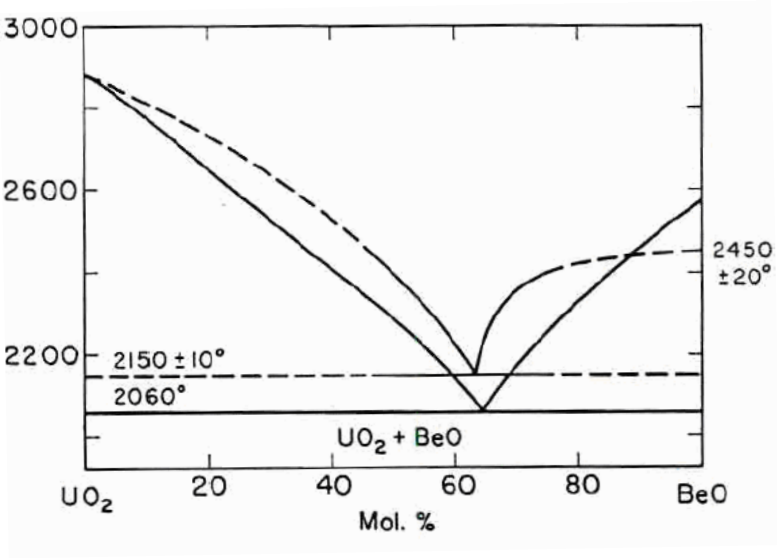

Figure 1.3 Phase diagram for uranium dioxide, Beryllium oxide fuel. Temperature in Celsius. [8]

2 CORE SIMULATION METHODS

2.1 Core Modeling Overview

There are many approaches and tools that can be used for core neutronic modeling and simulation. A direct core modeling approach is time consuming and not suitable for optimization purposes. In many situations, a core analysis may be repeated many times with only minor changes, such as a new assembly shuffle location. Performing a core-level analysis using MCNP or deterministic 3D transport tools repeatedly would be inefficient and therefore is not widely used.

An alternative to a 3D transport core modeling is based on a "divide and conquer" approach:

1. Lattice-level stage: Small portions of the reactor (2D infinite medium fuel assemblies) are treated with a high level of fidelity and resolution (transport calculations with many energy groups and fine spatial grids).
2. Homogenization stage: Characteristic features of the previous fine-level simulations are collapsed into node-averaged, two energy group cross sections.
3. Core stage: 3D, two energy group diffusion is performed at the entire core level.

Instead of regenerating the input data for each core simulation, all the necessary input data is generated prior to the core analysis. A database is built from the lattice and homogenization levels. Then the input data can then be reused many times for different core shuffle patterns, cycle optimization, or iterations for equilibrium cycles. One drawback to this approach is that the range of input parameters (variations in burnup, temperature, boron concentration, etc.) required for any future core simulations must be known or estimated. A core simulation cannot be performed with an inadequate range of input parameters.

The bulk of the input data comes from nuclear cross sections. Cross-sections are needed for any neutronic calculations. However, cross-sections can be a function of many core parameters such as temperature, boron concentration, and moderator density. Therefore, cross-sections are generated for a range of core parameters, a process known as branching cases. The ranges of these parameters are chosen based on expected core simulation requirements.

Cross-section data is generated for each assembly type placed in the core. Generally the number of different assembly types for each core is small. For example, the EPR reactor uses only three different assembly types for a 241 assembly core [9]. Primarily the assembly types differ based on the Uranium enrichment or the number and placement of Gadolinium pins. The cross-section data is generated using a 2D transport code. Assemblies are typically symmetric so a 1/8 symmetry is used to reduce the computational requirements. An illustration of the divide and conquer method is shown in Figure 2.1.

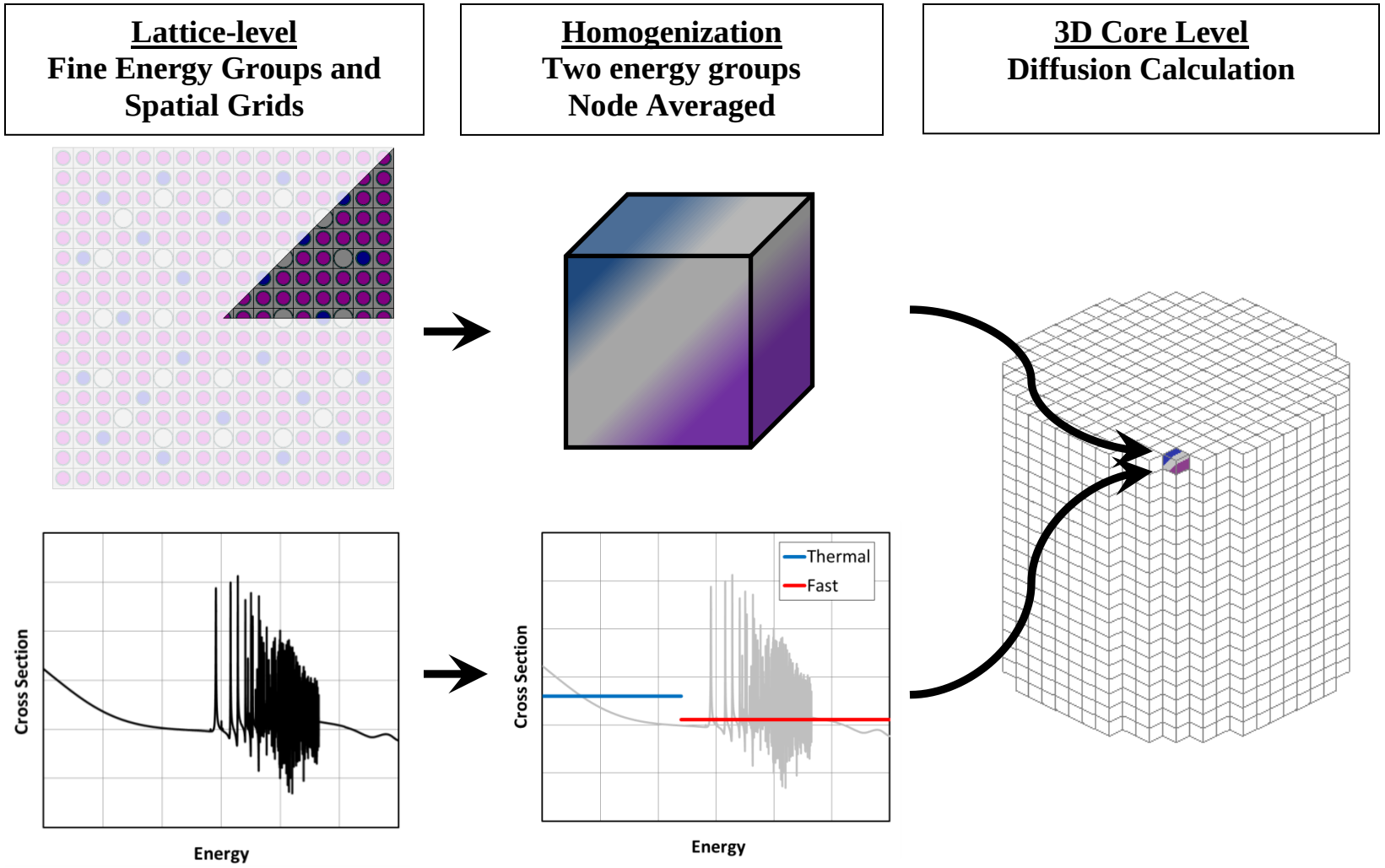

Figure 2.1 Illustration of fine group assembly cross-sections reduced to homogenized two-group cross-sections. Homogenized two-group cross-sections are then used for 3D core simulation.

2.2 Lattice Physics

Lattice physics calculations are performed in many steps and do not necessarily follow sequentially. An important lattice physics calculation is nominal assembly depletion. A nominal depletion is performed at typical core parameters and power densities. Results from a nominal depletion can show the effect of Uranium enrichment and Gadolinium rods. After a nominal depletion has been performed, one can use the linear reactivity model to estimate the cycle length and burnup of a given assembly design. In addition, a nominal depletion calculation is performed prior to branching cases and the generation of cross section data.

Another important lattice physics calculation is a moderator curve. Moderator curves are generated to determine the reactivity effect due to a change in the moderator density. Assemblies are designed to be under-moderated to provide a negative reactivity feedback. A change in the moderator curve due to the BeO addition is important for safety analysis of the fuel.

2.2.1 Nominal Depletion

Lattice physics calculations are performed on a 2D infinite assembly lattice. Assembly symmetry is used whenever possible to decrease computation time. Gadolinium rods are placed within the assembly to suppress some excess reactivity of the fresh fuel assemblies. Strategic placement of the Gadolinium rods reduces the local power peaking factors. An example assembly design is shown in Figure 2.2.

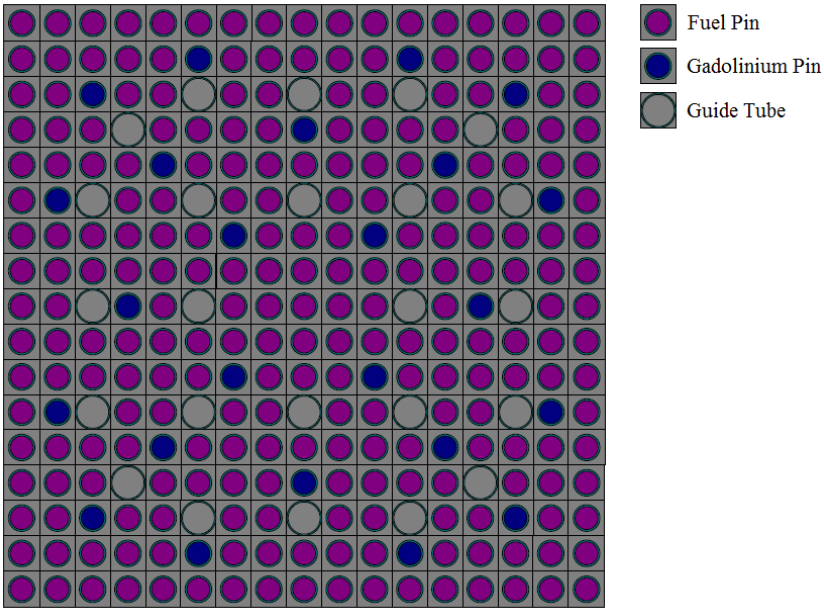

Figure 2.2 Design of a 24 Gadolinium pin assembly.

A nominal depletion is performed at core averaged fuel temperature, moderator density and boron concentration. The total number of burnup steps is estimated from the average cycle burnup and the number of batches. For the chosen UK EPR reactor (later described in Section 3), the final burnup is estimated to be 70 GWd/t. An example of the nominal depletion for UO_2 is shown in Figure 2.3.

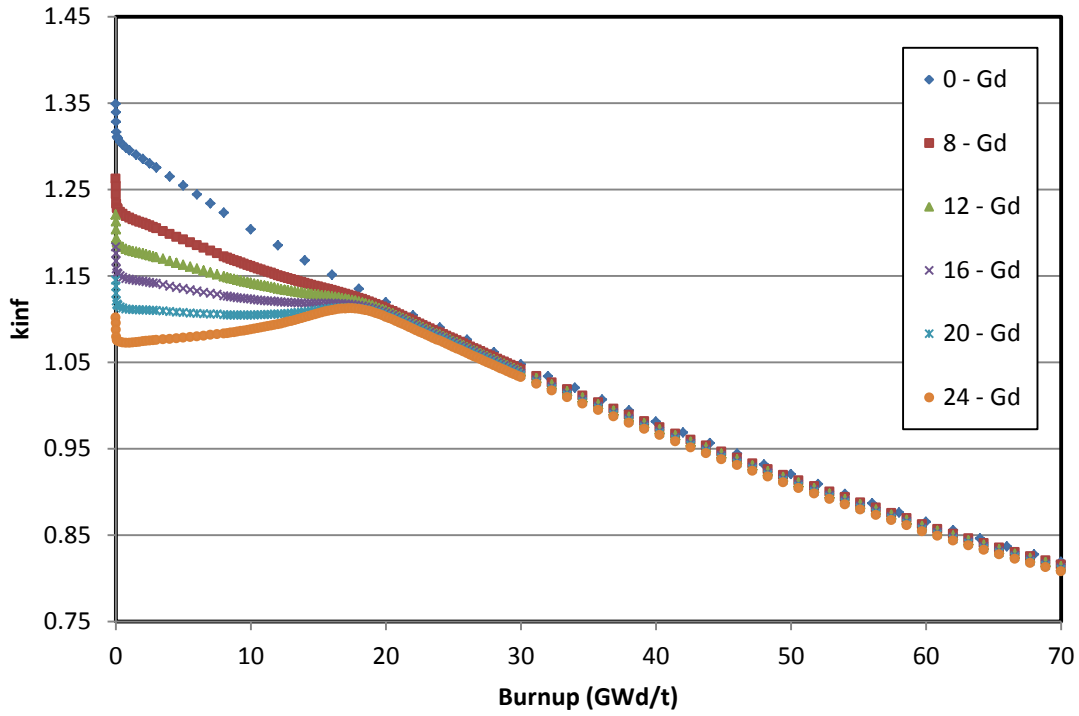

Figure 2.3 Nominal depletion of 5wt% UO_2 fuel with different assembly types.

As shown in Figure 2.3, k_{inf} (infinite multiplication factor) varies almost nearly linearly with burnup for the non-gadolinium assembly. The assemblies containing Gadolinium exhibit suppressed reactivity during the first 20 GWd/t but eventually vary linearly with burnup as the Gadolinium is depleted. A slight burnup penalty is incurred in the Gadolinium assemblies (due to the slightly lower ^{235}U loading in these pins), but the Gadolinium is necessary for BOC reactivity management.

2.2.2 Linear Reactivity Model

The cycle length of a full core can be estimated using an infinite lattice assembly calculation. As previously shown in Figure 2.3, k_{inf} varies nearly linearly with burnup. The cycle burnup can be determined at the end-of-reactivity life for a fuel assembly using a linear reactivity model (LRM). An important parameter for burnup calculations is the power density. Equation (2-1) shows the calculation for power density.

$$pd = \frac{Q\gamma}{m_{fuel}} \tag{2-1}$$

pd is the power density (MW/MTU), Q is the total thermal power (MWth), γ is the fraction of heat generated in the fuel, and m_{fuel} (MTU) is the total fuel loading in the core. The burnup is determined by multiplying the power density by the time at full power, as displayed in Eq. (2-2).

$$BU = pd \cdot T \cdot CF = pd \cdot EFPD \tag{2-2}$$

BU is the fuel burnup (MWd/MTU), T is irradiation time (days), CF is the capacity factor, and $EFPD$ is the effective full power days.

2.2.2.1 Simple Cycle Analysis

The LRM can be applied with varying degrees of complexity. A simple analysis is performed first to gain a basic understand of how the LRM is applied. Basic burnup relationships from the LRM are given in Eq. (2-3) [10].

$$BU_d = nBU_c = \left(\frac{2n}{n+1}\right)\left(\frac{\rho_0}{A}\right) = \left(\frac{2n}{n+1}\right)BU_{avg} \tag{2-3}$$

BU_d is the assembly discharge burnup, n is the number of cycles, BU_c is the cycle burnup increment, and BU_{avg} is the average core burnup at the end-of-cycle. The terms ρ_0 and A are determined from a nominal depletion curve. Figure 2.4 illustrates these terms required for a LRM calculation. The initial reactivity ρ_0 and the slope A are determined after Xenon is in equilibrium. Xenon causes an initial decrease in reactivity at BOC and is ignored for LRM calculations.

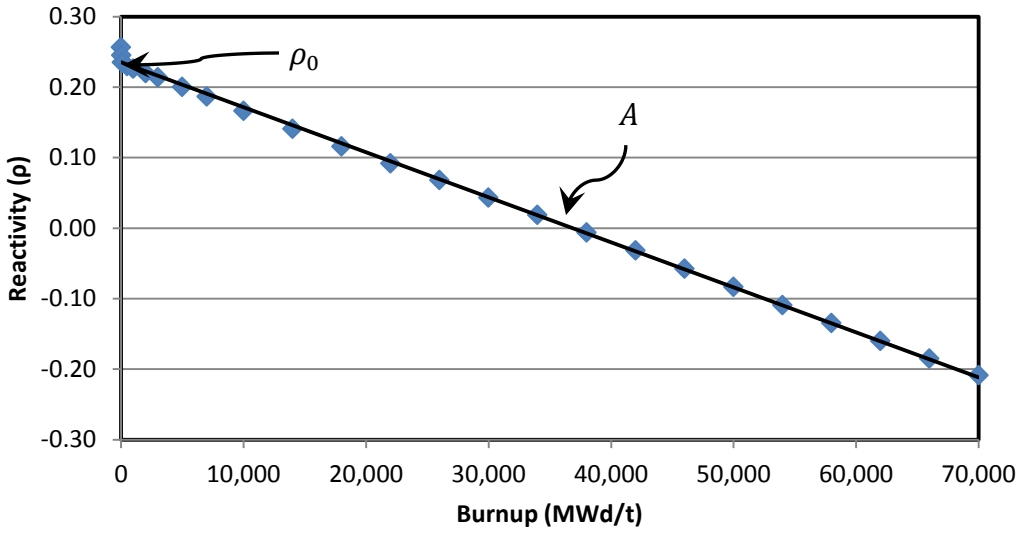

Figure 2.4 Example of the linear reactivity model. The initial reactivity and slope are determined after Xenon is in equilibrium.

The cycle burnup is an important parameter to consider for cycle length calculations. Equation (2-3) can be rearranged to provide the cycle burnup calculation, as shown in Eq. (2-4) [10]. The cycle length (EFPD) can then be determined by dividing by the power density, as shown in Eq. (2-2).

$$BU_c = \left(\frac{2}{n+1}\right)\left(\frac{\rho_0}{A}\right) \qquad (2\text{-}4)$$

2.2.2.2 Unequal Batch Size

An equal batch size assumption may be inaccurate for an aggressive core reload pattern. Equation (2-5) is a more accurate calculation of the EOC cycle burnup with an added unequal batch size term in the denominator [10]. If the batch sizes are all equal, then Eq. (2-5) would be simplified to Eq. (2-4).

$$BU_c = \frac{\left(\frac{2}{n+1}\right)\left(\frac{\rho_0}{A}\right)}{1-\left(\frac{n-1}{n+1}\right)\left(\frac{nN_B}{N_T}-1\right)} \qquad (2\text{-}5)$$

N_B represents the batch size, or number of reload assemblies, and N_T represents the total number of core assemblies. The assembly discharge burnup can be computed using Eq. (2-6) once the cycle burnup is determined [10].

$$BU_d = \left(\frac{N_T}{N_B}\right) BU_c \qquad (2\text{-}6)$$

2.2.2.3 Assembly Weighting

It is important to consider the different assembly types in each reload batch. For example, the assembly types containing Gadolinium have a slight cycle length penalty compared to a Gadolinium-free assembly due to the neutron poison. In addition, the Gadolinium pins typically contain a lower enrichment than standard pins, resulting a slightly reduced cycle length. Therefore, the term $\left(\frac{\rho_0}{A}\right)$ can be weighted by the assembly types in the reload batch. Equation (2-7) shows how to calculate the assembly type weighting factor.

$$\left(\frac{\rho_0}{A}\right) = \sum_{i=1}^{S} \left(\frac{\rho_0}{A}\right)^i \frac{N_i}{N_T} \qquad (2\text{-}7)$$

The index i represents the assembly type and S is the total number of assembly types. N_i is the number of assembly types. For example, there may be three assembly types: Gd-8, Gd-12, and Gd-16 within the reload batch. Each assembly type would have a slightly different $\left(\frac{\rho_0}{A}\right)^i$ term from their respective nominal depletion curve. Figure 2.5 illustrates the different terms that may result from the different assembly types.

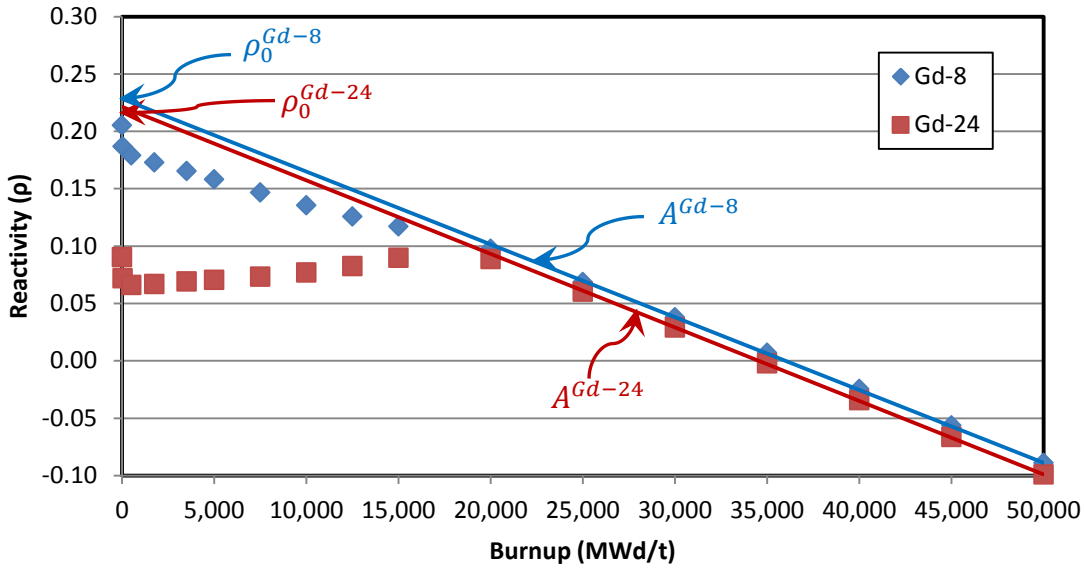

Figure 2.5 Linear reactivity model with different assembly types.

In addition to weighting the $\left(\frac{\rho_0}{A}\right)$ term, the power density must also be correctly computed to provide an accurate cycle length calculation. The power density is weighted by the number of in-core assembly types. Equation (2-8) shows the weighted power density calculation.

$$pd = \sum_{i=1}^{S} (pd)^i \frac{N_i}{N_T} \qquad (2\text{-}8)$$

2.2.3 Moderator Curves

A moderator curve is an important figure used to evaluate fuel safety. The ratio of moderator-to-fuel has a large effect on lattice physics. For example, an increase in power will reduce the moderator density. With an under-moderated assembly, the reactivity will decrease and curb the power increase. An over-moderated assembly would exhibit a reactivity increase with increasing power, creating an inherently unstable and unsafe behavior. Figure 2.6 illustrates a typical LWR moderator curve.

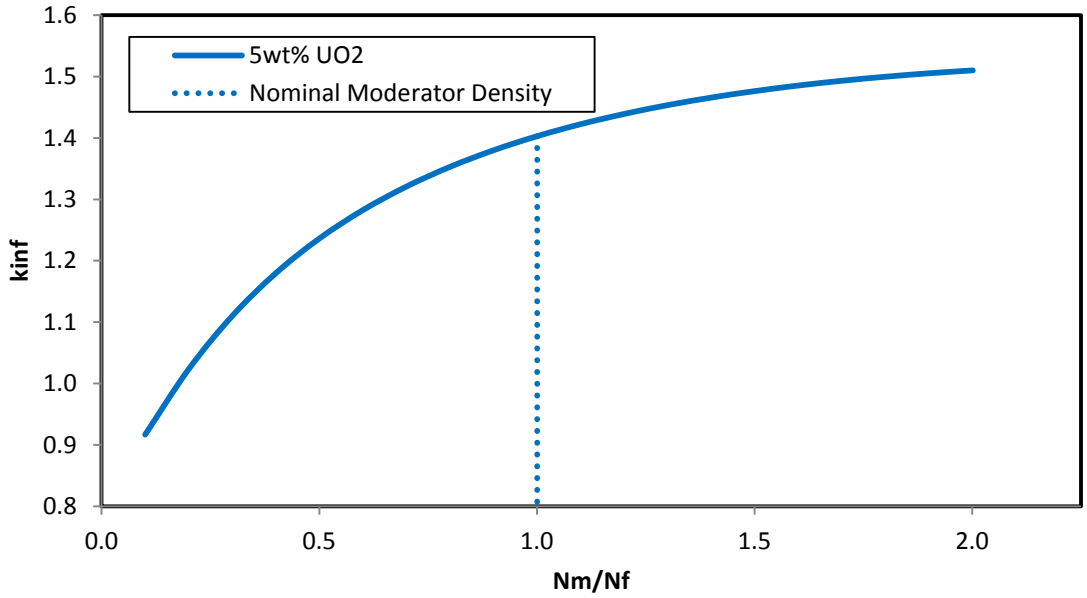

Figure 2.6 Moderator curve for 5wt% UO_2 cell lattice.

Moderator curves can be represented using either k_{inf} or reactivity. In certain situations, it is more convenient to express k_{inf} in terms of reactivity. The conversion to reactivity is shown in Eq. (2-9).

$$\rho = \frac{k - 1}{k} \qquad (2\text{-}9)$$

A change in reactivity can be calculated using Eq. (2-10).

$$\Delta\rho = \frac{1}{k_{initial}} - \frac{1}{k_{final}} \qquad (2\text{-}10)$$

Since the units of reactivity are typically small, it is convenient to express reactivity in terms of percent millirho (pcm). The conversion to pcm is shown in Eq. (2-11).

$$1\ pcm = 10^5 \Delta\rho \qquad (2\text{-}11)$$

2.2.4 Branching Cases

Branching cases are performed following a nominal depletion. The main parameter for a branching case is burnup. At each burnup step, additional user-defined parameters are varied over a specified range. Typically, these parameters include: fuel temperature, moderator density, boron concentration, and control rod presence. The range of values chosen is based on experience or expected values during cycle depletion. An illustration of branching cases is shown in Figure 2.7.

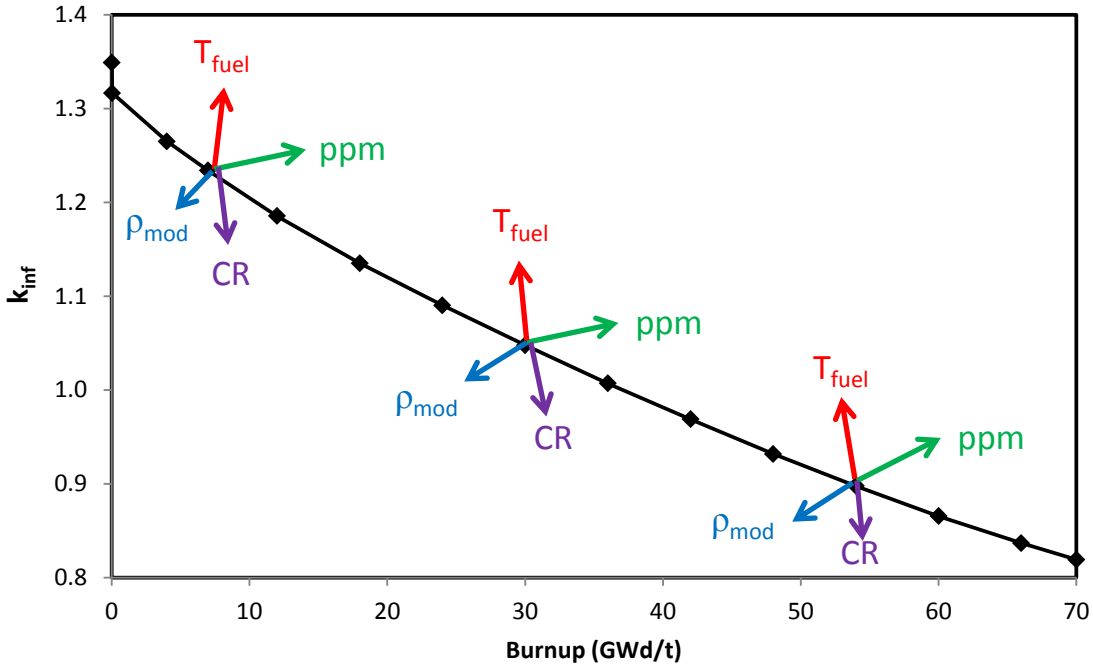

Figure 2.7 Illustration of branching cases during a nominal depletion.

A database of branching cases is required for a 3D core simulation. On a 3D core level, it is impossible to know the isotopics in a given core location because of the distribution of parameters. For instance, the high power, fresh fuel assemblies in the core will have a higher fuel temperature than the low power, periphery fuel assemblies. The distribution of temperatures will cause a distribution of isotopic concentrations. To account for the 3D distribution, the important core parameters are perturbed over a user-defined range.

Branching cases are performed so that multi-parameter cross-sections can be tabulated. Cross-sections are homogenized to two energy groups. With branching cases, the homogenized cross-sections are then functions of additional user-defined core parameters. Multi-parameter, homogenized cross-sections are computed once for each type of fuel assembly, before a core level computation is performed. Since cross-sections are not computed during a 3D core simulation, the user-defined range of parameters must be appropriately chosen in order to successfully complete the core computation.

2.2.5 Cross-section Generation

Assembly level calculations are first performed with fine energy group cross-section libraries. Multi-group cross-sections can then be generated for various burnup steps and core parameters. The multi-group cross sections are weighted based on energy, as shown in Eq. (2-12) [11].

$$\sigma^g = \frac{\int_{E_g}^{E_{g-1}} dE\sigma(E)w(E)}{\int_{E_g}^{E_{g-1}} dEw(E)} \qquad (2\text{-}12)$$

The weighting function (w) can be a constant such as the appropriate energy averaged flux. An example of calculating the scattering cross section is shown in Eq. (2-13) [11].

$$\sigma^{g\to g'} = \frac{\int_{E_g}^{E_{g-1}} dE\sigma_s(E)w(E)\int_{E_{g'}}^{E_{g'-1}} dE'p_n(E')w(E)}{\int_{E_g}^{E_{g-1}} dEw(E)} \qquad (2\text{-}13)$$

where p_n are the Legendre components pointwise in energy.

Once the fine multi-group cross sections are calculated, they are further reduced to few group cross sections [11]. This step requires the assembly-level calculations to generate a proper weighting spectrum (flux) to be utilized in the few-group cross-section collapsing. The cross section collapsing is shown in Eq. (2-14) [11].

$$\sigma^j = \frac{\sum_{g\in j}\sigma^g\phi_g}{\sum_{g\in j}\phi_g} \qquad (2\text{-}14)$$

and is based on the notion that reaction rates, computed either using fine scale data or few-group data, must be equal. Similarly the scattering cross section collapsing is shown in Eq. (2-15) [11].

$$\sigma_n^{j\to j'} = \frac{\sum_{g\in j}\sum_{g'\in j'}\sigma_n^{g\to g'}\phi_g}{\sum_{g\in j}\phi_g} \qquad (2\text{-}15)$$

$g \in j$ represents a sum over fine groups g to few groups j. Typically j is equal to two for two-group collapsing while g can be on the order of 200 energy groups depending on the accuracy desired and cross-section library used.

2.2.6 Tools

The DRAGON computer code was developed at École Polytechnique de Montréal. DRAGON is designed to perform neutronic calculations for a unit cell or a single fuel assembly [12]. The code includes many modules and algorithms used to solve the neutron transport equation. Some of the key functions of DRAGON include: interpolation of microscopic cross sections from supplied libraries, calculation of resonance self-shielding, and calculation of neutron leakage. In post-processing, DRAGON can supply condensed and homogenized cross sections as well as isotopic depletion concentrations.

2.3 Core Level

2.3.1 Equilibrium Cycle Methodology

Calculation of an equilibrium cycle is an iterative process. An equilibrium cycle is performed when previous cycle burnup data is unavailable. In addition, an equilibrium cycle is used to analyze current and future cycle performance. To calculate an equilibrium cycle, iterations are performed on cycle depletion, critical boron search, steady-state neutronics, and steady-state thermal-hydraulics. The goal of an equilibrium cycle is to repeat the cycle depletions until the EOC burnup remains constant. An iteration diagram is shown in Figure 2.8.

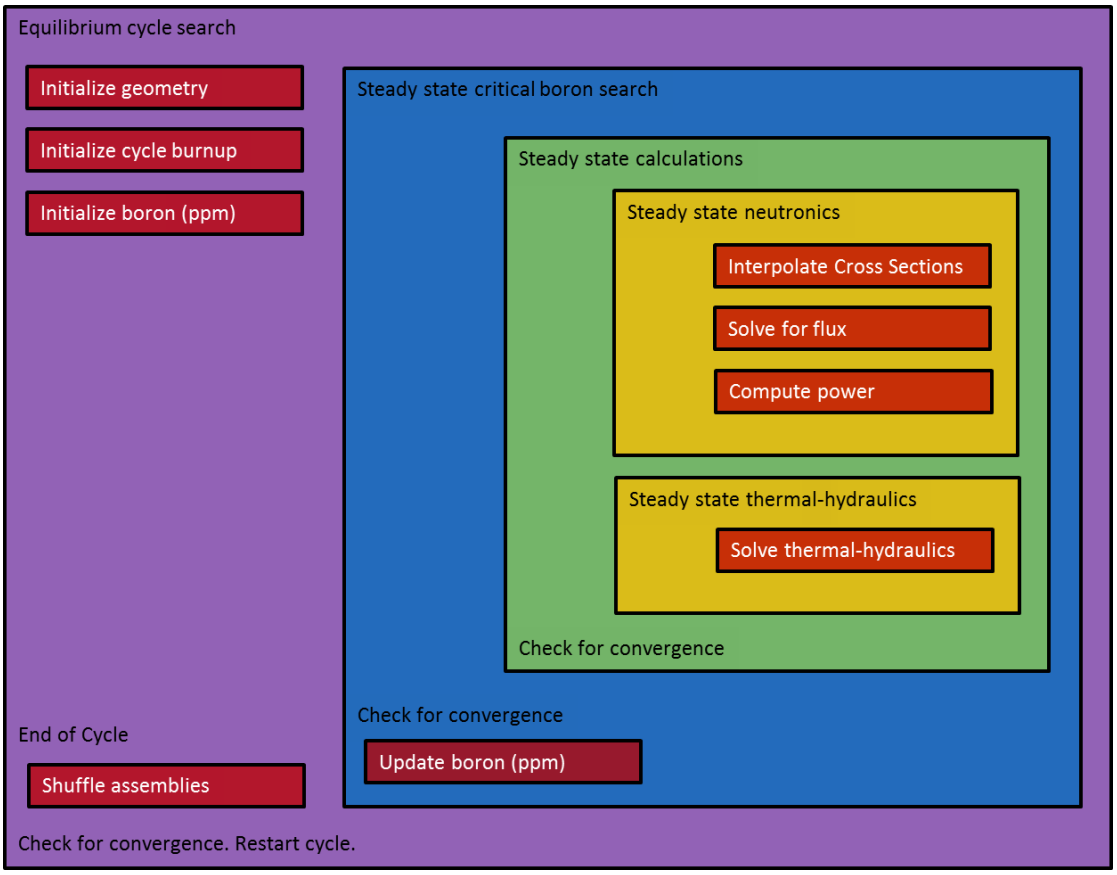

Figure 2.8 Steps involved to calculate an equilibrium cycle.

Iteration of the cycle depletion is necessary if the previous cycle burnup data is unknown. A guess of the previous cycle's assembly burnup is made and then an initial cycle depletion is performed. After the initial cycle depletion is completed, the assemblies are shuffled and the next cycle depletion is initiated. After several repeated cycle depletions, the burnup distribution will converge to an equilibrium value. The number of cycles that must be performed may depend on the initial assembly burnup guess.

The initial burnup guess is important because of cross-section limitations. A poor initial burnup guess may exceed the parameter range of the cross-sections. For example, one could choose zero burnup for all assemblies during the first cycle depletion. However to compensate for the high reactivity of un-burnt assemblies, the critical boron

concentration may exceed the maximum specified range. Alternatively, one could choose a high burnup for all assemblies for the initial cycle depletion. However then the maximum burnup range specified may be exceeded. The proper initial burnup guess is made based on experience or a trial and error process.

2.3.2 Neutronics

Typically for LWR's, a 3D diffusion code is the preferred choice for neutronic calculations. A diffusion code is less computationally intensive and provides sufficient accuracy for cycle analysis. The general form of the multi-group diffusion equations can be written as [11]:

$$-\bar{\nabla} D_g \bar{\nabla} \phi_g + \Sigma_r^g \phi_g = \sum_{g' \neq g}^{G} \Sigma_s^{g' \to g} \phi_{g'} + \frac{\chi_g}{k} \sum_{g'=1}^{G} \nu \Sigma_f^{g'} \phi_{g'} \qquad (2\text{-}16)$$

Variables shown in Eq. (2-16) are dependent on position as well as energy. The removal cross section is given in Eq. (2-17). Equation (2-18) represents the diffusion coefficient.

$$\Sigma_r^g = \Sigma_a^g + \sum_{g' \neq g} \Sigma_s^{g \to g'} \qquad (2\text{-}17)$$

$$D_g = \frac{1}{3\Sigma_{tr,g}} \qquad (2\text{-}18)$$

Σ_{tr} represents the transport-corrected cross section. The diffusion coefficient arises from Fick's approximation, which relates the current to the flux. Fick's approximation allows a simplification of the transport equation from angular flux to scalar flux. A two-group energy approximation is assumed in order to solve the general multi-group diffusion equation. The two-group diffusion equations can provide power level calculation with an error on the order of a few percent.

2.3.3 Simplified Thermal-hydraulics

Since the coolant remains in single phase for a PWR, a simplified thermal-hydraulic calculation can be performed based on a steady-state enthalpy balance. Thermal-

hydraulic parameters such as the moderator density are coupled to the neutronic analysis through the cross-section dependency. Development of a simplified thermal-hydraulic analysis begins with a conservation of energy in the coolant region. The general form of the energy balance accounts for the change rate of the total internal energy in a given volume. Eq. (2-19) shows the general energy balance in terms of enthalpy [13].

$$\rho \frac{Dh}{Dt} = -\nabla \vec{q}'' + q''' + \frac{Dp}{Dt} + (\bar{\bar{\tau}} : \nabla \vec{v}) \qquad (2\text{-}19)$$

ρ is the density of the fluid, D represents the substantial derivative, h is the fluid enthalpy, $\vec{q}''$ is the heat flux at the clad boundary, q''' is the volumetric heat generation rate in the fluid, p represents pressure, and $(\bar{\bar{\tau}} : \nabla \vec{v})$ represents a dissipation function due to viscous forces. The following assumptions are applied to reduce Eq. (2-19) to a form that is easier to solve by numerical methods.

- Steady state conditions
- Coolant mass flux is constant
- Pressure is constant with axial height
- Frictional energy losses are ignored
- Heat flux is constant
- Internal heat generation from (n,γ) reaction is negligible

Using these assumptions and applying cylindrical coordinates, Eq. (2-19) is simplified to the following.

$$\rho_m \bar{v} \frac{\partial}{\partial z}(h_m) = \frac{q''_{co} P_h}{A_H} \qquad (2\text{-}20)$$

$\rho_m \bar{v}$ represents the coolant mass flux (equal to the inlet mass flux in steady state), h_m is the coolant enthalpy, q''_{co} is the heat flux at the outer cladding, P_h is the heated perimeter of the fuel rod, and A_H is the hydraulic flow area. Using definitions for the heated perimeter and hydraulic flow area in cylindrical geometry, Eq. (2-20) can be rearranged to the following.

$$\frac{\partial}{\partial z}(h_m) = \frac{q''_{co}\pi D_{co}}{\left(p^2 - \frac{\pi}{4}D_{co}^2\right)\rho_m \bar{v}} \qquad (2\text{-}21)$$

D_{co} is the outer diameter of the cladding and p is the flow channel pitch. The average heat generation in the fuel, also known as the power density, can be determined from the following relationship.

$$q''' = \frac{Q\gamma}{N_{FA}N_{rods}\pi R_{co}^2 H} = \frac{q'}{\pi R_{co}^2} \qquad (2\text{-}22)$$

Q is the total thermal power, γ is the fraction of heat generated in the fuel, N_{FA} is the total number of fuel assemblies, N_{rods} is the number of fuel rods per assembly, and H is the active fuel height. The relationship between the power density, heat flux, and linear power density is given by Eq. (2-23).

$$q''' = \frac{2q''_{co}}{R_{co}} = \frac{q'}{\pi R_{co}^2} \qquad (2\text{-}23)$$

The core mass flow rate (kg/s) can be calculated using Eq. (2-24).

$$\dot{m}_{core} = \dot{V}_{pump} N_L (1 - B_{core})\rho_m \qquad (2\text{-}24)$$

$\dot{V}_{pump}$ is the volumetric flow rate of a pump (m^3/s), N_L is the number of reactor flow loops, B_{core} is the core bypass fraction. The assembly mass flux (kg/m^2-s) is calculated using Eq. (2-25).

$$G_{assmb} = \frac{\dot{m}_{core}}{N_{FA}A_H} \qquad (2\text{-}25)$$

The flow area for an assembly is the cross sectional area of the assembly minus the total area of the fuel rods and guide tube area. Once the assembly mass flux is known, the fluid velocity can be calculated with Eq. (2-26).

$$\bar{v} = \frac{G_{assmb}}{\rho} \qquad (2\text{-}26)$$

Nominal values for clad radius, power density, hydraulic area, and inlet velocity are calculated prior to analysis and are held constant. Equation (2-21) is solved numerically by discretizing over different axial zones. The discretization of the coolant enthalpy is shown in Eq. (2-27).

$$h_{m,i+1} - h_{m,i} = (z_{i+1} - z_i)\frac{\pi R_{co}^2 q'''}{A_H \rho_m \bar{v}} \qquad (2\text{-}27)$$

Subscripts i and $i+1$ represent different axial zones and z represents the axial height. The number of axial zones for the thermal-hydraulic analysis is chosen by the user and the accuracy desired. In Eq. (2-27), $\rho_m \bar{v}$ is a constant and equal to the inlet parameters because we have assumed steady-state conditions and no cross-flows between the fuel assemblies.

With the enthalpy calculated and using appropriate fluid state equations (or water tables), the temperature of the coolant can be determined. The coolant temperature is then used as input for the heat conduction equation so that the fuel temperature can be determined. Next the fuel temperature is used to determine the appropriate cross-section branching case. Iteration between thermal-hydraulics and neutronics must be performed until there is convergence of the thermal-hydraulic variables (fuel temperature and coolant enthalpy) and neutronic variables (flux). Convergence between thermal-hydraulics and neutronics represents a single steady-state calculation, as shown previously in the block diagram of Figure 2.8.

2.3.4 Burnup Steps

The size of a burnup step is chosen by the user and the accuracy desired. Usually the burnup step is performed in 1 GWd/t increments or greater. For example, a cycle depletion of 20 GWd/t would require 20 depletion steps. Choosing a coarse burnup step, however, requires special consideration at EOC, as described in the following.

The EOC cycle boron concentration is expected to be zero. We have chosen to determine the EOC when the boron concentration falls in the range between 0 and 10 ppm. During a typical cycle depletion, the boron concentration decreases approximately by 100 ppm per GWd/t. To guarantee the boron concentration is not negative near EOC, the burnup steps would need to be very small. A negative boron concentration is a non-real solution. Using a burnup step approximately less than 0.1 GWd/t would ensure that the next critical boron search does not exceed the 10 ppm EOC window. Figure 2.9 illustrates the boron concentration near EOC.

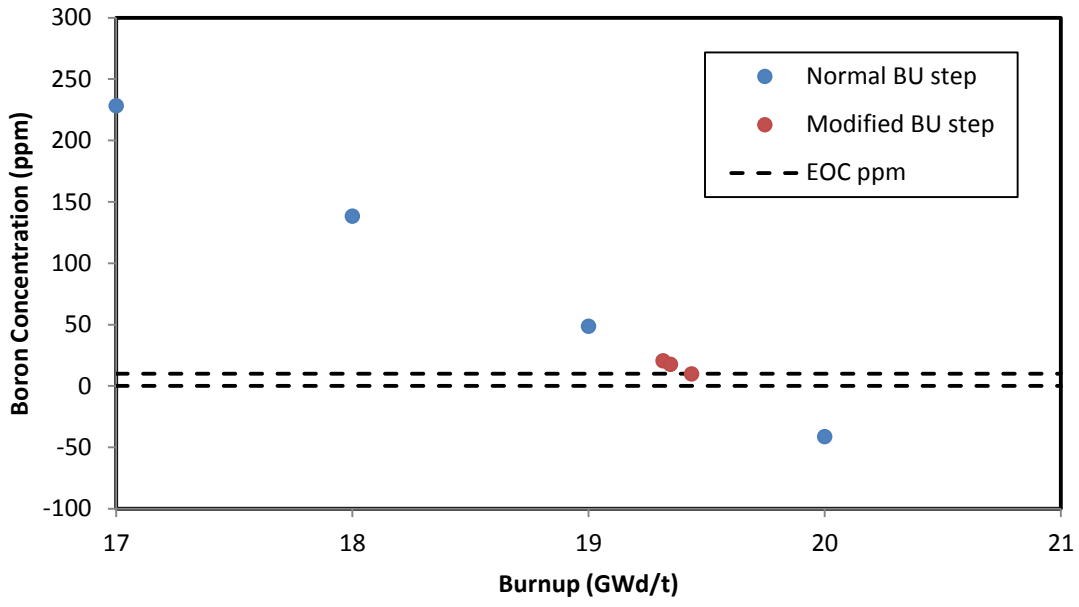

Figure 2.9 EOC boron concentration with and without a modified burnup step.

The exact EOC burnup is typically unknown the first time a cycle analysis is performed. Choosing a small burnup step of 0.1 GWd/t would be impractical. A cycle depletion of 20 GWd/t would then require 200 depletions steps. This needlessly increases the computational time with little or no improvements in accuracy. Therefore, a program was created to decrease the burnup step size near EOC. As Figure 2.9 illustrates, only a few additional fine burnup steps are required to meet the EOC boron window. Coarse burnup steps are used throughout the majority of the cycle depletion and fine burnup steps are generated near EOC.

2.3.5 Tools

Two well-known 3D core simulation tools are SIMULATE and CRONOS. Both codes are capable of solving two-group diffusion equations using homogenized cross-sections. The goal of these codes is to perform cycle calculations, fuel management optimization, and core safety parameters. For PWR's, the thermal-hydraulic calculations are a simple single-phase model. Calculations performed are at steady-state conditions only. Separate codes are used for a transient condition such as an overpower event.

3 CHOSEN REFERENCE CORE

The UK-EPR was chosen as the reference core for UBO fuel comparisons [9]. The EPR was chosen because of the publically available reference data. Specific data on assembly design and nominal core parameters were provided. In addition, cycle results were available for standard UO_2 fuel type. Therefore, the cycle length and reactivity coefficients using the standard UO_2 fuel type could be verified with our core simulations methods before analyzing the Beryllium-doped fuel types.

3.1 Fuel Assembly Design

The fuel assembly design chosen is typical of a PWR. The assembly lattice is 17x17, for a total of 289 channels with a varying number fuel pins, Gadolinium pins, and guide tubes. Nominal assembly parameters are given in Table 3.1. Values for gap and bulk heat convection were not provided by EPR but are representative values for a PWR. The average value of LHGR can be calculated with the parameters given. The peak LHGR at nominal conditions is determined by a transient loss-of-coolant (LOCA) analysis performed for the EPR design. Another peak LHGR protection setpoint is defined for prevention of fuel damage.

Table 3.1 Assembly dimensions and nominal parameters

Parameter	Value	Unit
Active fuel height	420	cm
Number assemblies	241	
Number fuel rods per assembly	265	
Radius fuel	0.4095	cm
Thickness gap	0.0085	cm
Thickness clad	0.057	cm
Average bulk temperature	313	°C
h_{gap}	10000	W/m^2-°C
h_{bulk}	36000	W/m^2-°C
Average LHGR	163.4	W/cm
Peak LHGR nominal conditions	470	W/cm
Peak LHGR protection setpoint	590	W/cm

Power density values were calculated using APOLLO and not taken from the EPR reference. The power density for each assembly design and fuel type is given in Table 3.2. The core average power density is determined by weighting the assembly power density by the number of assembly designs in the core.

Table 3.2 Power density for different assembly designs

	Power Density (kW/kgU)		
Assembly Design	**UO_2**	**UBO 5vol%**	**UBO 10vol%**
Gd-0	34.4721	36.285	38.3020
Gd-8	34.5900	36.359	38.3190
Gd-12	34.6496	36.396	38.3250
Gd-16	34.7089	36.432	38.3330
Gd-20	34.7685	36.469	38.3420
Gd-24	34.8282	36.506	38.3482

3.2 Core Thermal-hydraulics

Nominal thermal-hydraulic parameters were taken from the EPR reference. Mass flow rates and velocities were calculated using Eq. (2-24) and (2-26). A summary of the nominal thermal-hydraulic parameters and initial calculations can be found in Table 3.3.

Table 3.3 Nominal thermal-hydraulic parameters

Parameter	Value	Unit
Power	4500	MWth
Fraction heat generated in fuel	0.974	
Number of Loops	4	
Pressure	155	bar
Thermal design flow/loop	27185	m^3/h
Nominal inlet temperature	295.6	°C
Average core temperature	313.6	°C
Average rise in core	36	°C
Core bypass	5.5	%
Inlet density	742	kg/m^3
Core volume flow rate	28.54	m^3/s
Core mass flow rate	21,194	kg/s
Assembly mass flow rate	3584	kg/m^2-s
Inlet velocity	483	cm/s

3.3 Core Description

The mesh size and number of nodes for a 3D core calculation are determined by the user and the accuracy desired. In the radial direction, the assemblies were divided into four sections, resulting in a square 10.75 cm in length. In the axial direction, the core was split into 42, 10 cm high nodes. Therefore the core was composed of approximately cubic nodes with dimensions of 10x10.75x10.75 cm. Figure 3.1 illustrates the 3D core nodes.

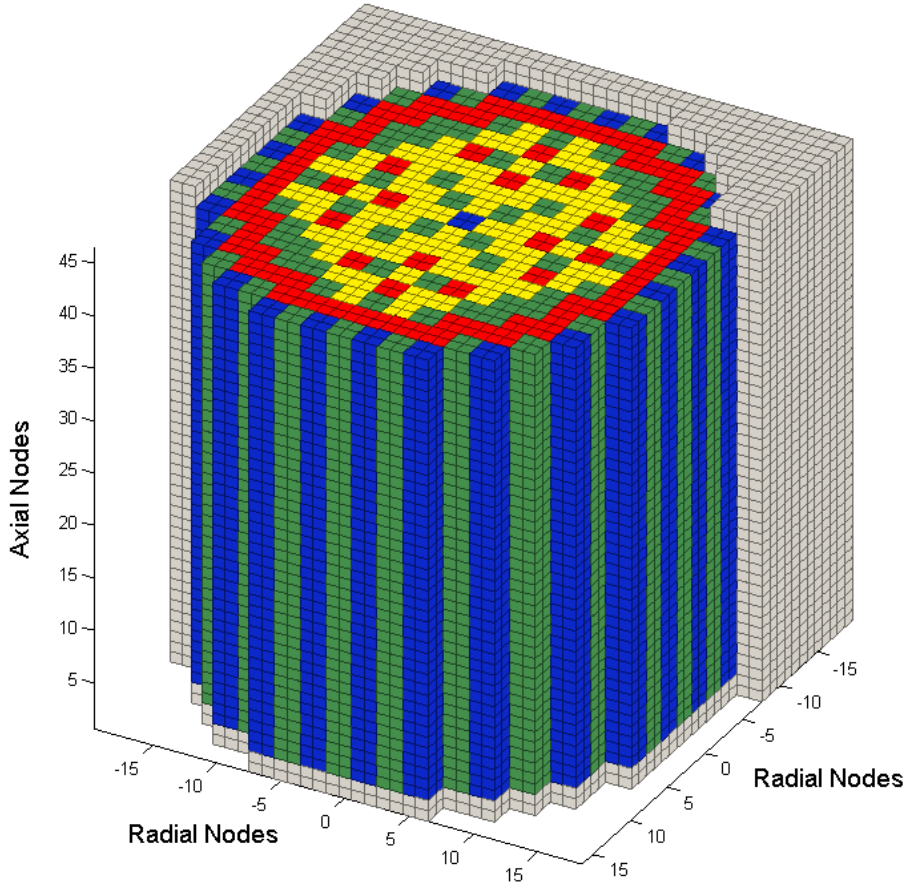

Figure 3.1 Computational mesh size for 241 assembly core. Reflectors (gray) are on top and bottom of each assembly and surround the periphery of the active core.

In addition to the core nodes, reflector nodes are placed at the periphery of the active core. Two reflector nodes are placed on the top and bottom of each assembly and a varying number of radial reflector nodes surround the core. The 241 assembly core subdivided into four assembly sections with 42 axial nodes contains 40,488 nodes plus the additional reflector nodes.

3.4 Shuffle Pattern

A shuffle map is used to determine the reload pattern for a new cycle depletion. The coordinate system for a shuffle map is typically alphabetical for the columns and

numerical for the rows. Letters “I”, “O”, and “Q” are omitted to prevent confusion with the one and zero digits.

The coordinates of the shuffle map indicate where the assembly is moving to. The assembly names on the shuffle map indicate where the assembly came from. Figure 3.2 shows an example of a shuffle pattern. The number 8 in coordinate R5 indicates that this assembly is fresh and contains 8 Gadolinium rods. Gadolinium weight percent and fuel enrichment were omitted from the map because these values were constant in all assembly designs.

The shuffle map can be read as follows. The assembly formerly located in coordinate R5 currently resides in the coordinate M7 (meaning the assembly came from the coordinate R5 and is moving to coordinate M7). Next this assembly will be moved to coordinate S5 and then to coordinate S4. Assemblies that are to be shuffled off the map will not exist on the map. For example, the assembly located in coordinate S4 is to be shuffled off the map at the next repositioning.

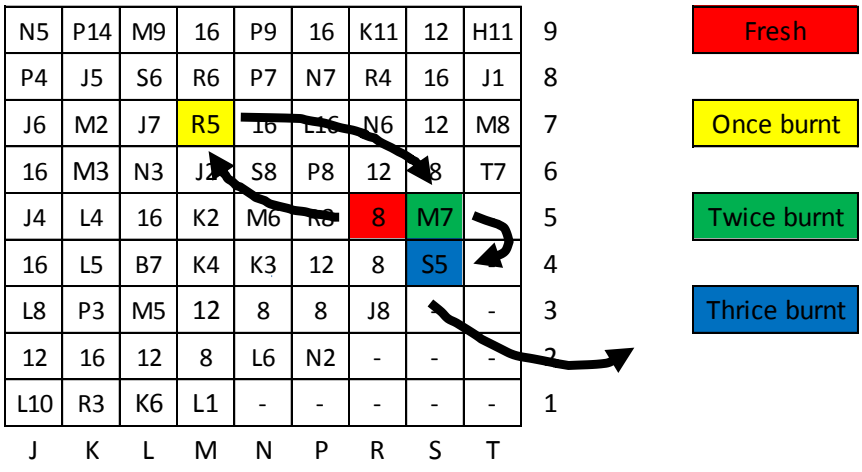

Figure 3.2 Example of coordinate system used to determine shuffle locations.

3.4.1 18-Month Equilibrium Cycle

The shuffle map for the 18-month equilibrium cycle is determined from the EPR reference design. The core uses four batches with an IN-OUT shuffle pattern. With an IN-OUT shuffle pattern, the once burnt assemblies are shuffled toward the center of the core while the twice or thrice burnt assemblies are shuffled out to the periphery of the core. Figure 3.3 shows the reload pattern for an 18-month equilibrium cycle.

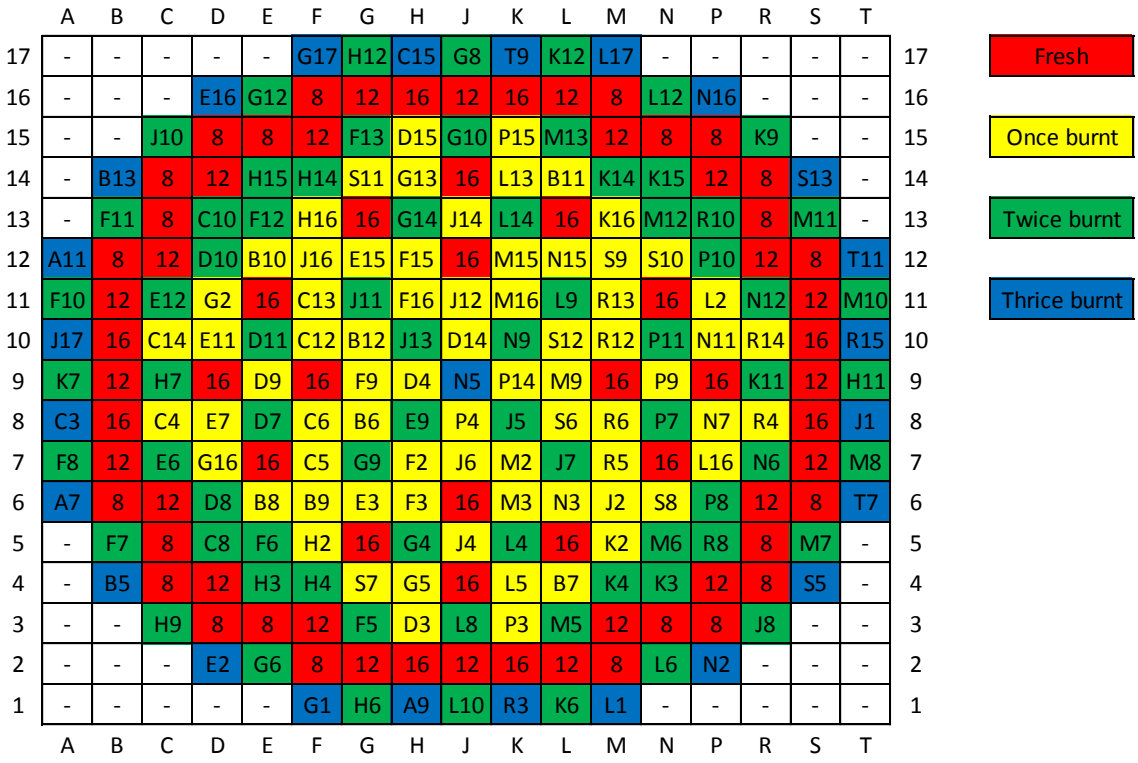

Figure 3.3 Original reload pattern for the 18-month equilibrium cycle.

3.4.2 22-Month Equilibrium Cycle

The 22-month equilibrium cycle follows a more aggressive core loading pattern. An IN-OUT shuffle pattern is used with a three batch strategy. The reload pattern is shown in Figure 3.4.

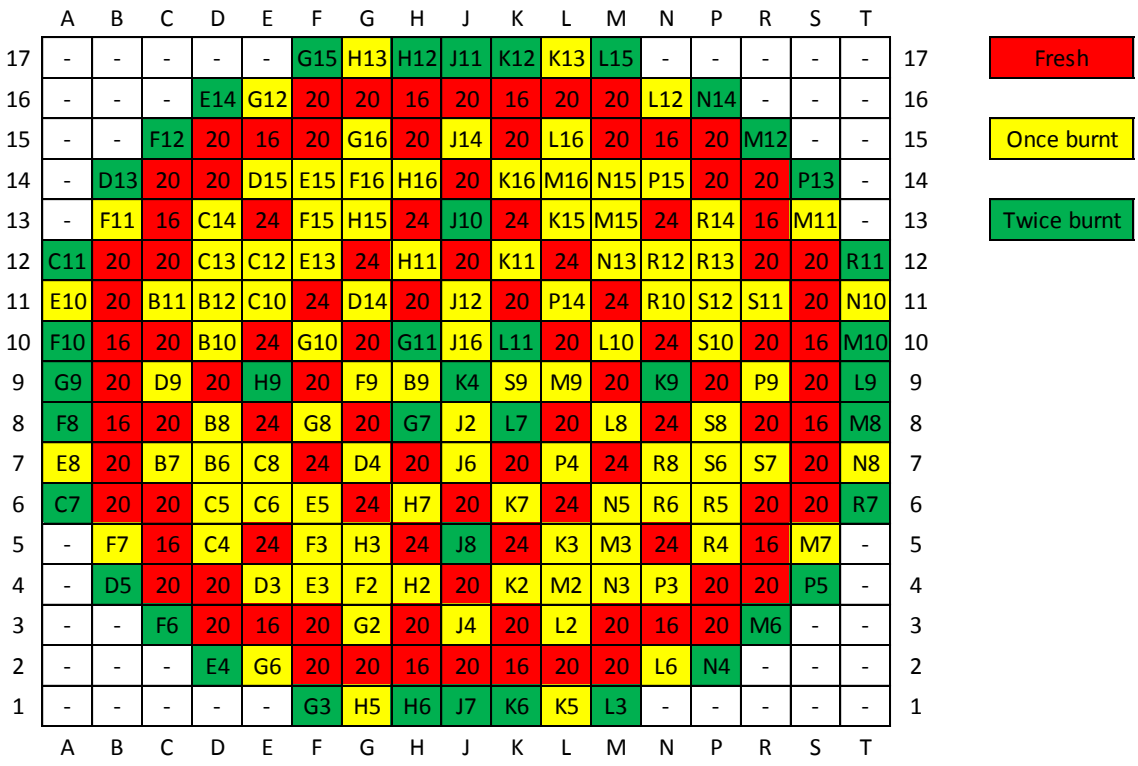

Figure 3.4 Original reload pattern for the 22-month equilibrium cycle.

4 PELLET HEAT CONDUCTION

Detailed analysis of the heat conduction for each pellet is not a required step for a 3D core simulation. On the 3D core level, only an average fuel temperature is considered per node (a node is a fraction of an assembly, typically one quarter, for a given height increment). The fuel thermal conductivity is used as an input to the 3D computation to calculate the effective fuel temperature only. A detailed description of the pellet radial temperature distribution is optionally calculated separately. Comparison of the UO_2 and UBO pellet heat conduction is performed to better understand the effect of a higher thermal conductivity.

4.1 Fuel Thermal Conductivity

Thermal conductivity studies at Purdue University were performed for a range of BeO volume percent addition. The volume percent of BeO parameter was varied between zero and ten percent BeO [4]. The reference thermal conductivity for UO_2 was obtained from Fink [1]. A power fit was used to represent the conductivity data and is shown in Eq. (4-1).

$$k_{UO2}(T) = 257.99(T)^{-0.627} \tag{4-1}$$

where k is the thermal conductivity (W/m-K) and T is the temperature in Kelvin. The temperature range for the power fit is 273-2073 K. The thermal conductivities for UBO fuel are from the green granule manufacturing process. A power fit for UBO 5vol% and UBO 10 vol% can be found in Eq. (4-2) and Eq. (4-3), respectively [4].

$$k_{UBO\ 5vol\%}(T) = 1362.3(T)^{-0.829} \tag{4-2}$$

$$k_{UBO\ 10vol\%}(T) = 7117(T)^{-1.037} \tag{4-3}$$

Thermal conductivity for UO_2 and UBO fuels are plotted as a function of temperature in Figure 4.1. Results from Figure 4.1 show increasing thermal conductivity as more

volume percent BeO is added to the fuel. At a nominal average reactor temperature of 550 °C, the thermal conductivity for UBO 5vol% and UBO 10vol% is increased 36% and 72%, respectively.

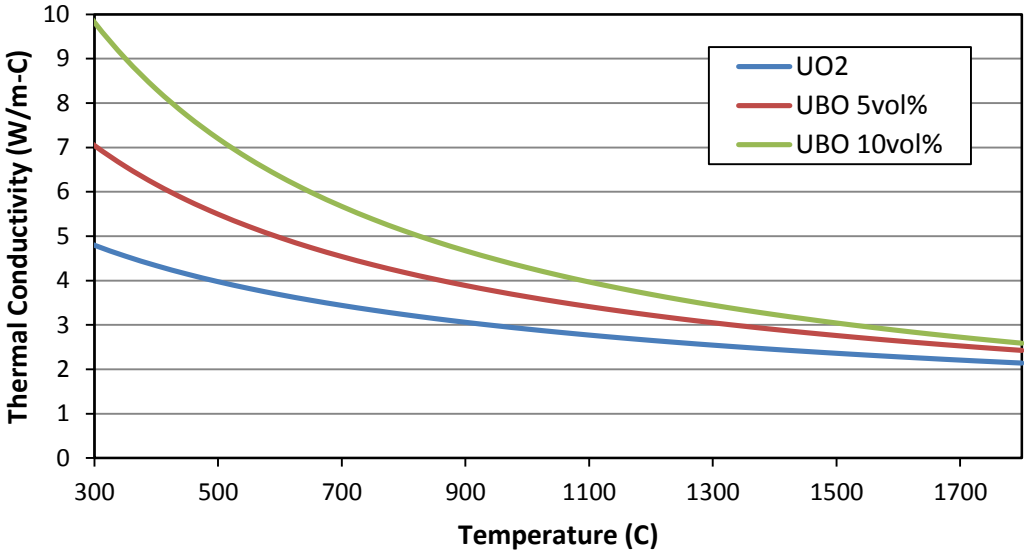

Figure 4.1 Thermal conductivity for UO_2 and UBO fuel [4].

4.2 Heat Conduction Solutions

A change in the fuel thermal conductivity has a significant effect on the pin temperature distribution. The temperature distribution can be analyzed by solving the general heat conduction equation. The steady-state heat conduction equation in a solid is given by Eq. (4-4).

$$-\nabla k(\vec{r},T)\nabla T(\vec{r}) = q'''(\vec{r}) \qquad (4\text{-}4)$$

Assumptions are made to reduce Eq. (4-4) to a simpler form. The first assumption is that the thermal conductivity is a function of temperature only within a given material. The second assumption is that the heat generation is uniform within the fuel. In addition, cylindrical coordinates are used to represent the fuel pin. Using cylindrical coordinates it

is also assumed that there is symmetry with the cylinder centerline and that the heat diffusion is only in the radial direction (no axial diffusion of heat). Using these assumptions, Eq. (4-4) can then be rewritten in polar coordinates as:

$$-\frac{1}{r}\frac{d}{dr}\left(kr\frac{dT}{dr}\right) = q''' \qquad (4\text{-}5)$$

q''' represents the volumetric heat generation rate in the fuel. After integrating Eq. (4-5), the constant of integration is solved by applying the boundary condition that the temperature gradient at the centerline is equal to zero. The resulting equation is shown in Eq. (4-6).

$$-k(T)\frac{dT}{dr} = \frac{1}{2}R_{co}q''' = q''_{co} \qquad (4\text{-}6)$$

R_{co} is the outer radius of the cladding and q''_{co} is the heat flux at the outer cladding boundary. To obtain the temperature of the fuel, the bulk coolant temperature must be coupled to the wall (outer clad) temperature. This is typically accomplished using a heat transfer coefficient between the coolant and clad, as shown in Eq. (4-7).

$$T_{co} - T_b = \frac{q''_{co}}{h_b} \qquad (4\text{-}7)$$

T_{co} is the temperature at the outer clad, T_b is an average bulk coolant temperature, and h_b is an effective bulk heat transfer coefficient. The bulk heat transfer coefficient may be solved by the Dittus-Boelter relationship or an average bulk heat transfer coefficient may be assumed.

A typical fuel pin can be divided into three fuel regions and one coolant region. The fuel region consists of the fuel, gap, and cladding. Figure 4.2 illustrates the geometry for a fuel pin.

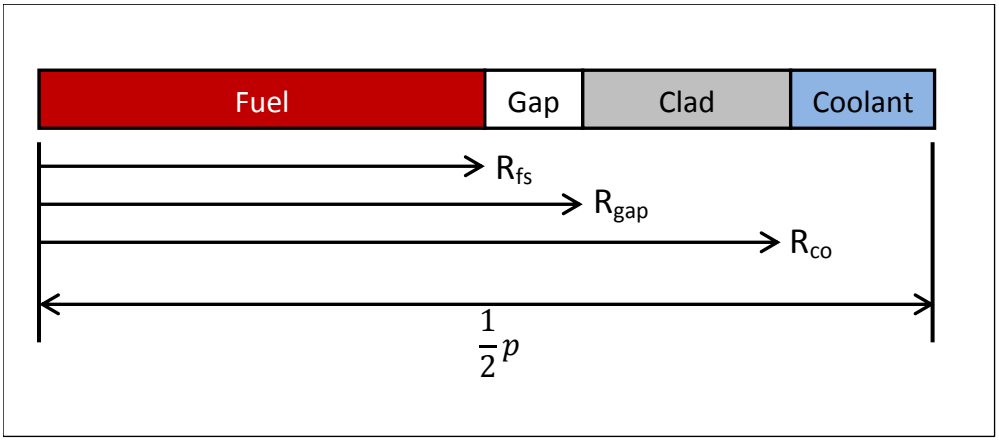

Figure 4.2 Symmetric geometry for half of a cylindrical fuel element.

Integrating Equation (4-5) over the gap and clad regions and combining the results is shown in Eq. (4-8).

$$T_{fs} = T_{co} + \frac{1}{2}R_{co}^2 q''' \left[\frac{1}{k_{gap}} ln\left(\frac{R_{gap}}{R_{fs}}\right) + \frac{1}{k_{clad}} ln\left(\frac{R_{co}}{R_{gap}}\right)\right] \qquad (4\text{-}8)$$

T_{fs} is the temperature at the fuel surface, k_{gap} is the conductivity of the gap, and k_{clad} is the conductivity of the clad. Integration of the heat conduction over the fuel region requires special consideration because the fuel conductivity is a function of temperature.

$$\int_{T_{fs}}^{T_{CL}} k(T')dT' = \frac{1}{4}R_{fs}^2 q''' \qquad (4\text{-}9)$$

T_{CL} represents the fuel centerline temperature. Equation (4-9) can be solved using Newton's method or other appropriate iterative techniques for non-linear equations.

Solving the heat conduction for the cylindrical fuel pin can provide information about the average clad temperature, fuel temperature, and centerline temperature. For neutronics calculations, one requires a representative average of the fuel temperature. Neutronic codes generally do not consider the radial pellet temperature distribution for self-shielding purposes. The fuel temperature has the greatest influence on the Doppler

broadening of isotopes. Since a simple volume weighted temperature average does not accurately represent the fuel physics, an effective Doppler temperature is used instead. The effective temperature is calculated using Rowland's formula.

$$T_{eff} = \frac{4}{9}T_{CL} + \frac{5}{9}T_{fs} \qquad (4\text{-}10)$$

4.3 Radial Temperature Distribution

With solutions for the heat conduction and known thermal conductivities, the pin temperature distribution can be compared for UO_2 and UBO fuels. For preliminary calculations, reactor thermal power is assumed to be divided evenly among the fuel assemblies. Within the assembly, the power is also divided evenly among the individual pins. The result is a temperature comparison that is a representative average of the power in each pin. Actual pin power and temperature on a core level will vary depending on the local power peaking factors.

Temperature comparisons were performed for UO_2, UBO 5vol%, and UBO 10vol% fuel. In addition, the temperature distributions were generated at nominal and maximum LHGR conditions. The nominal LHGR would represent expected temperatures during normal reactor operations. A maximum LHGR considers the local power peaking factors and provides the maximum temperatures in the fuel. Using an EPR design, the reference average and maximum LHGR are 163.4 and 590 W/cm, respectively [9]. Results of the temperature distributions for average LHGR are shown in Figure 4.3.

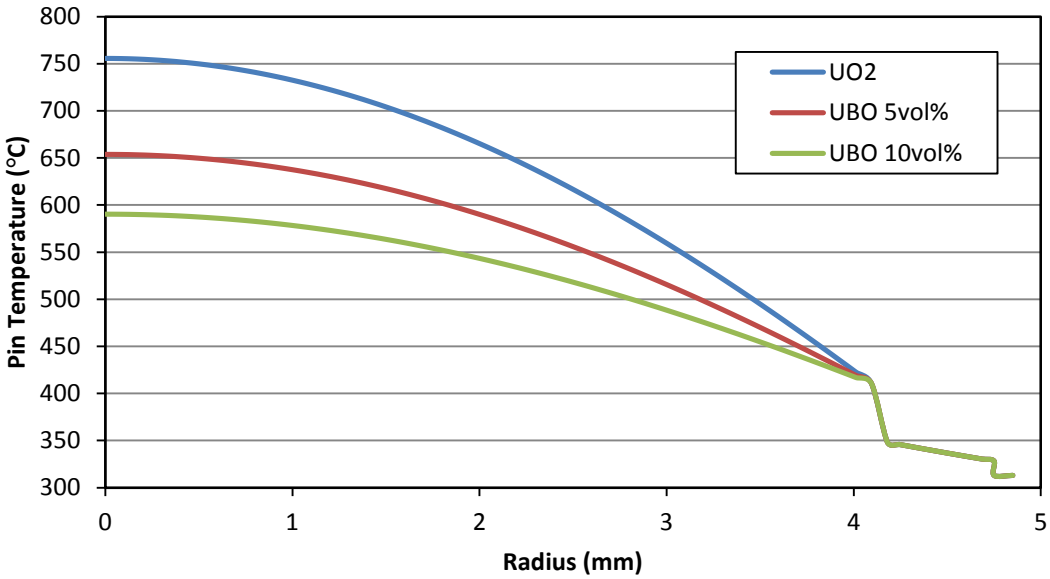

Figure 4.3 Radial pin temperature distribution for three fuel types at average LHGR (163.4 W/cm).

From Figure 4.3, the temperature is significantly reduced for the UBO fuel types. A summary of the temperature results for average and maximum LHGR are found in Table 4.1. Subtraction of the temperatures of UO_2 from UBO is summarized in Table 4.2.

Table 4.1 Results from the pin temperature calculations

		Temperature (°C)		
LHGR (W/cm)	**Temperature Type**	**UO_2**	**UBO 5vol%**	**UBO 10vol%**
163.4	Effective	564	519	490
	Centerline	756	654	590
590	Effective	1429	1308	1210
	Centerline	2389	2116	1896

Table 4.2 Reduction of the pin temperatures due to UBO

		ΔT (°C)	
LHGR (W/cm)	**Temperature Type**	**UBO 5vol%**	**UBO 10vol%**
163.4	Effective	45	74
	Centerline	102	166
590	Effective	121	219
	Centerline	273	493

Table 4.2 shows a significant reduction in the centerline temperature for the UBO fuels. However, UBO fuels have a lower melting point than standard UO_2 fuels because of the eutectic melting. Therefore the centerline temperature for UBO fuels at maximum LHGR is important for safety analysis. A comparison of temperature distributions at maximum LHGR is shown in Figure 4.4.

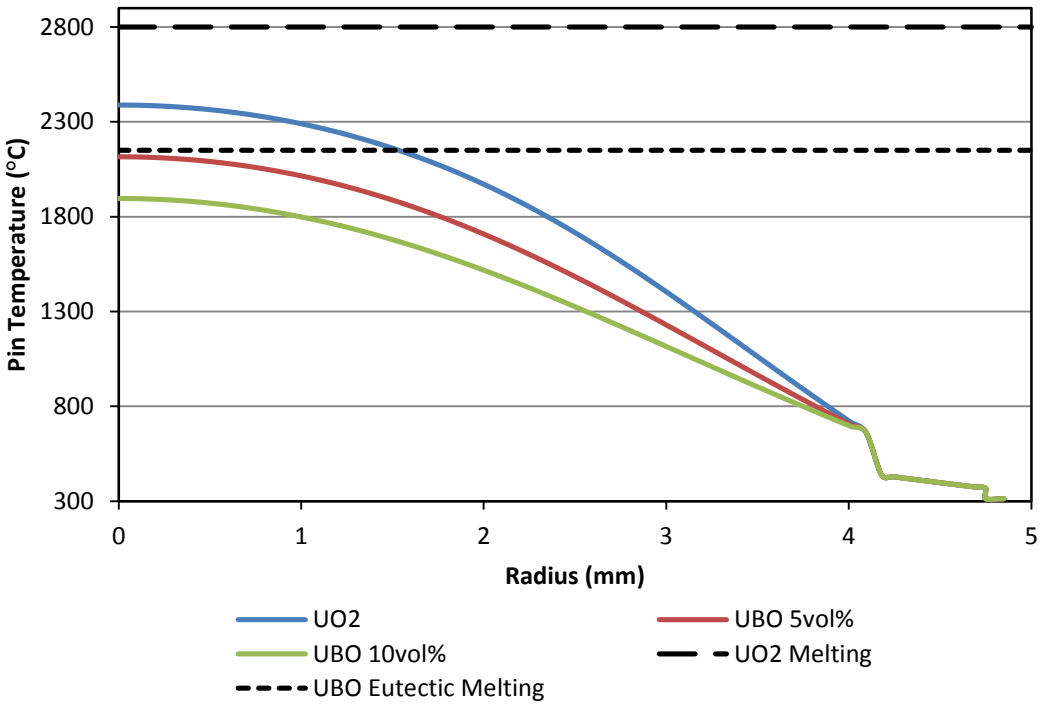

Figure 4.4 Radial pin temperature distribution for three fuel types at maximum LHGR (590 W/cm).

Melting margin for a given fuel type is calculated as the melting point minus the maximum centerline temperature. A comparison of the melting margins is found in Table 4.3. This calculation is only representative of a steady-state condition.

Table 4.3 Comparison of the melting limits

	Melting Margin (°C)		
LHGR (W/cm)	**UO_2**	**UBO 5vol%**	**UBO 10vol%**
163.4	2044	1496	1560
590	411	34	254

At nominal LHGR, there is significant margin for both UO_2 and UBO fuels. However at maximum LHGR, the margin is reduced for UBO fuels. UO_2 fuel has a margin of 411 °C whereas UBO 5vol% and UBO 10 vol% have a margin of 34 °C and 254 °C, respectively. The reduced centerline temperature of UBO fuel is not sufficient to overcome the large difference in melting points of UO_2 and UBO fuel. For BeO fuel additions of less than 5 vol%, there is the possibility of eutectic melting at the maximum LHGR.

5 2D LATTICE CALCULATIONS

Lattice physics calculations are an important precursor to 3D core simulation. Calculations results obtained during this stage are presented next. 2D assembly calculations can provide many important neutronic results. The input parameters and geometry of a 2D calculation can be carefully controlled to provide an accurate comparison of UO_2 and UBO fuels. Many lattice physics calculations can be performed such as: the four-factor formula, moderator curves, heterogeneous vs homogeneous fuel, spectrum analysis, and a nominal depletion. Lattice physics results can separate the significant benefits of the BeO addition. For instance, the relative importance of the BeO temperature effect compared to the moderating effect can be evaluated and distinguished using a 2D lattice physics calculation.

5.1 DRAGON

5.1.1 Initial Fuel Isotopics

Determining the fuel isotopics is an important input for neutronic calculations. The parameters necessary to calculate the fuel isotopics are found in Table 5.1. The fuel density is assumed to be 95% of the theoretical density.

Table 5.1 Parameters for fuel isotopic calculations

Parameter	Value	Unit
UO_2 fuel density	10.412	(g/cm^3)
BeO density	3.010	(g/cm^3)
(UO_2+Gd_2O_3) density	10.080	(g/cm^3)
M_{U235}	235.044	(g/mol)
M_{U238}	238.051	(g/mol)
M_U	237.899	(g/mol)
M_{UO2}	269.888	(g/mol)
M_{BeO}	25.007	(g/mol)

Most neutronic codes require an atom density input for each material specified. Atom densities for the main fuel constituents can be calculated using Eqs. (5-1) - (5-4). The atom density, N, is converted to mole/b-cm for input into DRAGON.

$$N_{Be9} = vf_{BeO}\frac{\rho_{BeO}N_a}{M_{BeO}} \qquad (5\text{-}1)$$

vf_{BeO} is the volume fraction of BeO in the UBO pellet, ρ_{BeO} is the density of BeO, N_a is Avogadro's number, and M_{BeO} is the molar mass of BeO. The atom density for the uranium isotopes are reduced depending on the volume of BeO added.

$$N_{U235} = (1 - vf_{BeO})\frac{\rho_{UO2}N_a}{M_{UO2}}\left(\frac{M_U}{M_{U235}}\right)wf_{U235} \qquad (5\text{-}2)$$

ρ_{UO2} is the density of UO_2 including any theoretical or dilution factors and wf_{U235} is the weight fraction of the ^{235}U isotope with respect to the uranium. M_U, M_{UO2}, M_{U235}, M_{U238}, are the molar masses for Uranium, Uranium dioxide, ^{235}U, and ^{238}U, respectively.

$$N_{U238} = (1 - vf_{BeO})\frac{\rho_{UO2}N_a}{M_{UO2}}\left(\frac{M_U}{M_{U238}}\right)(1 - wf_{U235}) \qquad (5\text{-}3)$$

The atom density for oxygen has contributions from both UO_2 and BeO. A variable amount of oxygen is present in the fuel depending on the volume fraction of BeO in the UBO fuel.

$$N_{O16} = 2(1 - vf_{BeO})\frac{\rho_{UO2}N_a}{M_{UO2}} + vf_{BeO}\frac{\rho_{BeO}N_a}{M_{BeO}} \qquad (5\text{-}4)$$

5.1.2 Mass Equivalence

There are two general methods to compare UO_2 to UBO fuel, a fixed mass or a fixed cycle length comparison. A fixed mass (or mass equivalent) approximation means that the amount of ^{235}U loaded into a pin is constant regardless of the BeO volume fraction. The weight fraction of ^{235}U for a mass equivalent comparison can be calculated using Eq. (5-5).

$$wf_{U235}^{eqv} = \frac{wf_{U235}}{(1 - vf_{BeO})} \qquad (5\text{-}5)$$

The equivalent ^{235}U weight fraction is increased by the volume displaced by the BeO addition. Combining Eq. (5-5) with the atom density calculation of Eq. (5-2), one can determine the equivalent atom density for ^{235}U.

$$N_{U235}^{eqv} = \frac{\rho_{UO2} N_a}{M_{UO2}} \left(\frac{M_U}{M_{U235}} \right) wf_{U235} \qquad (5\text{-}6)$$

The equivalent ^{235}U atom density calculation shown in Eq. (5-6) is no longer dependent on the volume fraction of BeO. However, the ^{238}U atom density calculation will be different between UO_2 and UBO fuels. The increased equivalent ^{235}U atom density will decrease the ^{238}U atom density. An illustration of the mass equivalence is shown in Figure 5.1.

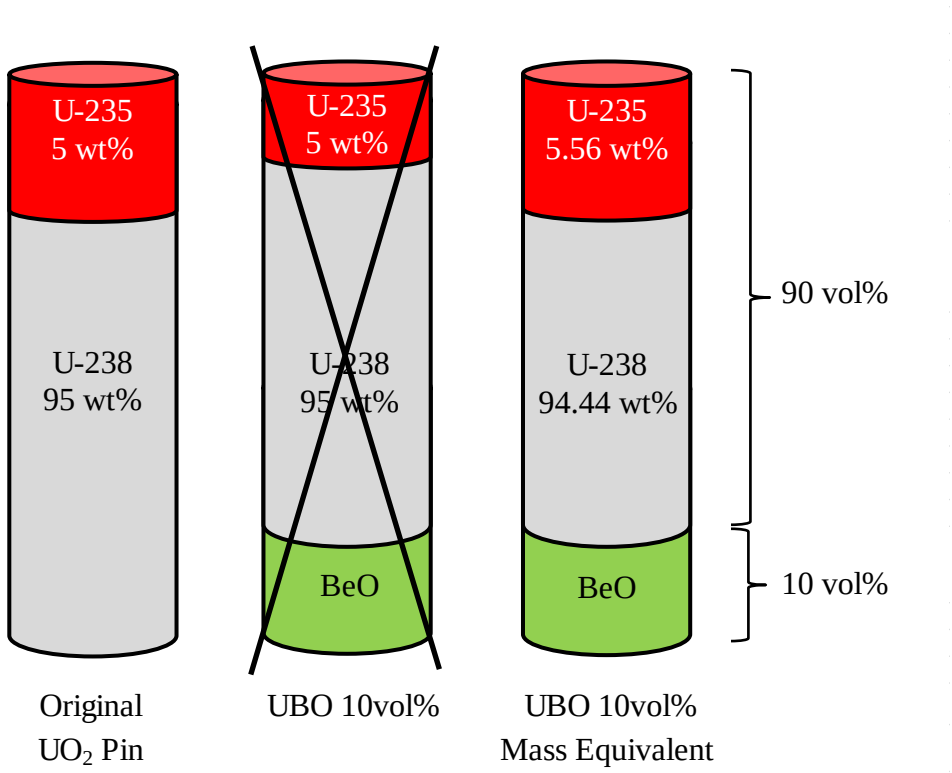

Figure 5.1 Example of three different pins to illustrate mass equivalence.

The equivalent mass comparison is intuitive because for the same amount of ^{235}U loading, one can potentially observe a cycle length increase due to the BeO addition. A mass equivalence is needed because otherwise removing some of the ^{235}U would shorten the cycle length. The disadvantage of the mass equivalence approach is that a higher enrichment is required. If the enrichment level is already near the maximum limit of 5 wt% for standard UO_2 fuel, then a UBO mass equivalent case may exceed the limit.

The alternative method of comparison is a fixed cycle length. Since UBO fuel has potential fuel cycle benefits, less ^{235}U mass may be require to reach a given cycle length. A fixed cycle length comparison is useful for facilities that want to keep a constant schedule. However, the fixed cycle length comparison is more difficult to perform because the enrichment savings must be interpolated after a cycle length analysis is

completed. The mass equivalent comparison is easier because the enrichment input is known before the cycle analysis is performed.

In addition, a fixed cycle length analysis on a full-core level is more complex. Multiple cross section inputs are necessary to make an interpolation of the enrichment savings. Calculating the enrichment savings for different assembly types would be difficult and time consuming. Therefore a mass equivalent comparison was chosen for fuel cycle comparisons. Subsequently, all the fuel cycle calculations use mass equivalence unless otherwise noted.

5.1.3 Single Cell Analysis

5.1.3.1 Description of Case Studies Performed

A single cell analysis was performed to determine the effect of a BeO addition. The single cell consists of a fuel, clad, and moderator region, as shown in Figure 5.2. Instead of modeling the small fuel-cladding gap, the cladding density was diluted over the gap region. Dilution of the cladding is a common assumption to avoid discretization of a very thin and neutronically unimportant gap zone.

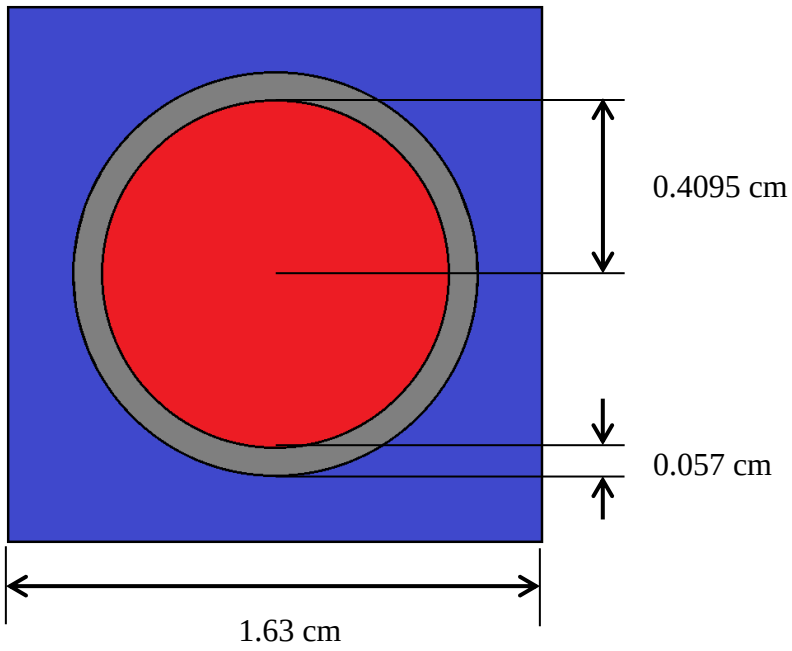

Figure 5.2 Single lattice cell dimensions for fuel case studies.

Four case studies were performed for comparison of UO_2 and UBO fuels. The first case study (Case A) was a reference UO_2 pin at nominal enrichment and fuel temperature. Three additional studies were performed using the UBO fuel type. Case B was a mass equivalent pin with a 10 vol% BeO addition at the reference UO_2 fuel temperature. Case C was the same as case B except that the temperature was reduced to the nominal UBO 10 vol% fuel temperature. Lastly case D was the same as case B except that the 10 vol% BeO density was set to zero so as to create a void. Figure 5.3 is an illustration of the four case studies performed.

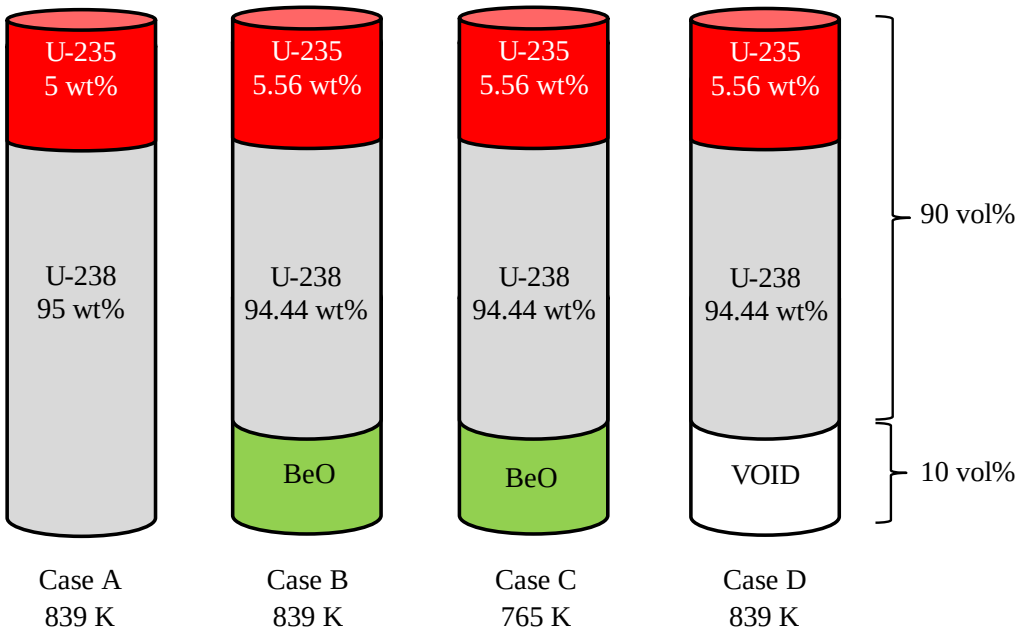

Figure 5.3 Illustration of four case studies performed.

The isotopics of the four case studies were slightly different. Since mass equivalence was assumed, the ^{235}U atom density was constant. To accommodate the BeO addition, the ^{238}U atom density was reduced. The oxygen content also varies depending on the presence of BeO. A summary of the fuel isotopics for the four case studies is found in Table 5.2.

Table 5.2 Atom densities for the four case studies performed.

	Atom Density (mol/b-cm)			
Isotope	**Case A**	**Case B**	**Case C**	**Case D**
U235	1.176E-03	1.176E-03	1.176E-03	1.176E-03
U238	2.206E-02	1.974E-02	1.974E-02	1.974E-02
Be9	0.000E+00	7.249E-03	7.249E-03	0.000E+00
O16 (UO2+BeO)	4.647E-02	4.907E-02	4.907E-02	4.182E-02

5.1.3.2 Four Factor Formula

A four-factor formula can be used to represent the infinite multiplication factor for a neutron cycle. The infinite multiplication factor (k_{inf}) describes the neutron population at some point in the cycle. A description of the infinite multiplication factor is given in Eq. (5-7).

$$k_{inf} = \frac{neutron\ population\ in\ current\ generation}{neutron\ population\ in\ previous\ generation} \qquad (5\text{-}7)$$

If k_{inf} is less than unity, the neutron population decreases with each subsequent generation whereas the neutron population increases for k_{inf} greater than unity. If k_{inf} is equal to unity the neutron population is constant, a condition known as critical. The infinite multiplication factor can be shown as a product of four factors, as given in Eq. (5-8).

$$k_{inf} = \eta \varepsilon f p \qquad (5\text{-}8)$$

Where η is the reproduction factor, ε is the fast fission factor, f is the thermal utilization factor, and p is the resonance escape probability factor. The four factors of the four factor formula can reveal which nuclear property of the infinite lattice is most affected by the BeO addition. A description of the fast fission factor is given in Eq. (5-9).

$$\varepsilon = \frac{total\ fission\ rate\ in\ fuel}{thermal\ fission\ rate\ in\ fuel} \qquad (5\text{-}9)$$

Using two energy groups, the fast fission factor can be represented mathematically using Eq. (5-10). Convention for representing the two energy groups is I for fast energy above approximately 0.625 eV and II for thermal energy below 0.625 eV. In addition, the infinite lattice is separated into fuel (F) and non-fuel (NF) regions. The non-fuel regions include the moderator, cladding, or any other structural material.

$$\varepsilon = \frac{\left(\nu \Sigma_f^F \phi^F\right)^I + \left(\nu \Sigma_f^F \phi^F\right)^{II}}{\left(\nu \Sigma_f^F \phi^F\right)^{II}} \qquad (5\text{-}10)$$

ν is the number of neutrons released per fission, ϕ^F is the neutron flux in the fuel, and Σ_f^F is the macroscopic fission cross-section of the fuel. The thermal utilization factor is described in Eq. (5-11).

$$f = \frac{thermal\ absorption\ rate\ in\ fuel}{thermal\ absorption\ rate\ in\ all\ components} \qquad (5\text{-}11)$$

Equation (5-11) is a mathematical representation of the thermal utilization factor.

$$f = \frac{(\phi^F \Sigma_a^F)^{II}}{(\phi^F \Sigma_a^F)^{II} + (\phi^{NF} \Sigma_a^{NF})^{II}} \qquad (5\text{-}12)$$

Σ_a^F and Σ_a^{NF} are the macroscopic absorption cross-section for the fuel and non-fuel, respectively. ϕ^{NF} is the flux in the non-fuel region. A description of the resonance escape probability is given in Eq. (5-13).

$$p = \frac{thermal\ absorption\ rate\ in\ all\ components}{total\ absorption\ rate\ in\ all\ components} \qquad (5\text{-}13)$$

The resonance escape probability can also be written as shown in Eq. (5-14).

$$p = \frac{(\phi^F \Sigma_a^F)^{II} + (\phi^{NF} \Sigma_a^{NF})^{II}}{(\phi^F \Sigma_a^F)^{I} + (\phi^{NF} \Sigma_a^{NF})^{I} + (\phi^F \Sigma_a^F)^{II} + (\phi^{NF} \Sigma_a^{NF})^{II}} \qquad (5\text{-}14)$$

Lastly, a description of the reproduction factor is given in Eq. (5-15). The reproduction factor accounts for the fact that not all absorptions in the fuel will cause fission.

$$\eta = \frac{thermal\ fission\ rate\ in\ fuel}{thermal\ absorption\ rate\ in\ fuel} \qquad (5\text{-}15)$$

Equation (5-16) is the mathematical representation of the reproduction factor.

$$\eta = \frac{\left(\nu \phi^F \Sigma_f^F\right)^{II}}{(\phi^F \Sigma_a^F)^{II}} \qquad (5\text{-}16)$$

The four factors were calculated for each of the four fuel case studies. A nominal moderator density of 0.695 g/cm^3 was used at a pressure of 155 bars and an average

coolant temperature of 314 °C. The atom density of H_2O at these conditions is 2.325 $x10^{-2}$ atoms/b-cm. DRAGON provided the two-group, two-region infinite lattice reaction rates necessary to calculate the four factors. A summary of the four factors is given in Table 5.3.

Table 5.3 Results from the four case studies performed

Factor	Case A	Case B	Case C	Case D
ε	1.39072	1.37431	1.37361	1.37866
f	0.95862	0.95835	0.95837	0.95837
p	0.54895	0.56137	0.56273	0.56071
η	1.91699	1.93254	1.93260	1.93272
kinf	1.40293	1.42887	1.43166	1.43185

Results of Table 5.3 can be difficult to interpret. There are three changes to the lattice physic parameters due to the BeO addition: reduced fuel volume, reduced temperature, and changes in moderation due to the Beryllium cross-section. A comparison of the various cases reveals the individual effect BeO has on lattice physics parameters. Subtracting case A from case D shows the effect of a reduced fuel volume due to a voided region. The moderating effect of the BeO material itself is shown by subtracting case D from case B. Subtracting case B from case C reveals the effect due to a reduced fuel temperature. Lastly, the total lattice physics effect due to the BeO addition is shown by subtracting case A from case C. A summary of the case comparisons can be found in Table 5.4.

Table 5.4 Comparison of the four factors

	Reactivity (pcm)			
Factor	**Reduced Fuel Volume (D-A)**	**Temperature Effect (C-B)**	**BeO Effect (B-D)**	**Total Effect (C-A)**
ε	-629	-37	-229	-895
f	-27	2	-2	-28
p	3822	431	210	4463
η	425	2	-5	421
k_{inf}	1440	137	-146	1431

The thermal utilization factor is nearly constant and therefore does not significantly change due to the BeO addition. The reduced fuel volume has the greatest effect on lattice physics parameters. An increase in the resonance escape probability is observed because less ^{238}U is present in the fuel. In addition, the fast fission factor decreases due to less ^{238}U. The reproduction factor is increased from the assumption of less neutron capture in the fuel.

The reduced temperature effect slightly affects the resonance escape probability. A lower fuel temperature reduces the Doppler broadening of ^{238}U. Therefore more neutrons are able to escape the resonance region of ^{238}U. The BeO addition slightly reduces the fast fission factor because of the increased moderation. Overall the temperature and BeO lattice physics effects are minimal compared to the reduction in fuel volume.

According to Table 5.4, the total reactivity difference between UO_2 and UBO fuel at their respective enrichments and fuel temperatures is 1431 pcm. However, close inspection of the cases reveals the majority of the reactivity increase is due to the reduced fuel volume. The positive reactivity gain from the temperature decrease is relatively small at 137 pcm. The BeO addition negatively contributes to the total reactivity by 146 pcm.

5.1.3.3 Moderator Curves

To generate the moderator curves, a series of lattice cell calculations were performed with a reduced or increased moderator density while the fuel density remained constant.

The multiplication factor is then plotted as a function of the ratio of the moderator density to fuel density. In addition, the four factors are plotted as a function of the moderator-to-fuel density as shown in Figure 5.4.

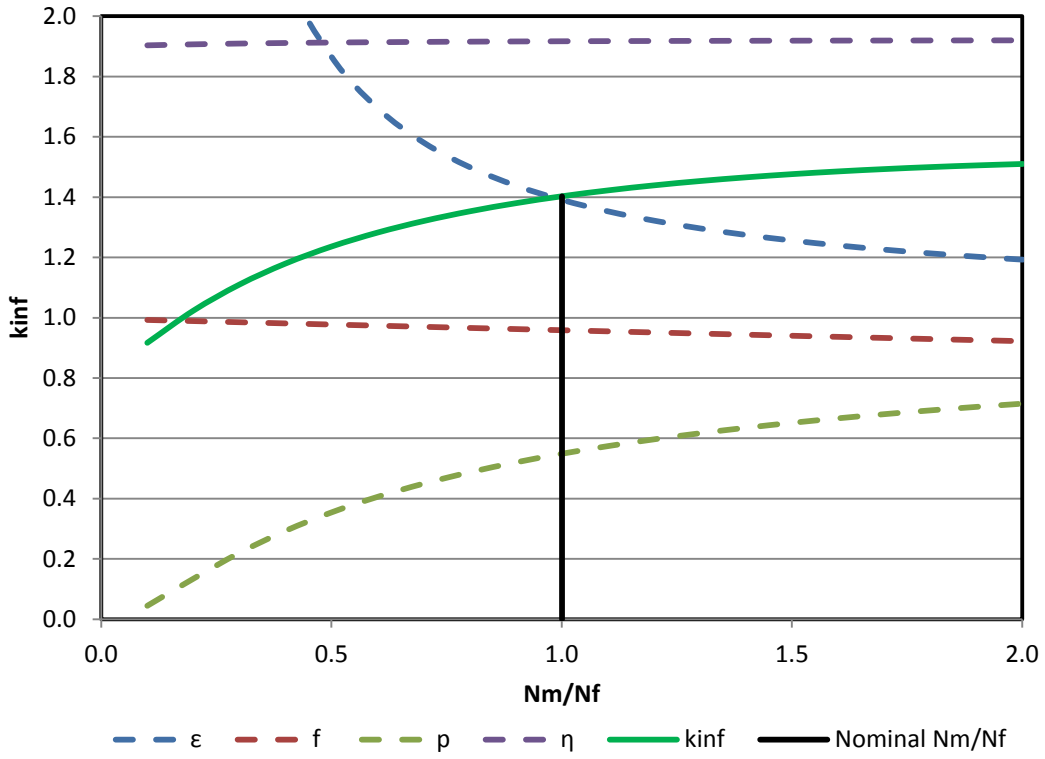

Figure 5.4 Four components of the infinite multiplication factor.

From Figure 5.4, the reproduction factor and thermal utilization factor are relatively constant. The fast fission factor decreases with increasing moderator density because of the increased moderation. Thermal fission becomes more probable as the moderator density increases. The resonance escape probability increases with increasing moderator density. This is due to more neutrons slowing down in the moderator region rather than the fuel region. Neutrons slowing down in the fuel regions are more likely to be absorbed by the ^{238}U resonance capture cross section. Figure 5.5 shows the moderator curves for the different fuel cases performed.

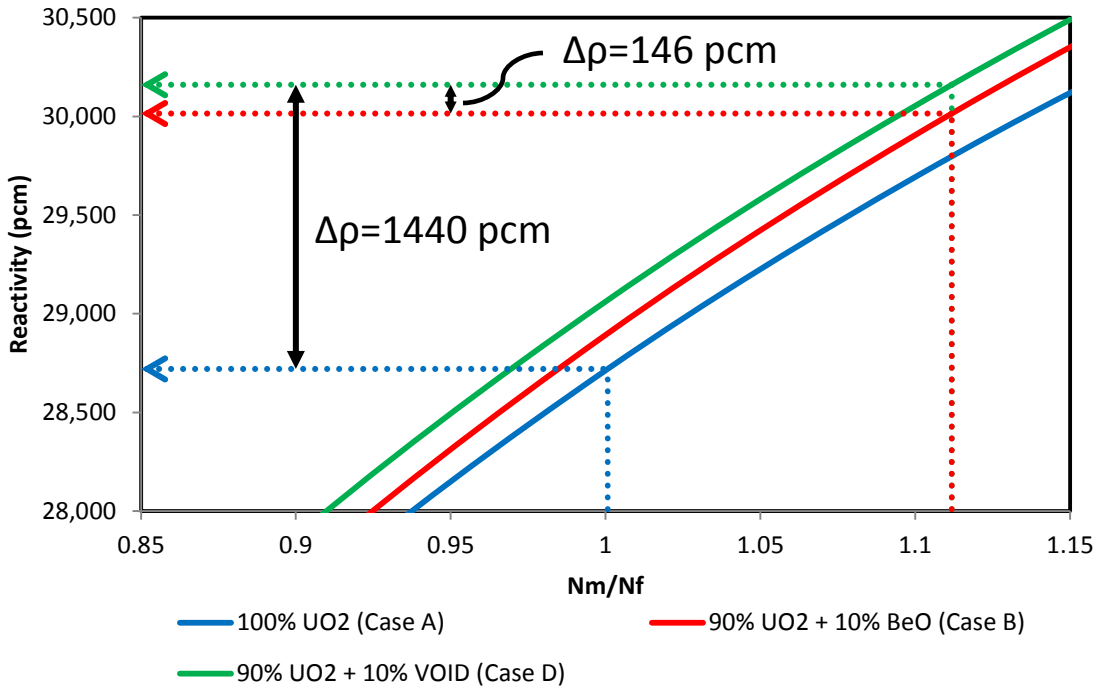

Figure 5.5 Moderator curves for different fuel cases. Case C omitted for clarity. Dashed lines indicate the nominal moderator density.

As shown in Figure 5.5, the moderator-to-fuel ratio for UBO fuel is shifted to the right of UO_2 due to the decreased fuel density. The moderator curve for Case C was nearly indistinguishable from Case D and therefore omitted. Subtracting the reactivity worth of the different cases reveals the effect of individual fuel properties. Overall, the reduced fuel volume is the greatest contribution to the reactivity increase while the BeO introduces a reactivity penalty.

5.1.3.4 Heterogeneous vs Homogeneous

To verify the reactivity effect of the BeO addition, a heterogeneous and homogeneous comparison of the UBO fuel type was performed. The temperature was held constant for both cases. For the homogenous case, the fuel region contained 90% UO_2 and 10% BeO by volume. In the heterogeneous case, the fuel region was modified so that 90 vol% was UO_2 and 10 vol% was void. Then BeO occupied the 10 vol% region surrounding the

fuel. A summary of the atom densities is found in Table 5.5. The lattice cell comparison is illustrated in Figure 5.6.

Table 5.5 Atom densities for homogeneous and heterogeneous fuels.

	Atom Density (mol/b-cm)	
Isotope	**Homogeneous**	**Heterogeneous**
U235	1.176E-03	1.176E-03
U238	1.974E-02	1.974E-02
O16 (UO_2+BeO)	4.907E-02	4.182E-02
Be9 (fuel)	7.249E-03	0.000E+00
Be9 (ring)	0.000E+00	7.249E-02

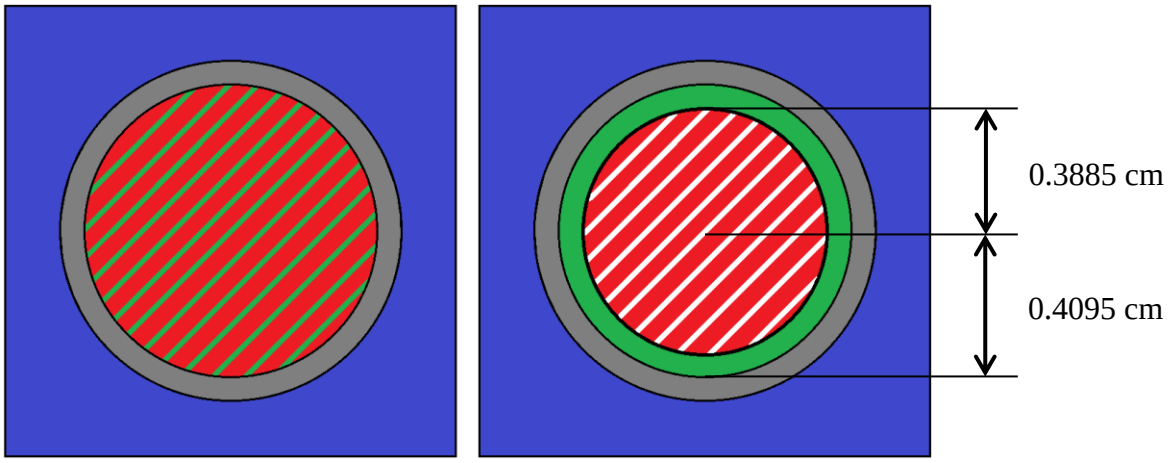

Figure 5.6 Homogeneous (left) and heterogeneous (right) comparison of UBO fuel.

Results from the lattice cell calculations were a k_{inf} of 1.45196 for the heterogeneous case and a k_{inf} of 1.43051 for the homogeneous case. The reactivity was 1033 pcm higher for the heterogeneous case. The result is consistent with the understanding of heterogeneous fuels. Therefore, it was confirmed that adding BeO directly to the fuel causes a slight reactivity penalty.

5.1.4 Spectrum Analysis

Changes in the lattice physics can be observed using a spectrum analysis. A single assembly in an infinite lattice was modeled. The neutron flux spectrum was produced for UO_2 and UBO 10 vol%, as shown in Figure 5.7.

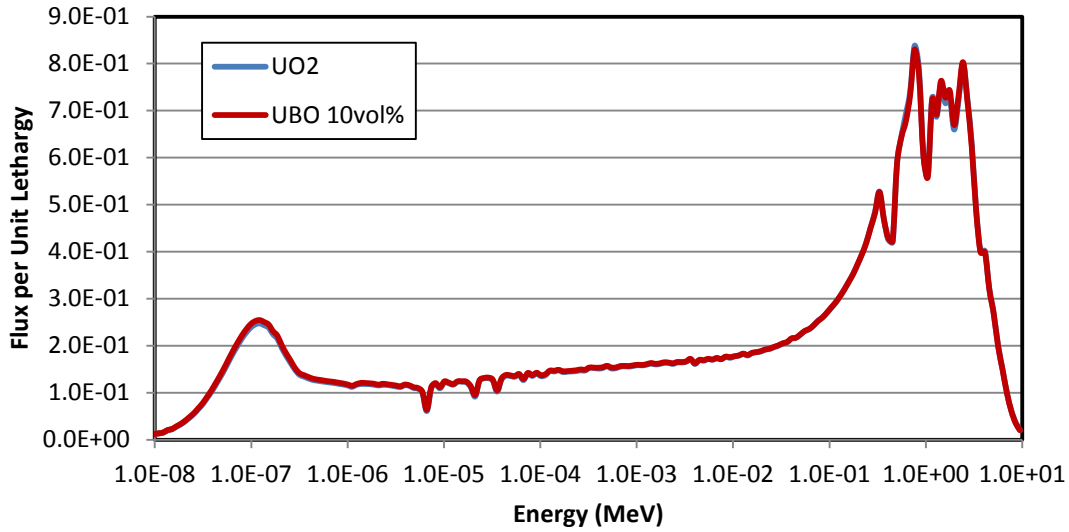

Figure 5.7 Flux spectrum for UO_2 and UBO 10vol% fuel.

The difference between the UO_2 and UBO 10 vol% flux spectrum is difficult to distinguish. A better comparison can be made by subtracting the UO_2 spectrum from the UBO spectrum. The flux difference can be seen in Figure 5.8.

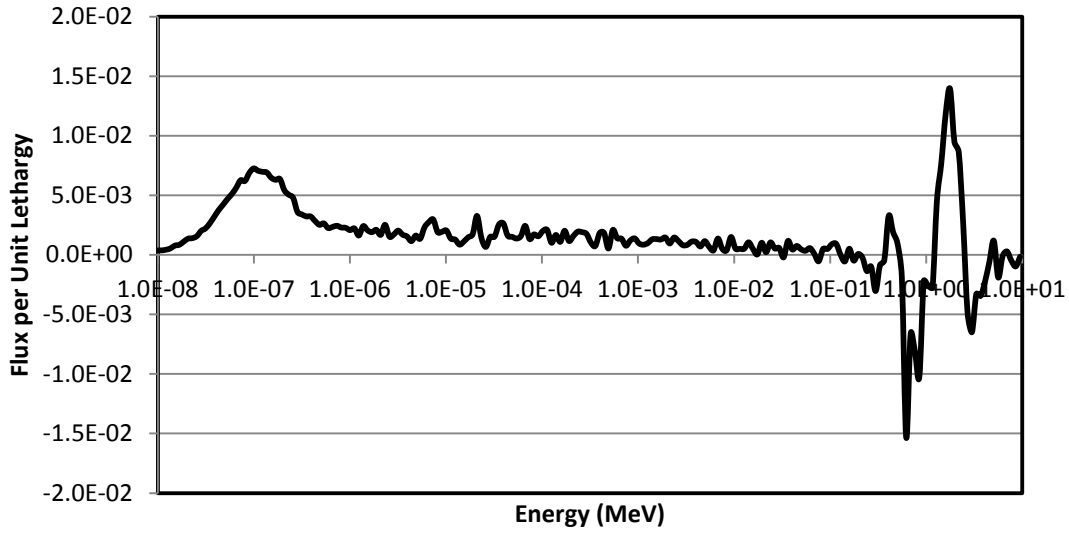

Figure 5.8 Flux spectrum difference between UBO 10vol% and UO_2 fuel.

The difference between the two neutron spectra is small. An increase in the thermal neutron spectrum is observed in Figure 5.8. However this increase cannot be contributed to the BeO addition. From the previous heterogeneous vs. homogeneous results, BeO decreases the thermalization. Therefore the increased thermal spectrum is due to more neutrons passing through the slowing down region because the amount of the resonant absorber ^{238}U is decreased. In addition to a flux spectrum, a fission density spectrum was produced for UO_2 and UBO 10 vol% fuel. Figure 5.9 shows the fission density spectrum.

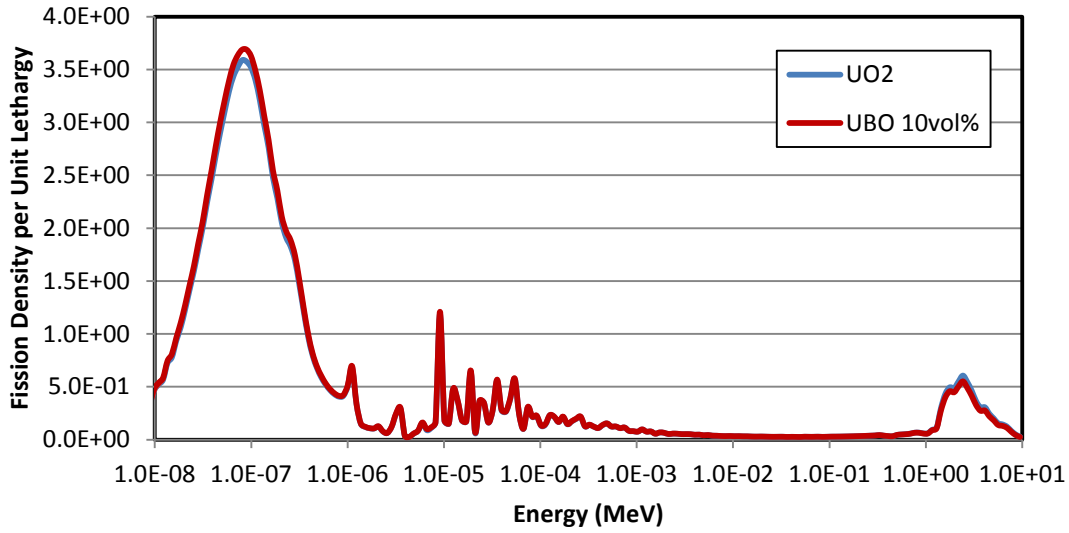

Figure 5.9 Fission density spectrum for UO_2 and UBO 10vol% fuel.

Again the difference between the UO_2 and UBO 10 vol% fission density spectrum is difficult to interpret. The fission density difference spectrum is shown in Figure 5.10.

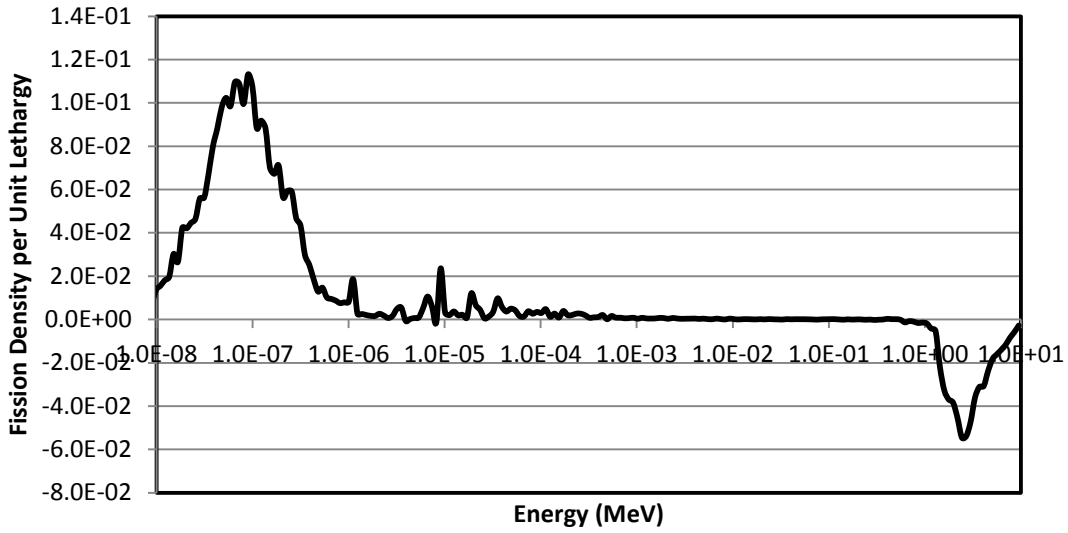

Figure 5.10 Fission density spectrum difference between UBO 10vol% and UO_2 fuel.

Results from Figure 5.10 reveal an increase in the thermal fission density and a decrease in the fast fission density. The decrease in fast fission density is because less ^{238}U is present in the UBO fuel. As before, the increase in thermal fission density is not due to the increased thermalization but rather more neutrons are able to escape the resonance region of ^{238}U.

5.1.5 Linear Reactivity Model

5.1.5.1 Simple Cycle Analysis

Nominal 2D cycle depletions were performed using DRAGON to estimate the cycle length of each fuel type. A simple cycle analysis was performed assuming a single assembly type with no Gadolinium pins. The first cycle depletions were performed without using mass equivalence. BeO was added in 5 vol% and 10 vol% amounts with a fixed enrichment of 5 wt%. Figure 5.11 shows the nominal cycle depletion results for three fuel types examined. The 1.035 k_{inf} reference was used to approximate a 3.5% core leakage.

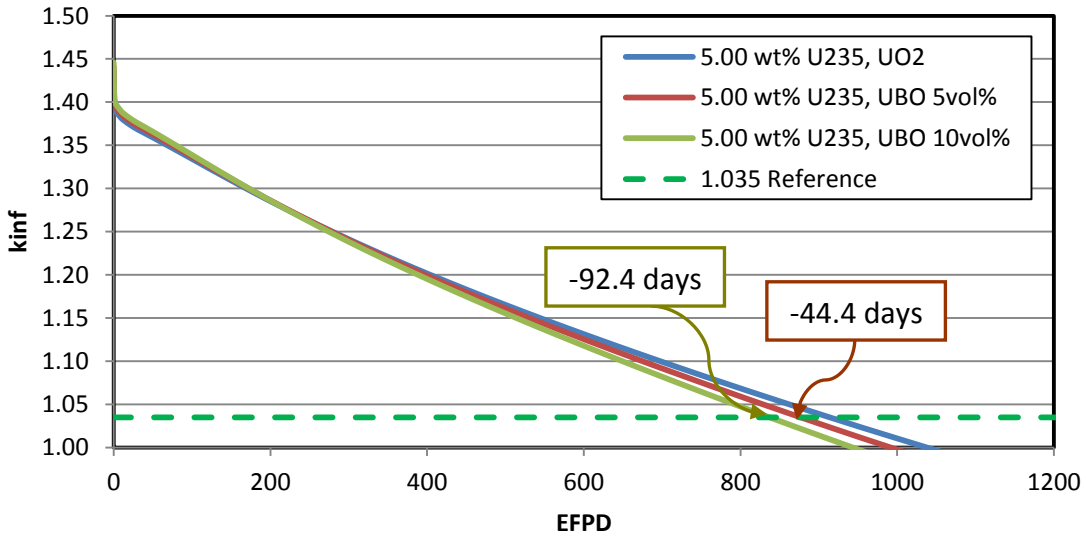

Figure 5.11 Core average cycle length analysis without mass equivalence. The assembly design was Gadolinium-free.

As shown in Figure 5.11, the UBO fuels are not able to meet the core average cycle length of the nominal UO_2 fuel. Without mass equivalence, the ^{235}U displaced by the BeO addition causes a shorter core average cycle of 44.4 and 92.4 days for the UBO 5vol% and UBO 10vol%, respectively. The core average cycle length analysis with mass equivalent UBO fuels is shown in Figure 5.12.

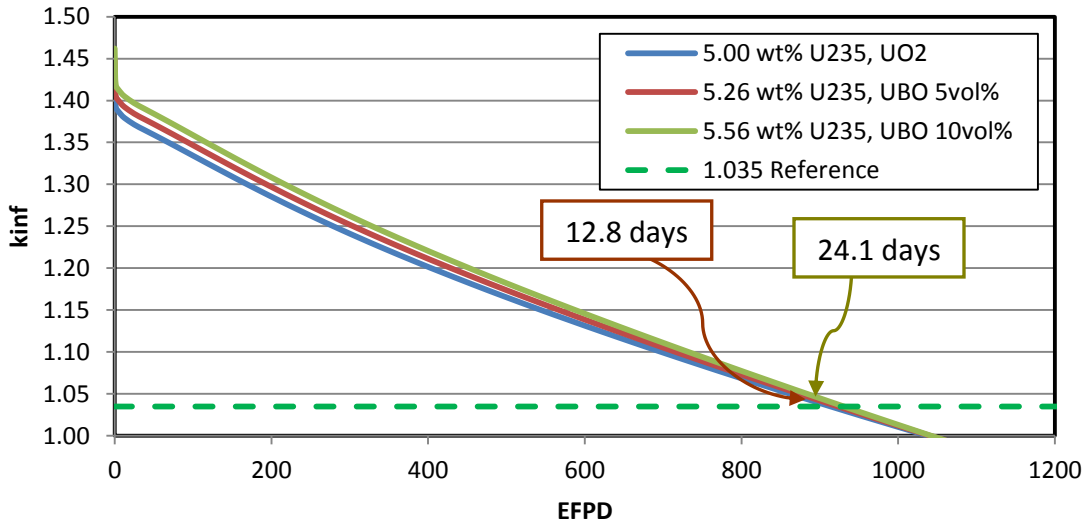

Figure 5.12 Core average cycle length analysis with mass equivalence. The assembly design was Gadolinium-free.

With a mass equivalent UBO fuel, the core average cycle length is increased. Figure 5.12 shows an increase of 12.8 and 24.1 days for the UBO 5vol% and UBO 10vol%, respectively. Since the ^{235}U mass is constant, the increased core average cycle length can be attributed to the positive benefits of UBO fuel. The overall reduced uranium mass of UBO fuels causes an increased power per kilogram of uranium. Due to the increased power density, the core average burnup is greater for the UBO fuels. Figure 5.13 illustrates the core average burnup for all three fuel types with a mass equivalent basis.

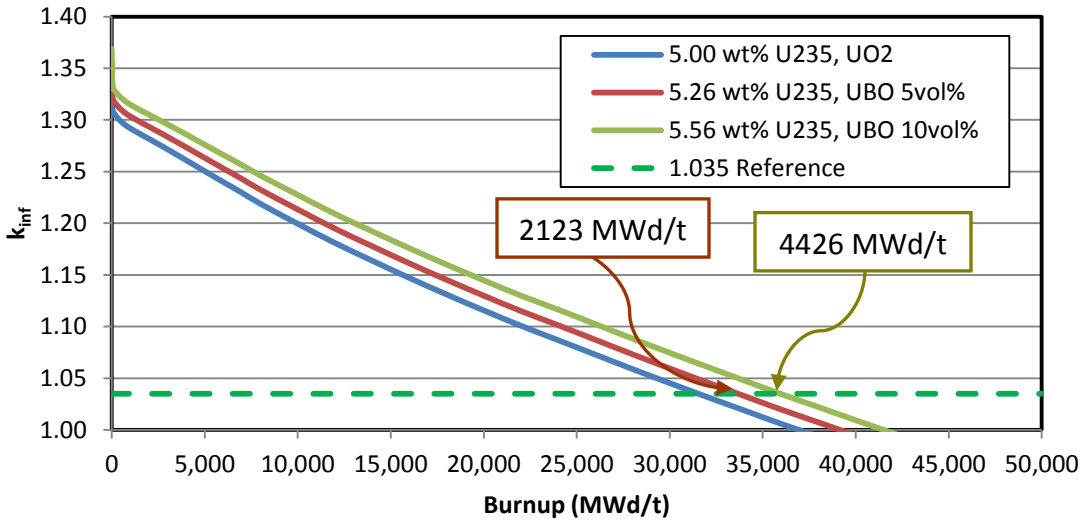

Figure 5.13 Core average burnup with mass equivalence. The assembly design was Gadolinium-free.

Core average burnup for the UBO 5 vol% and 10 vol% fuels was increased by 2123 and 4426 MWd/t, respectively, as shown in Figure 5.13. A summary of the core average parameters for each fuel type is found in Table 5.6. In addition, three different methods were used to obtain the core average results.

Table 5.6 Core average parameters using mass equivalence

Method	Parameter	UO_2	UBO 5vol%	UBO 10vol%
Leakage (k_{inf}=1.035 Reference)	BU_{avg} (MWd/t)	31,536	33,659	35,962
	Core average cycle (EFPD)	914.8	927.6	938.9
	Δ Core average cycle (EFPD)	-	12.8	24.1
No Leakage $\left(\frac{\rho_0}{A}\right)$	BU_{avg} (MWd/t)	36,702	39,067	41,647
	Core average cycle (EFPD)	1064.7	1076.7	1087.3
	Δ Core average cycle (EFPD)	-	12.0	22.6
Leakage $\left(\frac{\rho_0 - \rho_L}{A}\right)$	BU_{avg} (MWd/t)	31,337	33,524	35,903
	Core average cycle (EFPD)	909.0	923.9	937.4
	Δ Core average cycle (EFPD)	-	14.9	28.3

As shown in Table 5.6, leakage has a significant effect on the core average cycle length. A reduction of approximately 150 days occurs as a result of the leakage. The 1.035 k_{inf} leakage method and the $\left(\frac{\rho_0-\rho_L}{A}\right)$ leakage method provide similar results. A leakage reactivity of 0.03382 was assumed, equivalent to k_{inf}=1.035. The slight differences are due to the linear interpolation of either k_{inf} vs. burnup or reactivity vs. burnup. The reactivity curve tends to be more linear than the k_{inf} curve and therefore is the preferred method for analysis.

However, it can be deceptive to compare the cycle length increase using Figure 5.12 alone. The $\left(\frac{2}{n+1}\right)$ multiplier is required from Eq. (2-4) of the LRM. Omitting the LRM multiplier causes an overestimation of the cycle length. For simplicity, only the no leakage method was considered for cycle length comparisons. A summary of the cycle length results for the simple LRM model is shown in Table 5.7. The simple LRM model considers only the Gadolinium-free assembly design.

Table 5.7 Simple LRM cycle length analysis with no leakage

Cycle Type	Multiplier	Parameter	UO_2	UBO 5vol%	UBO 10vol%
4 batch (18-month)	$\left(\frac{2}{4+1}\right)$	BUc (MWd/t)	36,702	39,067	41,647
		Cycle (EFPD)	425.9	430.7	434.9
		Δ Cycle (EFPD)	-	4.8	9.1
3 batch (22-month)	$\left(\frac{2}{3+1}\right)$	BUc (MWd/t)	36,702	39,067	41,647
		Cycle (EFPD)	532.3	538.3	543.7
		Δ Cycle (EFPD)	-	6.0	11.3

Using the UBO 10vol% fuel as an example, an equal four batch reload core (18-months) would have a cycle increase of 9.1 days compared to UO_2 fuel. An equal three batch reload core (22-months) would have a cycle increase of 11.3 days. Therefore it is important to distinguish the difference between the core average cycle length and the cycle length. Further improvements in cycle length estimation can be performed using unequal batch sizes and assembly weighting.

5.1.5.2 Unequal Batch Size and Assembly Weighting

An accurate estimation of the cycle length can be calculated by considering unequal batch sizes and assembly weighting. This is accomplished using Eq. (2-5) and Eq. (2-7), respectively. The $\left(\frac{\rho_0}{A}\right)$ parameter is required for each assembly type and fuel type. A summary of these parameters is shown in Table 5.8. The previous Figure 2.5 illustrates how to obtain ρ_0 and A from the nominal depletion curve.

Table 5.8 Assembly parameters for the LRM

	(ρ_0/A)		
Assembly Type	**UO_2**	**UBO 5vol%**	**UBO 10vol%**
Gd-0	36,702	39,067	41,647
Gd-8	35,962	37,953	40,112
Gd-12	35,608	37,559	39,668
Gd-16	35,251	35,251	39,223
Gd-20	34,887	36,760	38,771
Gd-24	34,521	36,354	38,319

Unequal batch sizes were considered for the 18- and 22-month cycles. A summary of the in-core assembly types and batch size for the 18- and 22-month cycles are found in Table 6.2 and Table 6.7 of Section 6, respectively. The 18-month cycle contains Gd-8, Gd-12, and Gd-16 assembly types. The 22-month cycle contains Gd-16, Gd-20, and Gd-24 assembly types. Table 5.9 summarizes the LRM weighted parameters that account for the unequal batch size and assembly types.

Table 5.9 Weighted LRM parameters

Cycle Type	**Weighted Parameter**	**UO_2**	**UBO 5vol%**	**UBO 10vol%**
4 batches (18-months)	(ρ_0/A) (MWd/t)	35,625	37,578	39,690
	Power Density (MW/t)	34.647	36.394	38.325
3 batches (22-months)	(ρ_0/A) (MWd/t)	34,861	36,731	38,739
	Power Density (MW/t)	34.773	36.472	38.342

Using the weighted parameters in Table 5.9, an accurate cycle burnup is calculated using Eq. (2-5) and Eq. (2-7). After the cycle burnup is calculated, the cycle length is calculated by dividing the cycle burnup by the appropriate power density. The power density is weighted by the respective assembly types, as given previously in Eq. (2-8). Results of the cycle burnup and cycle lengths for the 18- and 22-month cycle cores are summarized in Table 5.10.

Table 5.10 Unequal batch size and assembly weighting results

Cycle Type	Multiplier	Parameter	UO_2	UBO 5vol%	UBO 10vol%
4 batches (18-months)	$\frac{\left(\frac{2}{4+1}\right)\left(\frac{\rho_0}{A}\right)}{1-\left(\frac{4-1}{4+1}\right)\left(\frac{4*72}{241}-1\right)}$	BUc (MWd/t)	16,138	17,023	17,980
		Cycle (EFPD)	465.8	467.7	469.1
		Δ Cycle (EFPD)	-	1.9	3.3
3 batches (22-months)	$\frac{\left(\frac{2}{3+1}\right)\left(\frac{\rho_0}{A}\right)}{1-\left(\frac{3-1}{3+1}\right)\left(\frac{3*100}{241}-1\right)}$	BUc (MWd/t)	19,862	20,927	22,071
		Cycle (EFPD)	571.2	573.8	575.6
		Δ Cycle (EFPD)	-	2.6	4.5

Table 5.10 results express the importance of unequal batch size and assembly weighting. A simple core average length comparison, as performed in Figure 5.12, would produce incorrect results. Using the UBO 10vol%, 22-month cycle as an example, a comparison of the core average cycle lengths would indicate a cycle increase of 24.1 days. Application of the LRM unequal batch size and assembly weighting multipliers indicates a cycle increase of 4.5 days.

The 2D LRM cycle length increase fuel comparisons are in good agreement with the 3D simulations performed in Section 6. However, the overall cycle length and burnup for the 2D LRM are shorter than the 3D simulation results. This discrepancy was due to different nominal depletions used for the 2D and 3D analyses. Originally, the 2D analysis was performed with slightly different dimensions and uranium loading. Later these parameters were changed for the 3D analysis but were not retroactively implemented for the 2D analysis.

Unequal power sharing would also improve the comparison of 2D and 3D results. However, unequal power sharing must be applied retroactively to the 2D results once the 3D simulations are completed. Therefore this option was not considered, introducing some discrepancy in the 2D cycle results.

5.1.6 Cycle Comparison Methods

A useful graph can be generated by varying the uranium enrichment. The core average cycle length, determined by the LRM method, is plotted as a function of enrichment. No LRM multiplier is considered for the batch size. Results of the enrichment variation are shown in Figure 5.14 for the UO_2 and UBO fuels.

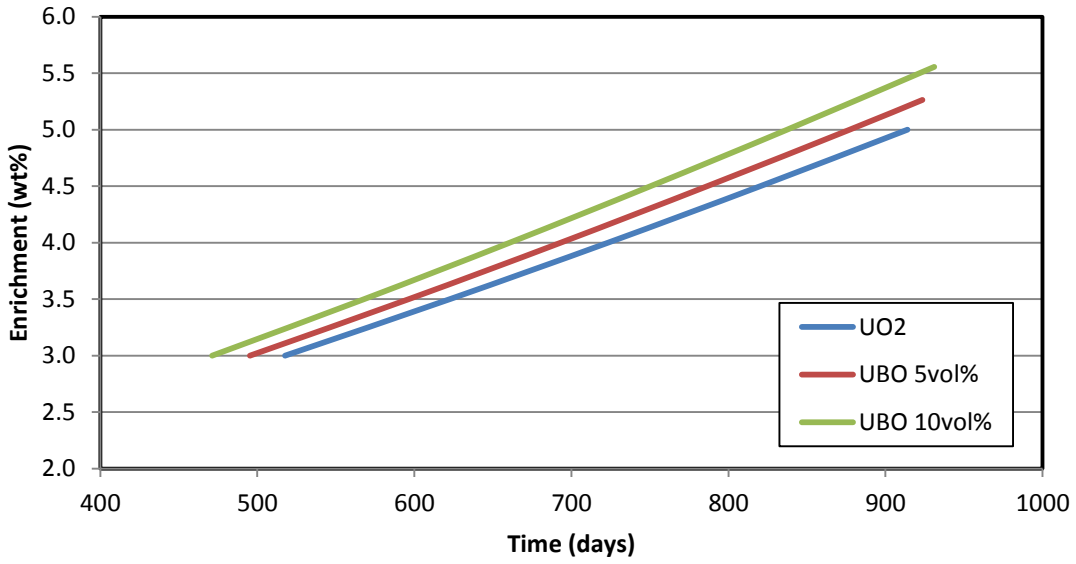

Figure 5.14 Cycle length as a function of U-235 enrichment (no LRM multiplier).

Figure 5.14 illustrates, as expected, that the cycle length for a given fuel type increases with increasing enrichment and that the relationship is nearly linear. Using Figure 5.14, one can then compare the UO_2 and UBO fuels using either a mass equivalence or fixed cycle length comparison. Figure 5.15 shows an example of the mass equivalence approach.

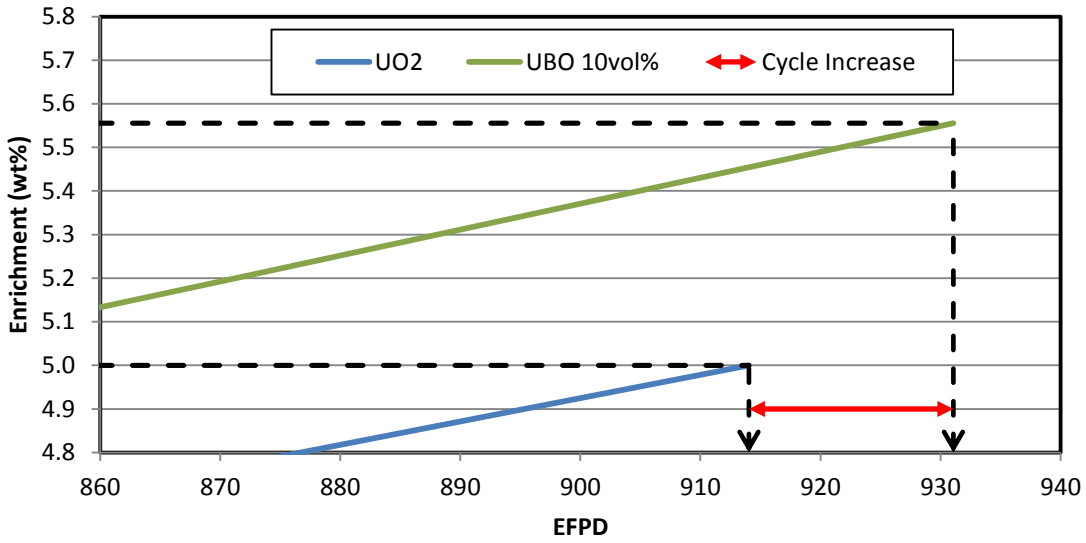

Figure 5.15 Mass equivalence analysis of cycle length for UO_2 and UBO fuel.

Figure 5.15 shows an example of a 5wt% enriched UO_2 fuel and a mass equivalent UBO 10vol% fuel with an enrichment of 5/0.9 = 5.56 wt%. The result is a cycle length increase due to the beneficial properties of the UBO fuel. Alternatively, the fuel comparison can be performed with a fixed cycle length, as shown in Figure 5.16.

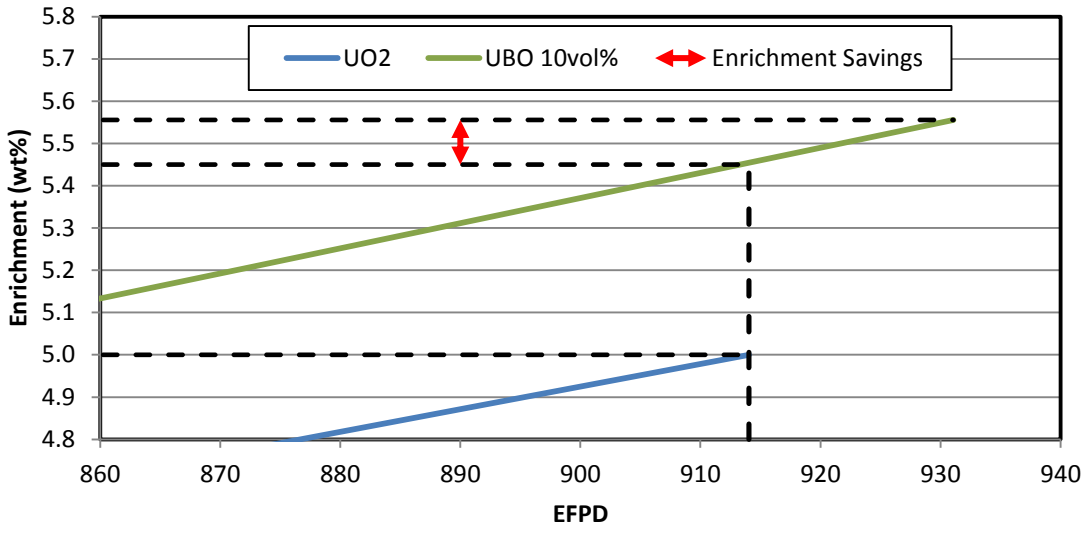

Figure 5.16 Fixed cycle length analysis for UO_2 and UBO fuel.

Using a fixed cycle length, the analysis is then performed assuming the cycle length is 1101 days for both fuel types (no LRM multiplier). According to Figure 5.16, the UO_2 fuel requires an enrichment of 5wt% to meet the fixed cycle length. However, the UBO 10vol% fuel requires less enrichment than the mass equivalent case in order to meet the cycle length. Although the UBO fuel has a higher enrichment than the UO_2 fuel, overall the amount of ^{235}U mass required in the pin is decreased. Any reduction in enrichment below the mass equivalent enrichment of 5.56wt% (for UBO 10vol%) can be viewed as an enrichment savings. The enrichment savings can be attributed to the beneficial properties of UBO fuel.

5.2 APOLLO

APOLLO is another 2D lattice physics code, similar to DRAGON. Both codes solve the neutron transport code using ENDF- or JEF-based cross-section libraries. APOLLO also has similar capabilities as DRAGON and can produce many of the same lattice physics results. APOLLO was used here to perform branching cases and generate the two energy group, multi-parameterized cross-sections. Two-group cross section generation and

management of the cross-section data for input into a 3D code is easier to perform using APOLLO.

5.2.1 Assembly Types

Nominal depletion and branching cases were performed for each of the different assemblies present in the core. Six different assembly designs were chosen for each fuel type. The assembly designs contained between 0 and 24 Gadolinium rods. Three different fuel types were analyzed: UO_2, UBO 5vol%, and UBO 10vol% for a total of 18 depletion cases.

The fuel enrichment for each assembly design was fixed at 5 wt%. However, rods that contained Gadolinium had a reduced ^{235}U enrichment of 3 wt%. All Gadolinium rods were 8 wt% Gd_2O_3 and 92 wt% fuel. In addition, no BeO was added to rods containing Gadolinium. Since the analysis was performed using mass equivalent ^{235}U, the enrichment for UBO fuels was increased accordingly. A summary of the fuel enrichment for each assembly design is shown in Table 5.11

Table 5.11 Description of assembly types for APOLLO calculations

		Fuel Rod Enrichment in ^{235}U			Gd Rod Enrichment
Assembly Design	**Number Gd Rods**	**UO_2**	**UBO 5vol%**	**UBO 10vol%**	**All Fuel Types**
1	0	5.00	5.26	5.56	3.00
2	8	5.00	5.26	5.56	3.00
3	12	5.00	5.26	5.56	3.00
4	16	5.00	5.26	5.56	3.00
5	20	5.00	5.26	5.56	3.00
6	24	5.00	5.26	5.56	3.00

The component masses of an assembly can be calculated from the geometry and densities. Approximately 26 kg of ^{235}U is present in assemblies of all fuel types. To accommodate the BeO addition, the amount of ^{238}U is reduced. The exact component masses slightly depend on the number of Gadolinium rods. A summary of the

component masses for a non-gadolinium assembly and a 24 Gadolinium rod assembly are found in Table 5.12 and Table 5.13.

Table 5.12 Component masses of a non-gadolinium assembly

Component (kg)	UO_2	UBO 5vol%	UBO 10vol%
Enriched Uranium	538.1	511.2	484.3
U-235	26.91	26.91	26.91
U-238	511.2	484.3	457.4
BeO	0.00	8.82	17.65
Gd_2O_3	0.00	0.00	0.00
Total Weight	538.1	520.1	502.0

Table 5.13 Component masses of a 24 Gadolinium assembly

Component (kg)	UO_2	UBO 5vol%	UBO 10vol%
Enriched Uranium	532.8	508.3	483.9
U-235	25.77	25.77	25.77
U-238	507.0	482.6	458.1
BeO	0.00	8.03	16.05
Gd_2O_3	4.28	4.28	4.28
Total Weight	537.1	520.6	504.2

Location of the gadolinium rods are from the reference EPR design [9]. Placement of the gadolinium rods are designed to reduce the local pin power peaking. A map of the gadolinium rod locations for all six assembly types are shown in Figure 5.17.

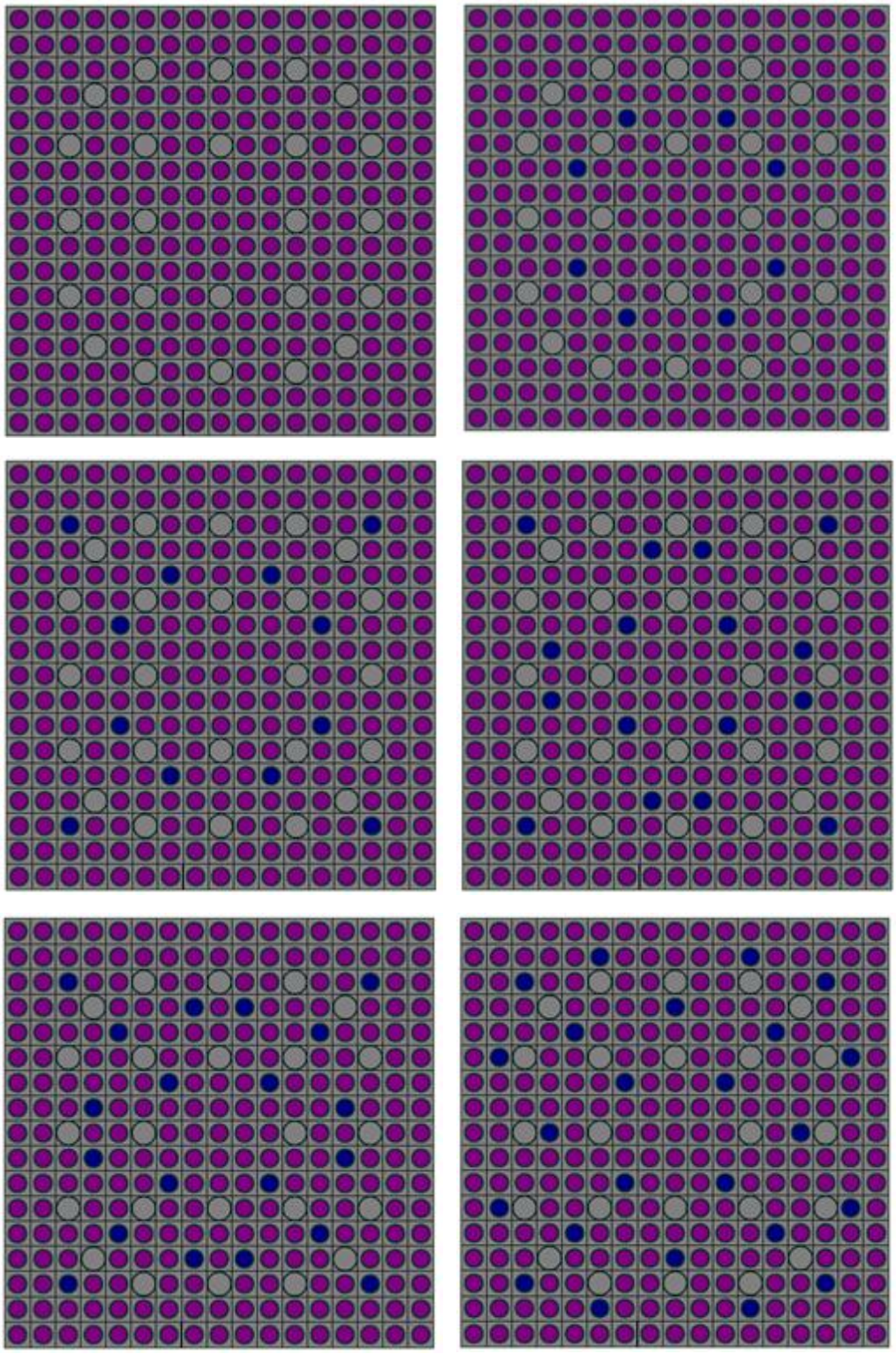

Figure 5.17 Location of the Gadolinium rods for the six different assembly designs.

6 3D CORE SIMULATION

3D core simulations were performed for both an 18- and 22-month equilibrium cycle. The cycles were chosen based on the published UK-EPR cycle design data. Use of the EPR data provided a reference to verify UO_2 cycle results were correctly reproduced using APOLLO and CRONOS. However, there were problems with the initial shuffle map provided. Incorrect assembly shuffle caused some assemblies to have a burnup much greater than the core average burnup. In addition, a lack of assembly rotation data resulted in assembly quadrant burnup much higher than NRC limitations. Therefore an initial cycle optimization was required before comparing the UO_2 and UBO fuels.

Performing an initial cycle optimization is a complex task. The number of variations that can be performed results in an enormous number of combinations. 241 assembly locations each with four different rotation possibilities (0°, 90°, 180°, 270°) is difficult to optimize. Optimizing cycle parameters using a computer algorithm is also complex and was not available for this work. Instead, engineering judgment, heuristic strategies, and recognizing cycle patterns were employed to perform a "best-estimate" cycle optimization. After the initial cycle optimization was completed, the UO_2 and UBO fuel cycles were compared.

Cycle optimization and fuel comparisons are described in full detail for only the 18-month cycle. A subsequent analysis of the 22-month cycle details becomes repetitive and therefore some results were moved to an appendix. The important 22-month cycle results, such as a brief cycle optimization and a cycle length comparison of UO_2 and UBO fuel, were retained. Other cycle results, such as reactivity coefficients, are similar for both the 18- and 22-month cycles and are not repeated.

The fuel comparisons were performed using the reference UO_2 fuel and a 5 vol% and 10 vol% UBO fuel. In general, only the 10 vol% UBO fuel comparisons are shown to reduce repetition of the similar 5 vol% UBO results. However, the 10 vol% UBO fuel is an upper bounding case for BeO addition. Beyond a 10 vol% BeO addition is a significant fuel change and results in an unrealistic enrichment increase. Also the comparison of 10 vol% UBO was chosen because any cycle variations are more apparent and can be readily attributed to the BeO addition. A more realistic UBO fuel may contain 5 vol% or less addition of BeO.

6.1 Detailed 18-Month Equilibrium Cycle

6.1.1 Initial Cycle Optimization

6.1.1.1 Burnup Analysis

An initial cycle was performed using the specifications of the EPR reference. Since an assembly rotation map was not provided, no initial rotation was assumed. The assembly burnup was analyzed for all four quadrants of an assembly. A partial burnup map is shown in Figure 6.1 to illustrate the burnup analysis. The initial optimization was performed on UO_2 fuel only. The UBO fuel then used the subsequent UO_2 optimized cycle shuffle map and assembly rotation.

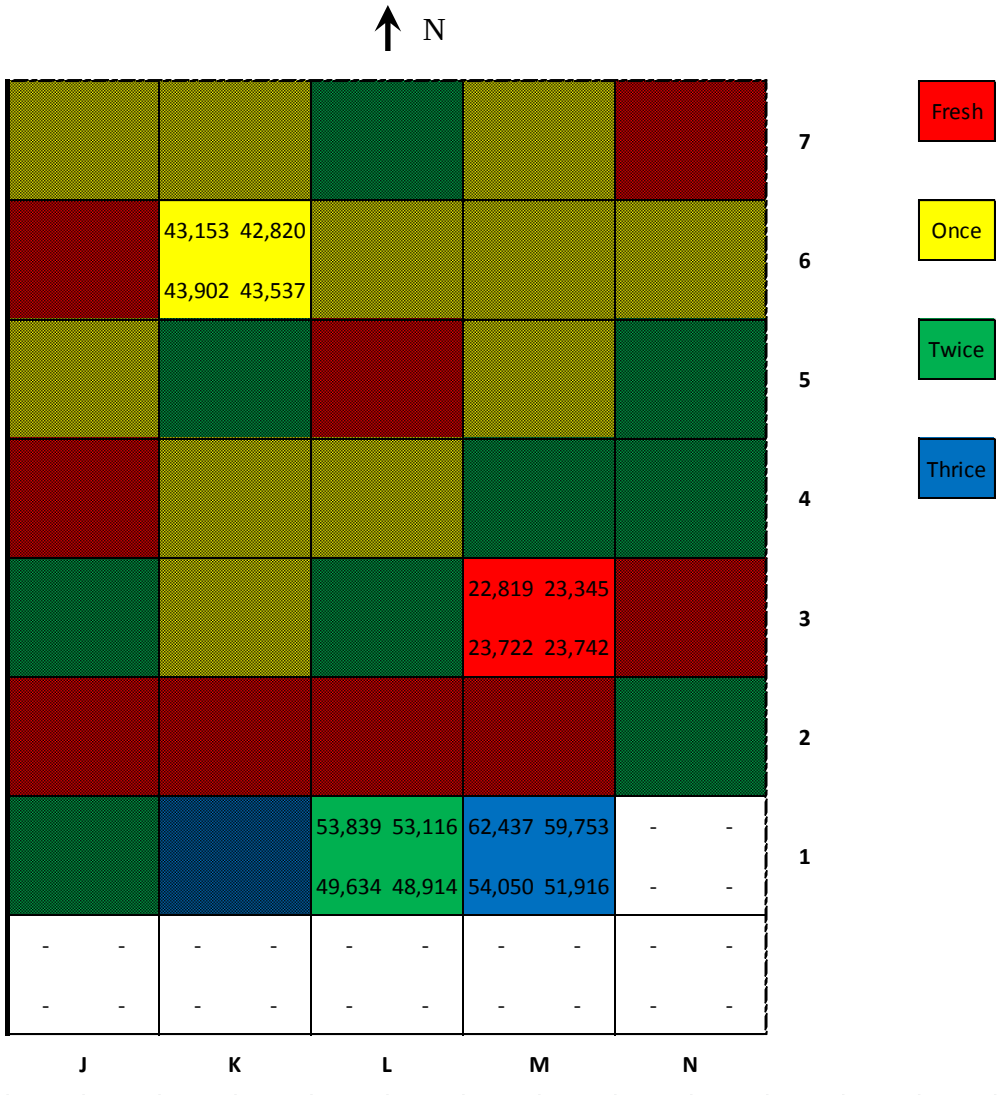

Figure 6.1 Partial burnup map of a selected assembly shuffle (M3-K6-L1-M1). Values indicate the burnup (MWd/t) in all four quadrants of an assembly location.

To analyze the assembly burnup following an equilibrium cycle, an incremental method was used. An incremental burnup method can indicate peaking in the four quadrants of an assembly and show the peaking during different burnup stages (fresh, once, twice, thrice burnt). Table 6.1 shows an example incremental assembly burnup during shuffling.

Table 6.1 Incremental burnup analysis of single assembly during shuffle

	Incremental Burnup (MWd/t)					
Quadrant	**Fresh (M3)**	**Once (K6)**	**Twice (L1)**	**Thrice (M1)**	**Total**	**Quadrant Peaking**
SE	23,742	19,795	5,377	3,002	51,916	91%
NE	23,345	19,474	10,296	6,637	59,753	105%
NW	22,819	20,334	10,686	8,598	62,437	109%
SW	23,722	20,180	5,732	4,415	54,050	95%

As shown in Table 6.1, the burnup during the fresh and once burnt stage is relatively even. However during the twice and thrice burnt stages, the quadrant assembly burnup becomes uneven. At the end of assembly lifetime, the difference between the SE and NW quadrant is 18%. An illustration of the quadrant assembly burnup is shown in Figure 6.2.

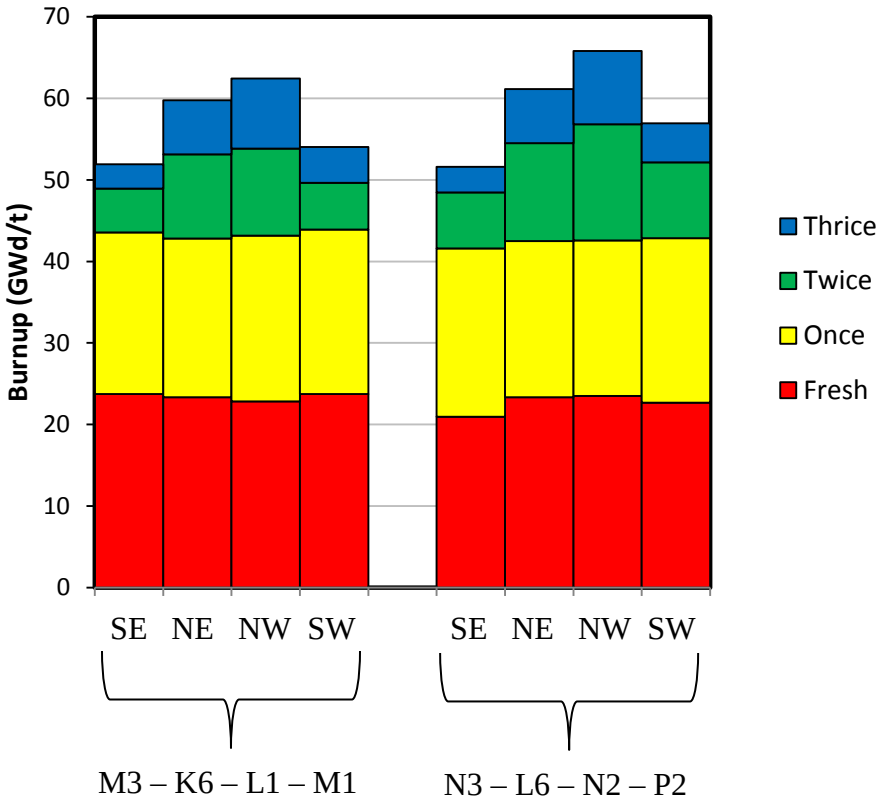

Figure 6.2 Incremental burnup in all four quadrants of an assembly for selected assemblies.

Figure 6.2 is a convenient way to analyze the quadrant assembly burnup. During the twice and thrice burnt stage, the northern side of the assembly is over-burned compared to the southern side. Reviewing Figure 6.1, one can see that the northern side of the assembly in coordinates L1 and M1 are always facing a fresh assembly while the southern side faces low burned, core periphery assemblies. An incremental analysis for all 241 core assemblies, including the quadrant burnup, is shown in Figure 6.3.

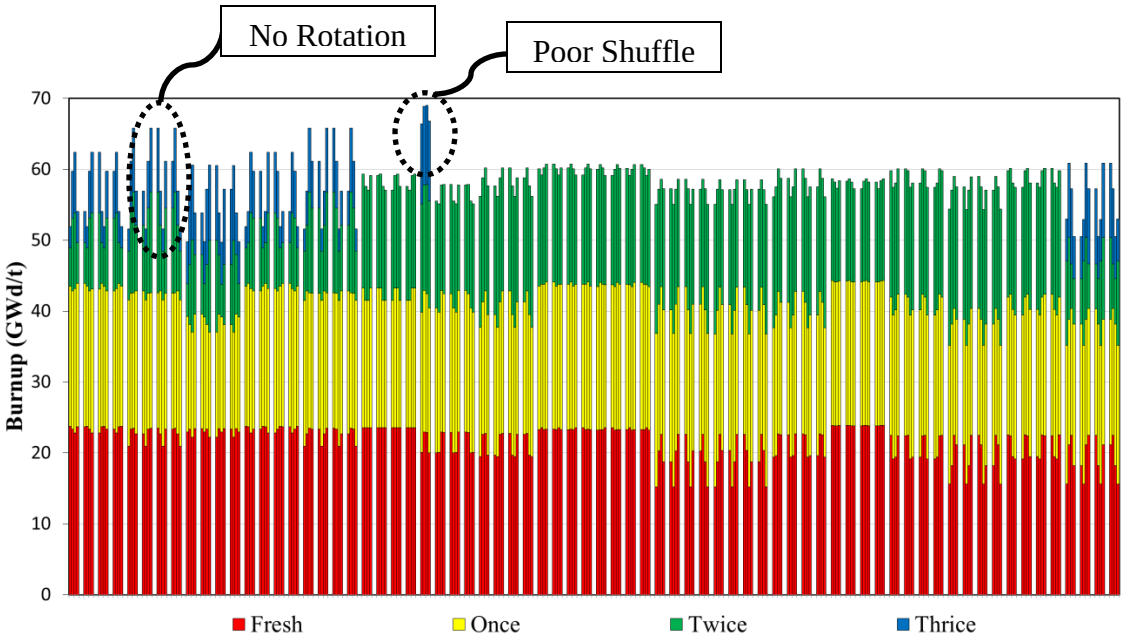

Figure 6.3 Initial incremental burnup analysis for all 241 assemblies, including the four assembly quadrants. The original EPR 18-month shuffle map with no assembly rotation was used for the UO_2 fuel.

As shown in Figure 6.3, all of the 72 reload assemblies are separated into individual groups. In addition, each assembly is further separated to show the four assembly quadrants (NE, NW, SE, SW). Groups of four assemblies with similar burnup appear in Figure 6.3 because these assemblies have quarter-core symmetry. The peak "noise" is due to the uneven burnup of the four quadrants as a result of no assembly rotation. Figure 6.3 is convenient for a burnup analysis because burnup peaking is easily identified and can be corrected with a proper shuffle map and assembly rotation.

6.1.1.2 New Shuffle Map

Figure 6.3 is the most valuable illustration used to analyze the assembly burnup. The incremental burnup for all assemblies, including the four assembly quadrants, can be viewed on a single graph. This can reveal uneven quadrant burnup compared to the assembly average as well as uneven assembly burnup compared to the core average burnup. Usually the quadrant peaking is due to improper assembly rotation. The assembly peaking is due to an inadequate shuffle map.

As shown in Figure 6.3, the highest 2D assembly burnup is 67,863 MWd/t and occurs in the center assembly coordinates J9. The 3D assembly burnup in J9 is 73,971 MWd/t, which is well above the NRC limit of 62.5 MWd/t. The maximum 3D peaking does not always correspond to the maximum 2D peaking. Therefore the 3D peaking must be verified following a 2D analysis.

To reduce the maximum 3D burnup, a new shuffle map was created. Five assemblies were identified that were above or below the average assembly burnup. Four low burnt assemblies would be used to compensate for the single, highly burnt assembly in the center coordinate J9. The method for choosing a new shuffle map is illustrated in Figure 6.4.

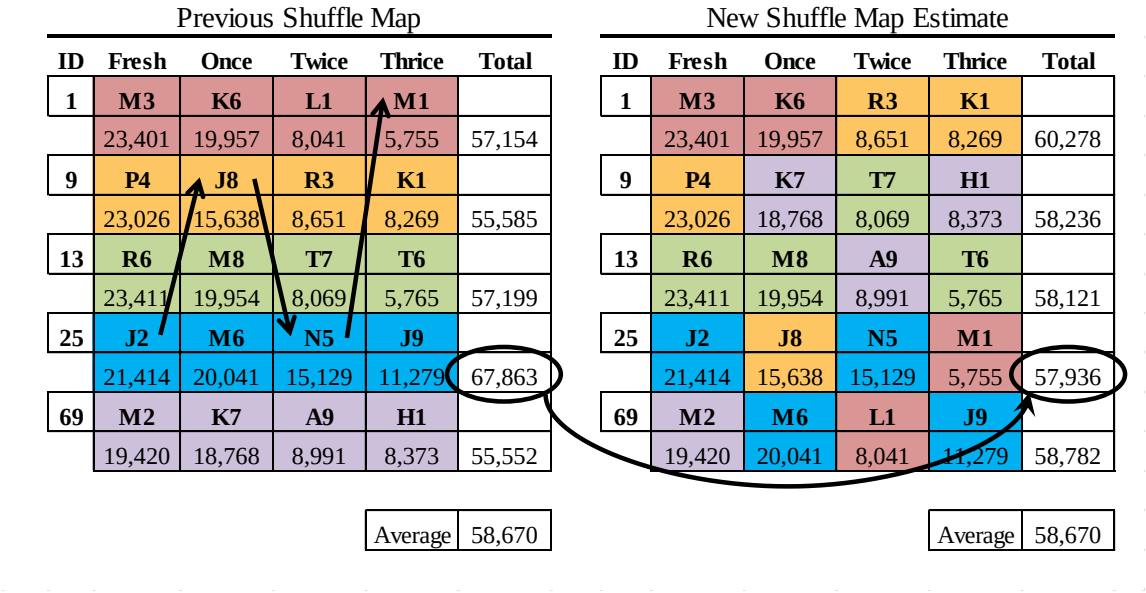

Figure 6.4 Illustration of the method used to estimate the new shuffle map. Assembly ID numbers are assigned to the 72 reload assemblies for convenience. Values indicate the incremental assembly burnup in MWd/t.

Figure 6.4 illustrates that the total assembly burnup for assembly ID 25 is well above the average burnup. Therefore a new shuffle path was chosen that would reduce the final EOL assembly burnup. The new path for assembly ID 25 would bypass the high incremental burnup incurred in locations M6 and J9. A lower burnt assembly would occupy the M6 and J9 coordinates instead.

After moving the assemblies to new coordinates, the burnup for the five assemblies are more even with respect to the average burnup. The final 2D burnup for assembly ID 25 is reduced from 67,863 to 57,936 MWd/t. However, this incremental burnup method is only an estimate. Another equilibrium cycle was performed with the new shuffle map to verify the 2D and 3D burnup. Multiple iterations were required to achieve the final optimized assembly burnup. Figure 6.5 shows the final shuffle map for the 18-month equilibrium cycle.

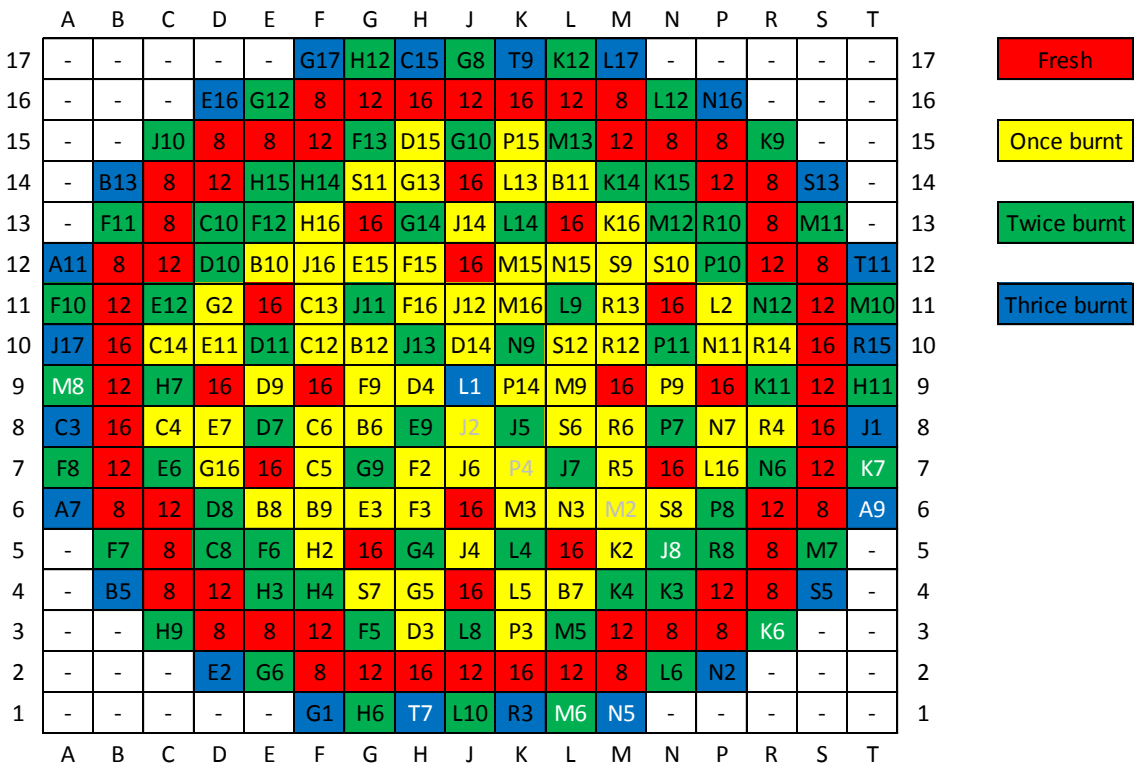

Figure 6.5 Final shuffle map chosen for the 18-month equilibrium cycle. White/grey highlighted locations represent a change from the original shuffle map.

The number of reload assemblies and assembly types remained unchanged from the initial EPR shuffle map. Only the assembly location during the once, twice, or thrice burnt stage was modified. The number of reload and in-core assemblies is summarized in Table 6.2.

Table 6.2 Number of assemblies in an 18-month equilibrium cycle

	Number of Assemblies	
Assembly Type	**Reload**	**In-core**
Gd-8	24	84
Gd-12	24	85
Gd-16	24	72
Total	72	241

To calculate the core average power density, the individual assembly power density was weighted by the number of in-core assemblies. The individual assembly power densities were calculated previously in APOLLO and can be found in Table 3.2. A summary of the core average power density for each fuel type is given in Table 6.3.

Table 6.3 Power densities for the 18-month equilibrium cycle

Fuel Type	**Core Avg Power Density (kW/kgU)**
UO_2	34.647
UBO 5vol%	36.394
UBO 10vol%	38.325

6.1.1.3 Assembly Rotation

In addition to correcting the shuffle map, an assembly rotation map was also required. Originally no assembly rotation was used so the assemblies always faced core-north during shuffling. An example shuffle (P4-J8-R3-K1) without rotation is shown in Figure 6.6.

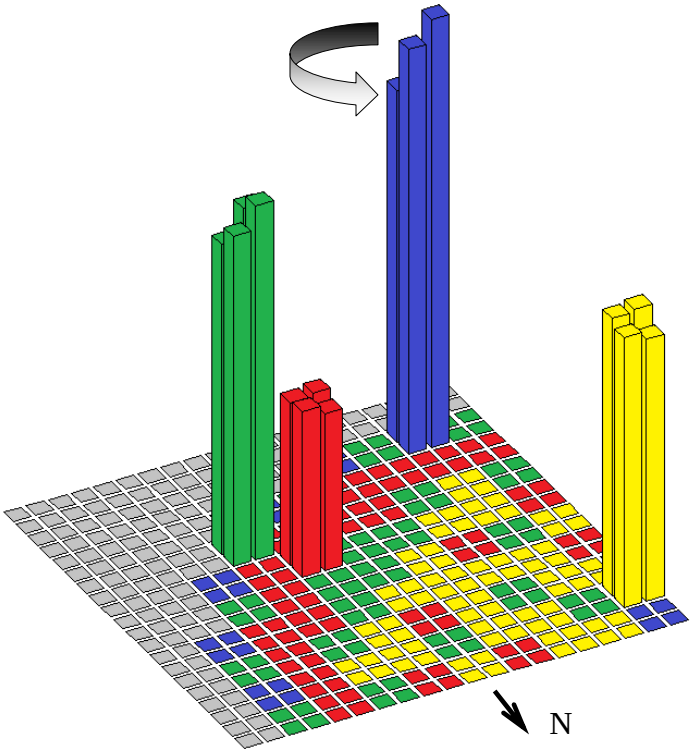

Figure 6.6 Illustration of assembly rotation necessary to reduce maximum peaking. NW assembly quadrant is adjacent to fresh assemblies during the second and third burnup stage that results in a high burnup.

As shown in Figure 6.6, the quadrant assembly burnup is relatively even during the fresh and first burnt stages but becomes uneven during the twice and thrice burnt stages. Initially an algorithm was implemented that rotated the assemblies based on their geometric location. The goal was to rotate a low burnt assembly quadrant toward the higher core flux gradient in the next shuffle location. However, using the core flux gradient alone was not sufficient to provide a good assembly rotation. The EOC burnup was marginally improved but the maximum 3D burnup peaking was greater than with no rotation.

Instead a good rotation is dependent on the quadrant location relative to neighboring assembly types (i.e. fresh or thrice burnt) and the cumulative quadrant burnup acquired during shuffling. Using Figure 6.6 as an example, a more even quadrant burnup would

occur if the assembly was not rotated during the first and second burnt stages, but rotated 180° during the last thrice burnt stage. The cumulative burnup in the SE quadrant during the twice burnt stage is relatively low due to facing a reflector assembly. By rotating the SE quadrant 180° during the thrice burnt stage, the SE quadrant will now face a fresh assembly rather than another reflector assembly. The resulting quadrant burnup will be higher due to facing a high-power, fresh assembly. Similarly, the NW quadrant during the twice burnt stage is relatively high compared to the average. The rotation will cause the NW quadrant to face a reflector assembly rather than a fresh assembly, resulting in a lower quadrant burnup.

An algorithm to perform assembly rotation based on quadrant location and burnup history was not implemented. Developing the algorithm would be difficult and increase the complexity of the analysis. Instead the rotation map was determined manually using multiple iterations until the maximum 3D quadrant burnup was within reasonable limits and the average assembly burnup was uniform. Iterations were performed using only the UO_2 fuel type. Once the final rotation map was determined, the subsequent UBO fuel types would use the same rotation map. A consistent cycle comparison would be achieved using a constant rotation map between fuel types.

With a few exceptions, the shuffle map has one-quarter core symmetry. Therefore the rotation map also has one-quarter core symmetry. The rotation map using the updated shuffle pattern is shown in Figure 6.7.

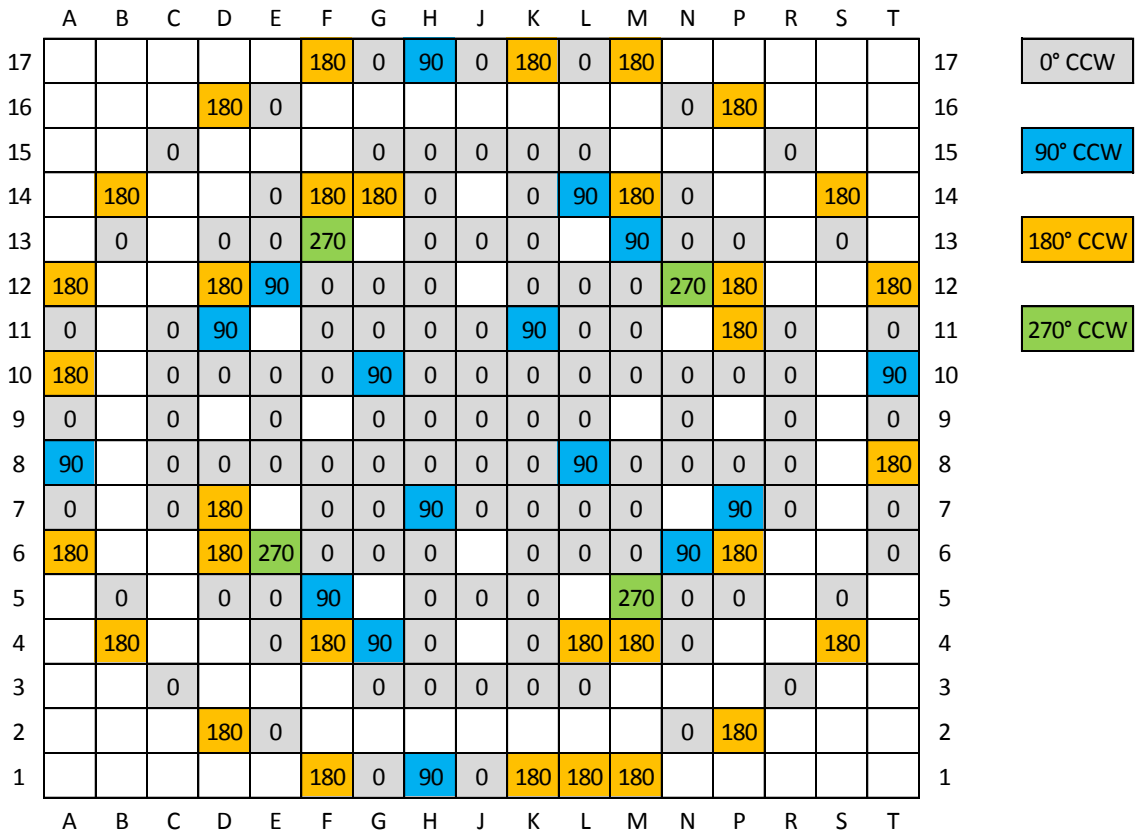

Figure 6.7 Rotation map for the final 18-month shuffle pattern.

6.1.1.4 2D Radial and Axial Power Peaking

Power peaking factors are applied for a single fuel cell, also known as a hot channel. The maximum linear power at a given core elevation is the product of radial and axial power peaking factors. Equation (6-1) shows the calculation of the maximum linear power.

$$Q(z) = F_{XY}(z)P(z) \qquad (6\text{-}1)$$

$Q(z)$ is the maximum linear power at elevation z, $P(z)$ is the average axial power distribution, and $F_{XY}(z)$ is the radial peaking factor at a given elevation [9]. Definitions for $F_{XY}(z)$ and $P(z)$ are given in Eq. (6-2) and (6-3), respectively.

$$F_{XY}(z) = \frac{max\ LHGR(x,y)\ at\ elevation\ z}{average\ LHGR(x,y)\ at\ elevation\ z} \qquad (6\text{-}2)$$

$$P(z) = \frac{average\ LHGR\ at\ elevation\ z}{average\ LHGR} \qquad (6\text{-}3)$$

The heat flux hot channel factor is the maximum linear power density without considering any uncertainties or penalties. Calculation of the heat flux hot channel factor is given in Eq. (6-4).

$$F_Q = \frac{maximum\ local\ LHGR}{average\ LHGR} = max[Q(z)] \qquad (6\text{-}4)$$

The hot channel factor (F_Q) may also be referred to as the maximum 3D power peaking factor. This is not to be confused with the 2D power peaking factor, which is only the radial power peaking $F_{XY}(z)$. The power distribution in the core changes as a function of cycle depletion. Generally the power peaking is highest at the BOC. Figure 6.8 illustrates the radial power peaking factor for the UO_2 fuel type.

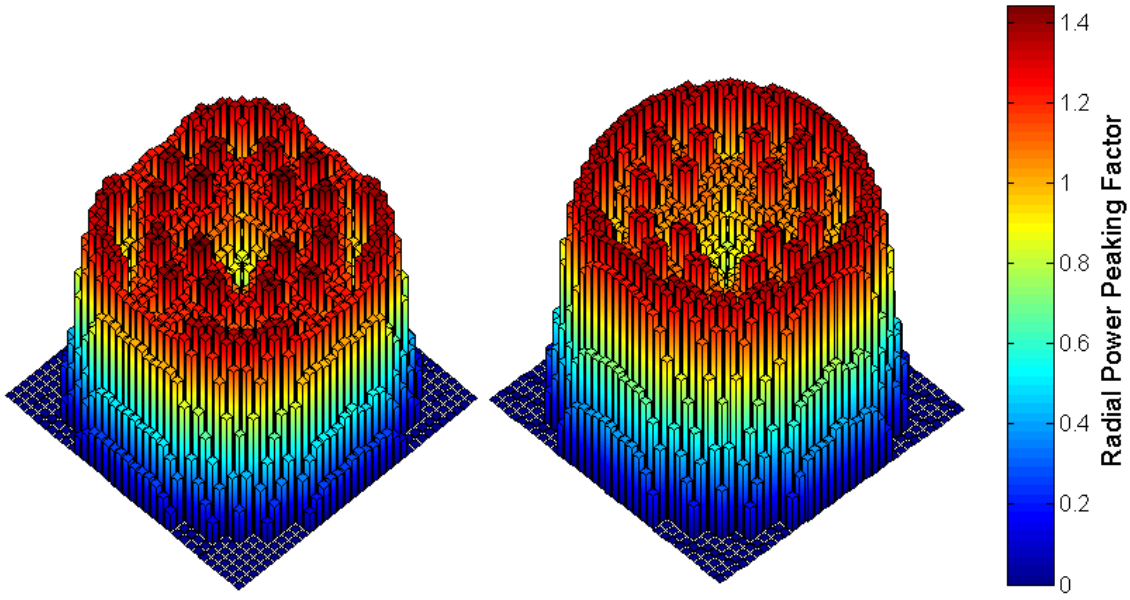

Figure 6.8 Radial power peaking factors at BOC (left) and EOC (right) for UO_2 fuel.

As expected, the radial PPF is highest for the fresh assemblies in the center and periphery of the core. Power is significantly lower for the twice and thrice burnt assemblies on the outermost periphery of the core. The radial power distribution changes as a function of cycle depletion, but this cannot be easily represented graphically. Figure 6.8 shows the radial PPF at BOC and EOC.

Figure 6.9 shows the axial distribution of the power peaking factors. The axial distribution of power also changes with cycle depletion. Evolvement of the axial distribution with depletion can be more readily represented, as shown in Figure 6.9.

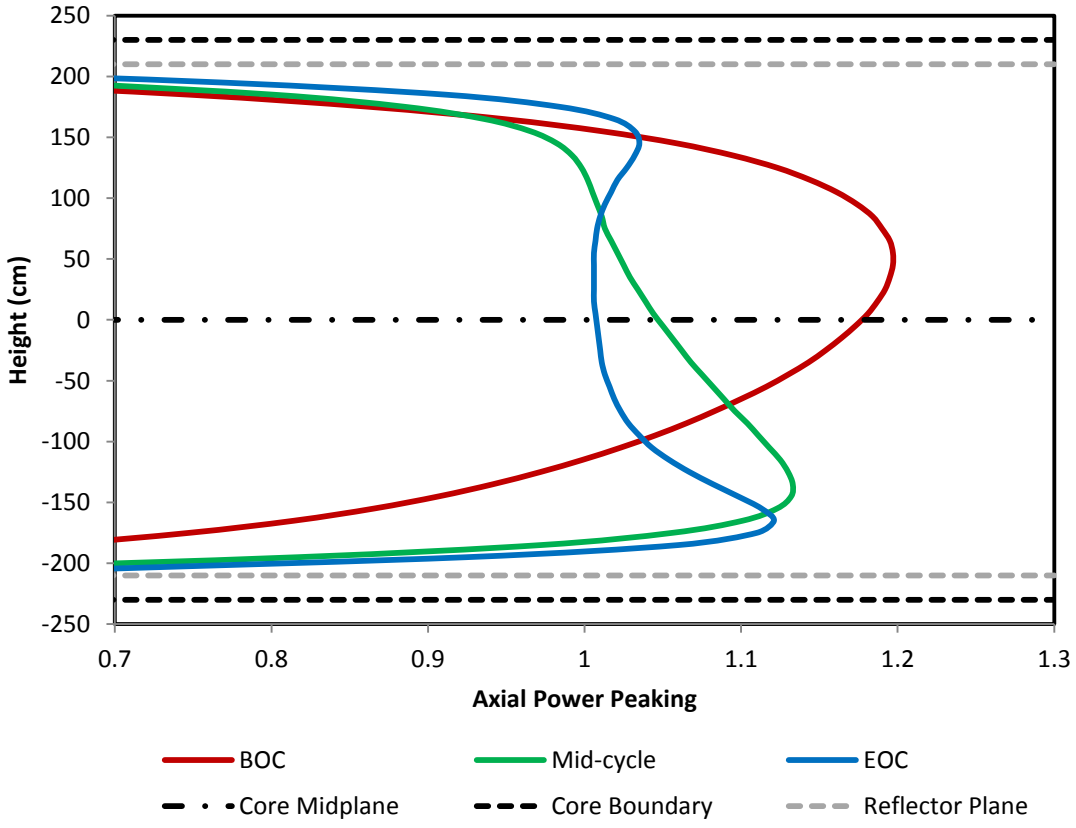

Figure 6.9 Axial power distribution during beginning, middle, and end of cycle depletion for the UO_2 fuel type.

At BOC, the axial power peaking is greatest and is peaked slightly above the core mid-plane. As the cycle depletion continues, the axial distribution becomes more flattened and peaked toward the bottom of the core. From the radial and axial distributions, the power peaking is primarily in the fresh assemblies and located below the core mid-plane.

6.1.1.5 3D Power Peaking

The 2D PPF is a representation of the assemblies with the highest fractional power. However, the 3D PPF location does not necessarily coincide with the 2D PPF location. Therefore it is important to know the location of 3D PPF. The magnitude of the 3D PPF is shown in Figure 6.10. In addition, Figure 6.10 shows which assembly coordinate has the 3D PPF as a function of cycle depletion.

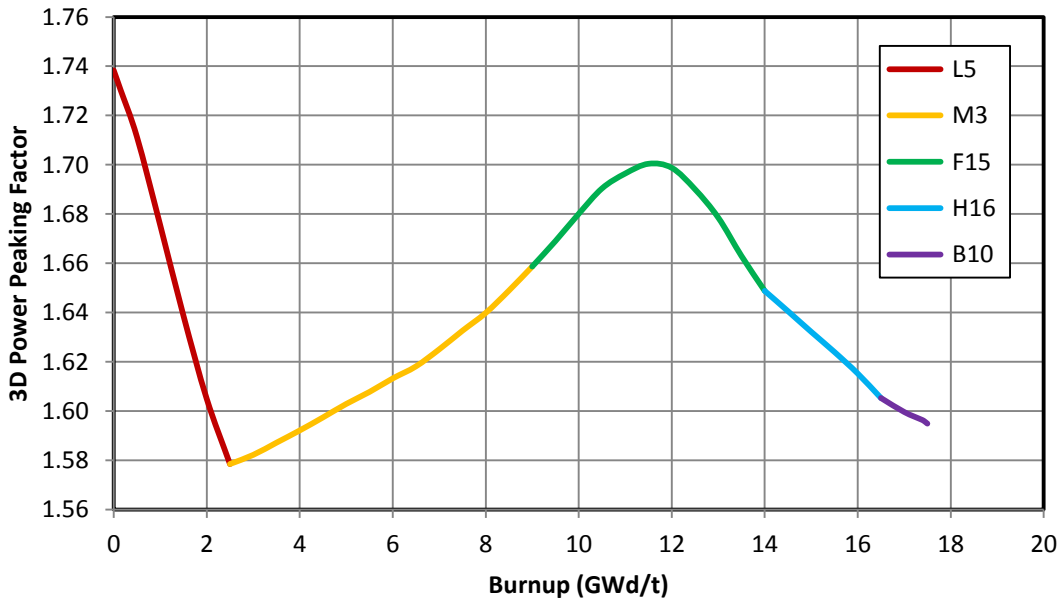

Figure 6.10 Magnitude of the 3D power peaking factor as a function of burnup and assembly type for UO_2 fuel type.

Figure 6.10 illustrates how the 3D PPF changes in magnitude and changes assembly location during cycle depletion. The 3D PPF decreases during the first 2 GWd/t of cycle depletion as the fuel is depleted. However the 3D PPF increases again as the power

suppression provided by the Gadolinium is depleted. Axial location of the 3D PPF varies significantly, as shown in Figure 6.11.

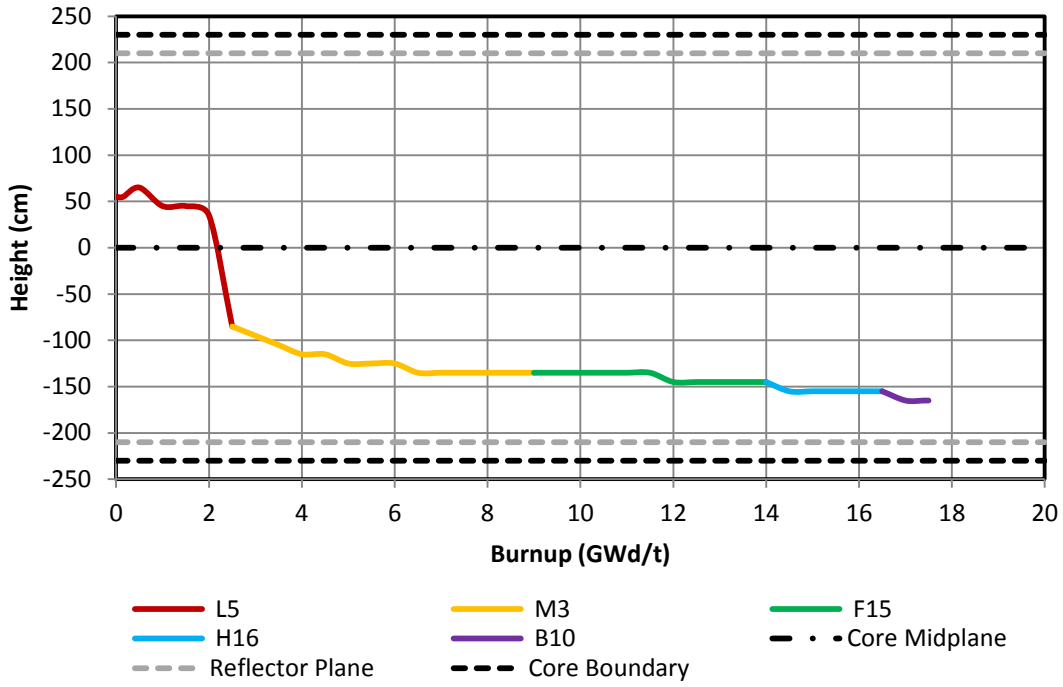

Figure 6.11 Axial location of the 3D power peaking factor as a function of burnup and assembly type for UO_2 fuel.

Initially, the 3D PPF is located above the core mid-plane. After the first 2 GWd/t, the 3D PPF falls below the core mid-plane and remains there for the rest of the cycle. Radially, the 3D PPF moves significantly during cycle depletion. For a majority of the cycle depletion, the 3D PPF is located in the fresh, periphery assemblies, as shown in Figure 6.12.

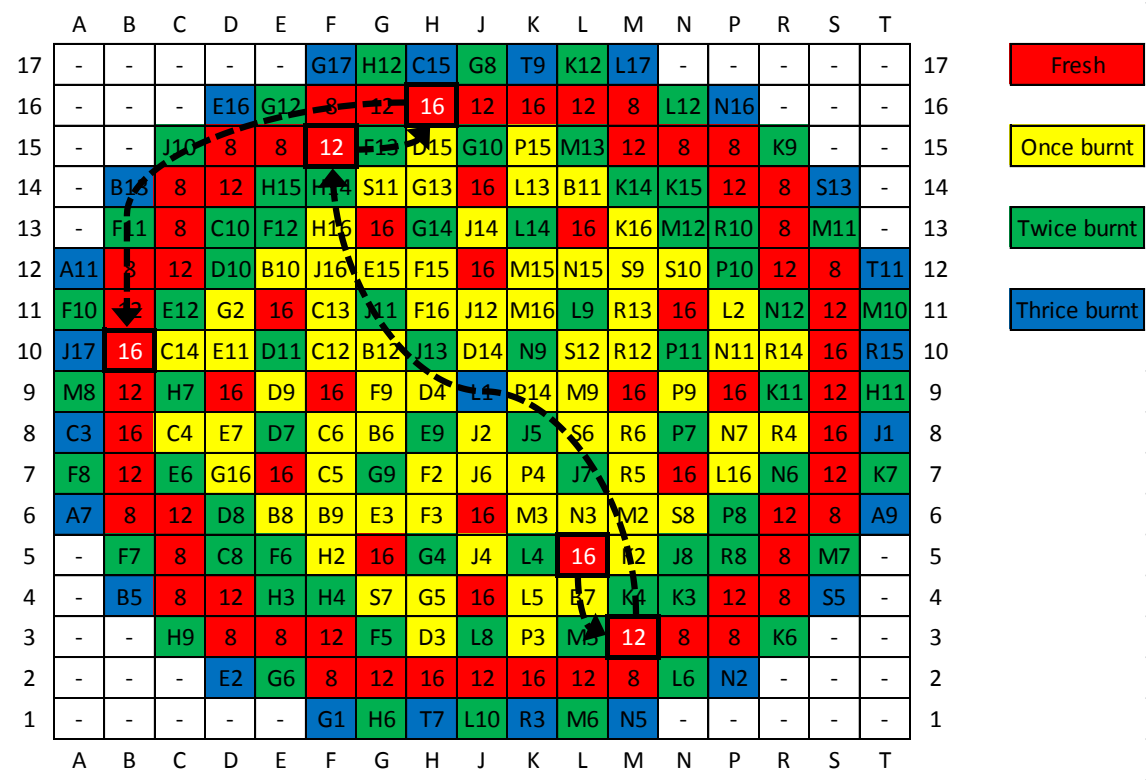

Figure 6.12 Radial location of the 3D power peaking factor for UO_2 fuel during depletion.

6.1.1.6 Enthalpy Peaking Factors

The enthalpy peaking factor is important for thermal-hydraulic considerations. A high enthalpy peaking can be unsafe for transient scenarios. If the enthalpy peaking is too high, a departure from nucleate boiling condition (DNB) may exist. DNB condition leads to rod dry-out and subsequent rod failure. Calculation of the enthalpy peaking factor is performed using Eq. (6-5).

$$F_{\Delta H} = \frac{maximum\ channel\ enthalpy\ rise}{core\ average\ enthalpy\ rise} = max\left[\frac{\Delta H}{avg\ \Delta H}\right] \qquad (6\text{-}5)$$

The enthalpy rise (ΔH) is simply the outlet enthalpy minus the inlet enthalpy for each individual fuel channel. Under normal operating conditions, the inlet enthalpy is uniform and constant for each fuel channel of the core. The inlet enthalpy chosen for the core

analysis was 1295 kJ/kg. An enthalpy rise map is given for the UO_2 fuel type at BOL in Figure 6.13.

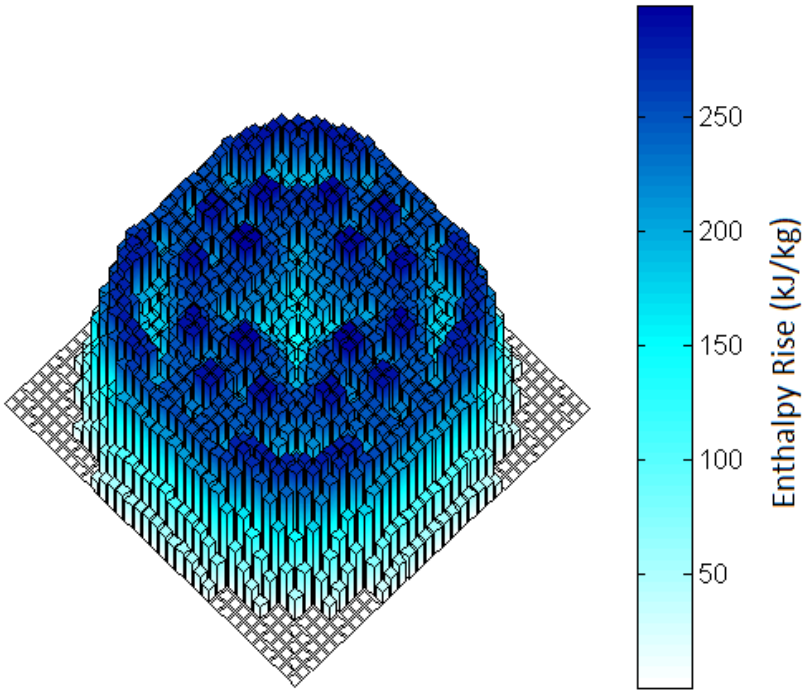

Figure 6.13 Enthalpy rise at BOL for UO_2 fuel type. The inlet enthalpy is 1294.6 kJ/kg.

Figure 6.13 is similar to the power peaking factor map shown in Figure 6.8. The enthalpy rise is high for assemblies with a high power fraction. Also the magnitude of the enthalpy rise factor as a function of cycle depletion follows a similar pattern to that of the 3D PPF, as shown in Figure 6.14.

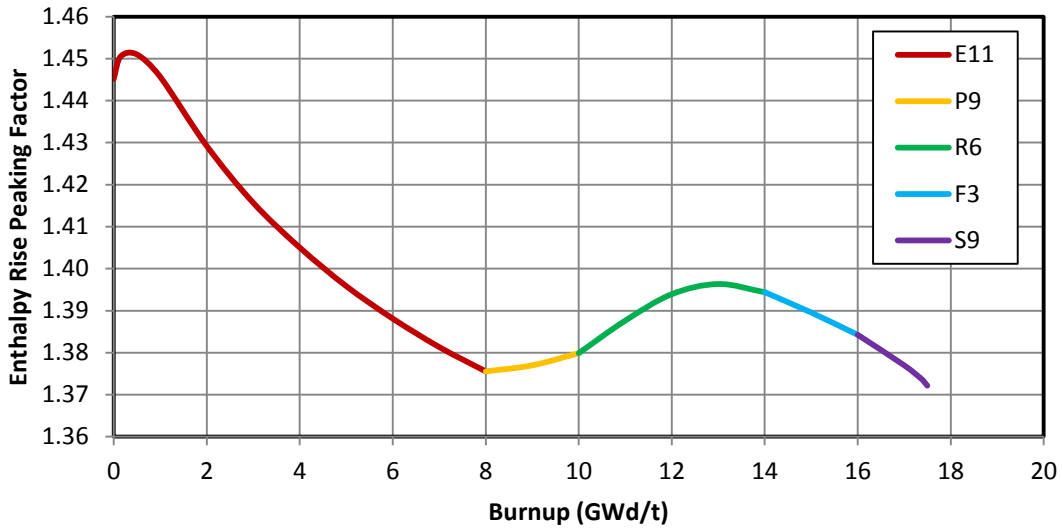

Figure 6.14 Magnitude of the enthalpy rise peaking factor as a function of burnup and assembly type for UO_2 fuel.

Radial location of the enthalpy rise factor is given in Figure 6.15. It is important to observe that the location of the enthalpy rise factor and the 3D PPF are not the same, despite the similar behavior. Therefore both 3D PPF and enthalpy rise factors must be considered when choosing a new assembly shuffle map.

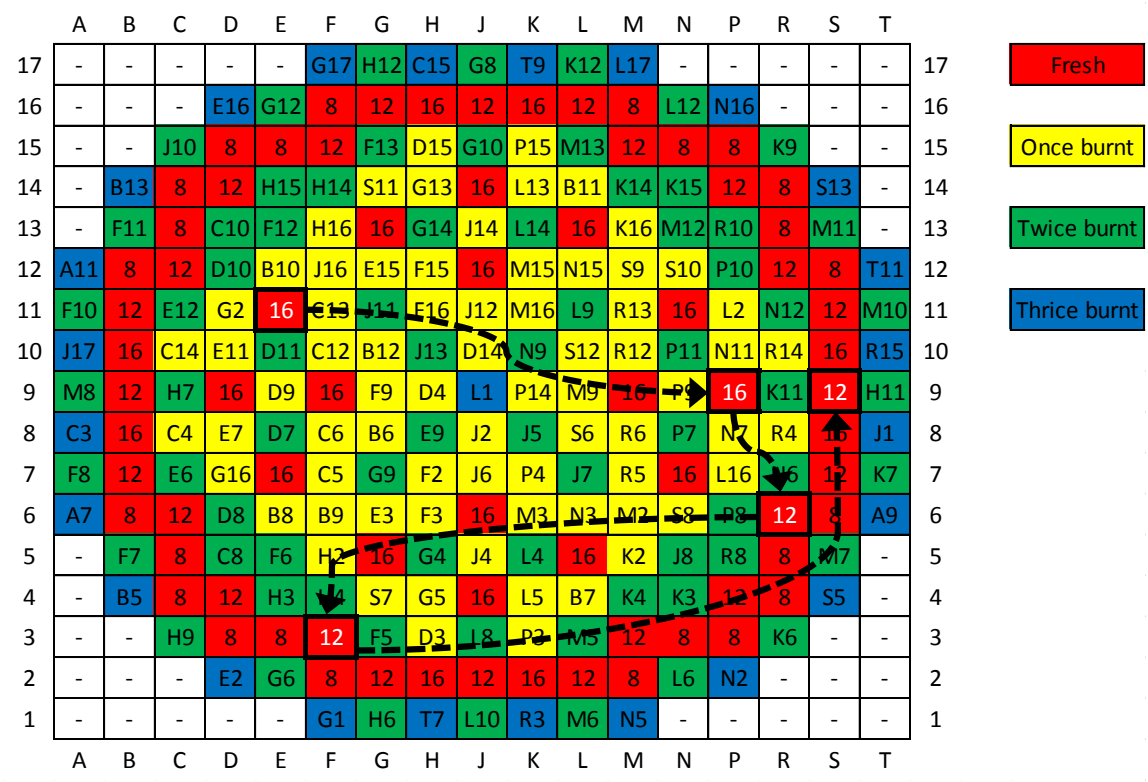

Figure 6.15 Radial location of the enthalpy rise peaking factor for UO_2 fuel type during depletion.

6.1.1.7 Optimized Cycle Parameters

Cycle optimization is a complex task because of the multiple parameters that must be considered. The main parameter to optimize is the cycle burnup. Efficient shuffle patterns and assembly rotation maps results in a longer cycle lengths; a clear benefit to the utility. However, a new shuffle map and assembly rotation must be weighed against any changes in safety parameters such as: power peaking, enthalpy peaking, maximum rod burnup, and reactivity coefficients.

The most prominent issue with the original shuffle and assembly rotation maps was the maximum 3D burnup. The center assembly J9 had an EOL burnup of 73,971 MWd/t, well above the rod burnup limitations. Analyzing the incremental assembly burnup graph was the simplest method by which to optimize cycle burnup. Figure 6.16 shows the final incremental burnup analysis.

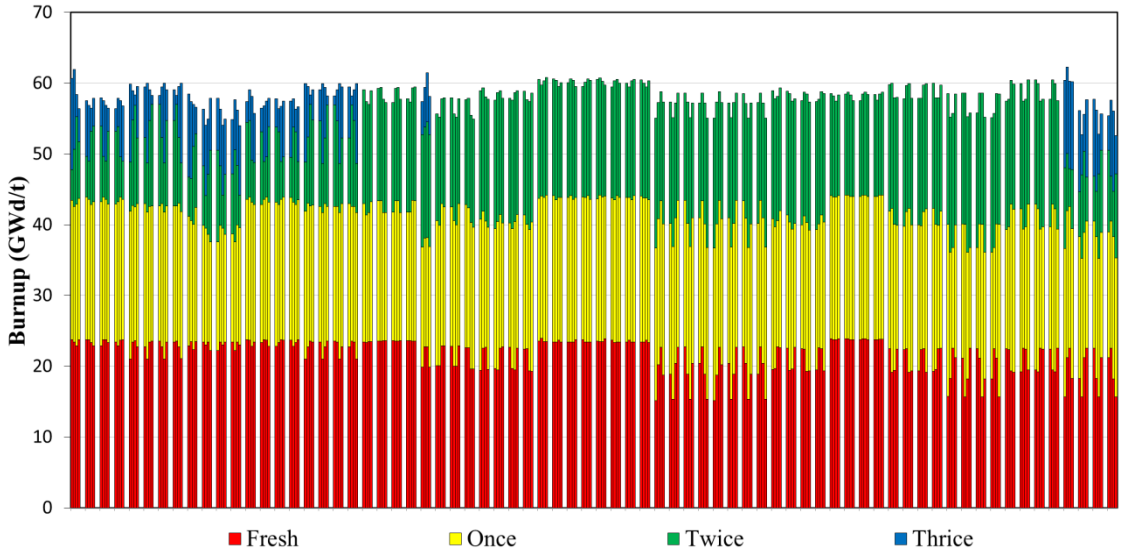

Figure 6.16 Final incremental burnup analysis for all 241 assemblies, including the four assembly quadrants. The updated 18-month shuffle map and assembly rotation was used for the UO_2 fuel.

A comparison of the original and optimized shuffle and rotation map, Figure 6.3 and Figure 6.16 respectively, can be made to verify the optimization. The EOC burnup for each assembly is divided by the average burnup at EOC, thereby providing an EOC burnup peaking factor. Comparison of the original and optimized EOC burnup peaking is shown in Figure 6.17.

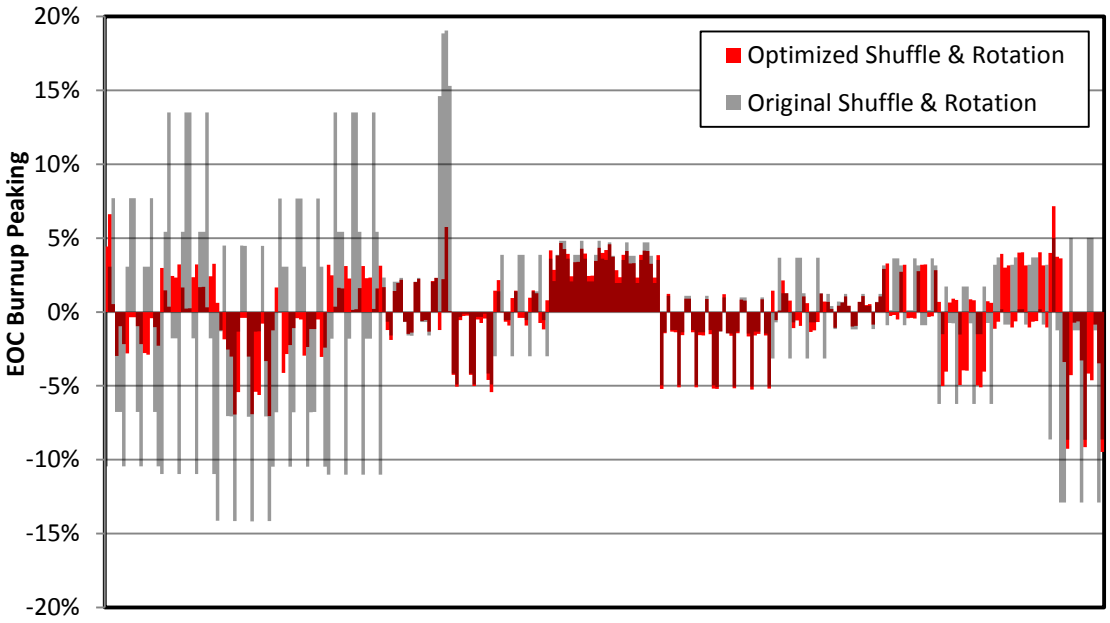

Figure 6.17 Comparison of the EOC burnup peaking for the original and optimized shuffle and rotation map.

Figure 6.17 shows a clear improvement of the EOC burnup peaking. The original shuffle and rotation map has a burnup peaking nearly 20% greater than the average EOC burnup. With a few exceptions, the optimized shuffle and rotation map shows a burnup peaking less than 5% of the average EOC burnup. Therefore, the EOC burnup is more uniform after the optimization. A 2D burnup map at EOC is shown in Figure 6.18.

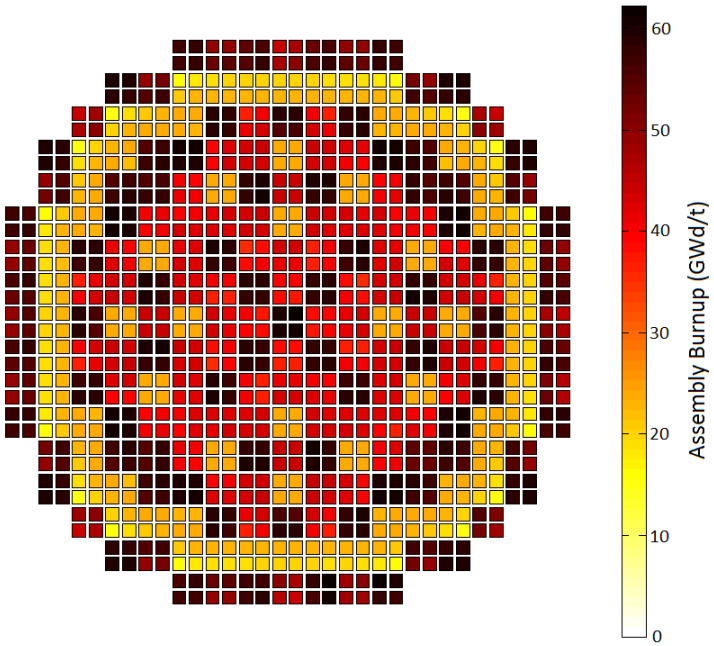

Figure 6.18 2D assembly burnup at EOC with optimized shuffle and rotation for UO_2 fuel type.

In addition to the burnup optimization, it is important to check key cycle parameters. Exceeding a safety parameter would cause a reassessment of the cycle optimization. A summary of key cycle parameters is given in Table 6.4.

Table 6.4 Optimized 18-month cycle parameters

Cycle Parameter	Original Shuffle Map with no Rotation	New Shuffle Map with Rotation
Core Avg Burnup (MWd/t)	41,452	41,544
EOC Burnup (MWd/t)	17,454	17,496
Cycle Length (days)	503.8	505.0
Max 3D Burnup (MWd/t)	73,971	68,570
Max 3D PPF	1.726	1.739
Max 3D Enthalpy Rise	1.443	1.451
BOL Boron (ppm)	1696	1700
BOL AO (%)	4.789	4.865
EOL AO (%)	-2.472	-2.509

Two notable cycle parameter changes in Table 6.4 are the cycle length and maximum 3D burnup. A cycle length increase of 1.2 days is observed from the optimized shuffle map and assembly rotation. The maximum 3D burnup is reduced by 5401 MWd/t. The other key cycle parameters do not present any significant changes due to the optimization. Therefore, the cycle optimization is an improvement and does not alter any safety parameters compared to the original cycle.

6.1.2 UBO-UO_2 Comparisons

6.1.2.1 Cycle Length

All subsequent cycle comparisons of UO_2 and UBO fuels were performed using the optimized shuffle map and assembly rotation. No further changes in the shuffle map or assembly rotation map were made for the UBO fuels to preserve a consistent cycle comparison to UO_2 fuel. In addition, no changes in the assembly design or number of Gadolinium rods were made for the UBO fuel cycle. The entire UO_2 fuel core would be replaced with either a UBO 5vol% or 10vol% fuel type. Comparison of the cycle burnup is shown in Figure 6.19. The following figures omit the UBO 5vol% results for clarity.

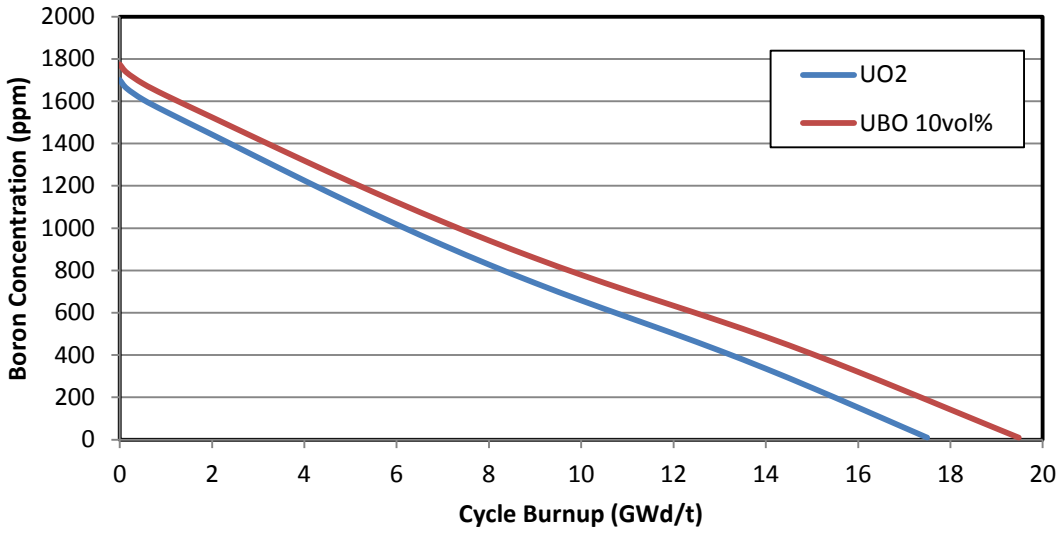

Figure 6.19 Boron concentration for the 18-month cycle depletion for UO_2 and UBO 10vol% fuels.

An important verification was performed for the UO_2 cycle before the UBO comparisons. The UK-EPR reference uses the computer codes APOLLO 2 for the macroscopic cross section data, SMART for the 3D, two-energy group diffusion theory, and FLICA III-F for the thermal-hydraulic design [9]. The EPR reference indicates an EOC burnup value of approximately 17,500 MWd/t for the standard UO_2 fuel in an 18-month equilibrium cycle [9]. As shown in Figure 6.19 and in Table 6.5, the EOC cycle burnup is in good agreement with the EPR value. This close agreement is a good indication that the cross section data used in this work and the thermal-hydraulic and neutronic analysis presented in this M.S. thesis are in good agreement with the UK-EPR Pre-construction Safety Report.

Comparison of cycle burnup parameters for UO_2 and UBO fuels is found in Table 6.5. The core average burnup is increased for the UBO fuels due to the higher power density. An increase of 2464 and 5096 MWd/t is shown in the core average burnup for the UBO 5vol% and 10vol%, respectively.

Table 6.5 18-month cycle length comparison between UO_2 and UBO fuels

Fuel Type	Core Avg Burnup (MWd/t)	Max 3D Burnup (MWd/t)	EOC Burnup (MWd/t)	Cycle Length (days)	Δ Cycle Length (days)
UO_2	41,544	68,570	17,496	505.0	-
UBO 5vol%	44,008	72,277	18,458	507.2	2.2
UBO 10vol%	46,640	76,194	19,481	508.3	3.3

Cycle length is determined by dividing the EOC burnup by the respective core average power density. The cycle length is increased by 2.2 and 3.3 days for the UBO 5vol% and 10vol%, respectively. However the maximum 3D burnup is increased significantly for the UBO fuels. The UBO 10vol% fuel shows an increase of 7624 MWd/t in the maximum 3D burnup. UBO fuels may require selective placement to reduce the burnup peaking.

6.1.2.2 2D Radial and Axial Power Peaking

Cycle peaking factors are important parameters for cycle safety analysis. One metric used by utilities is the axial offset. The axial offset indicates the power peaking in the two halves of the core. Calculation of the axial offset is given in Eq. (6-6).

$$Axial\ Offset = \frac{P_T - P_B}{P_T + P_B} \qquad (6\text{-}6)$$

P_T is the power fraction in the top half of the core and P_B is the power fraction in the bottom half of the core [9]. Figure 6.20 shows the axial offset of the UO_2 and UBO fuel relative to the core mid-plane.

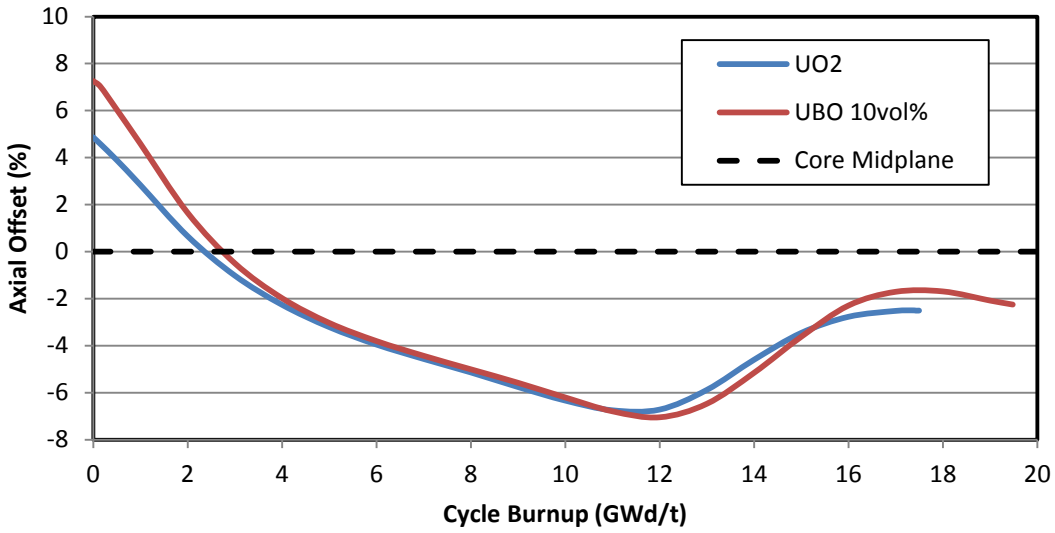

Figure 6.20 Axial offset for the 18-month cycle depletion.

The axial offset is briefly positive during the initial 2 GWd/t of cycle depletion but is negative for the remainder of the cycle. Coolant entering the bottom of the core is colder and denser than at the top of the core. The extra moderation provided by the denser coolant increases the power in the lower half of the core. However, the axial offset for the UBO 10vol% fuel shows only minor differences compared to the UO_2 fuel at the beginning and end of cycle.

Closely related to the axial offset is the axial power distribution. The axial power distribution reveals a more detailed analysis of all axial planes instead of only the two halves of the core. Local axial peaking can be observed, as shown in Figure 6.21.

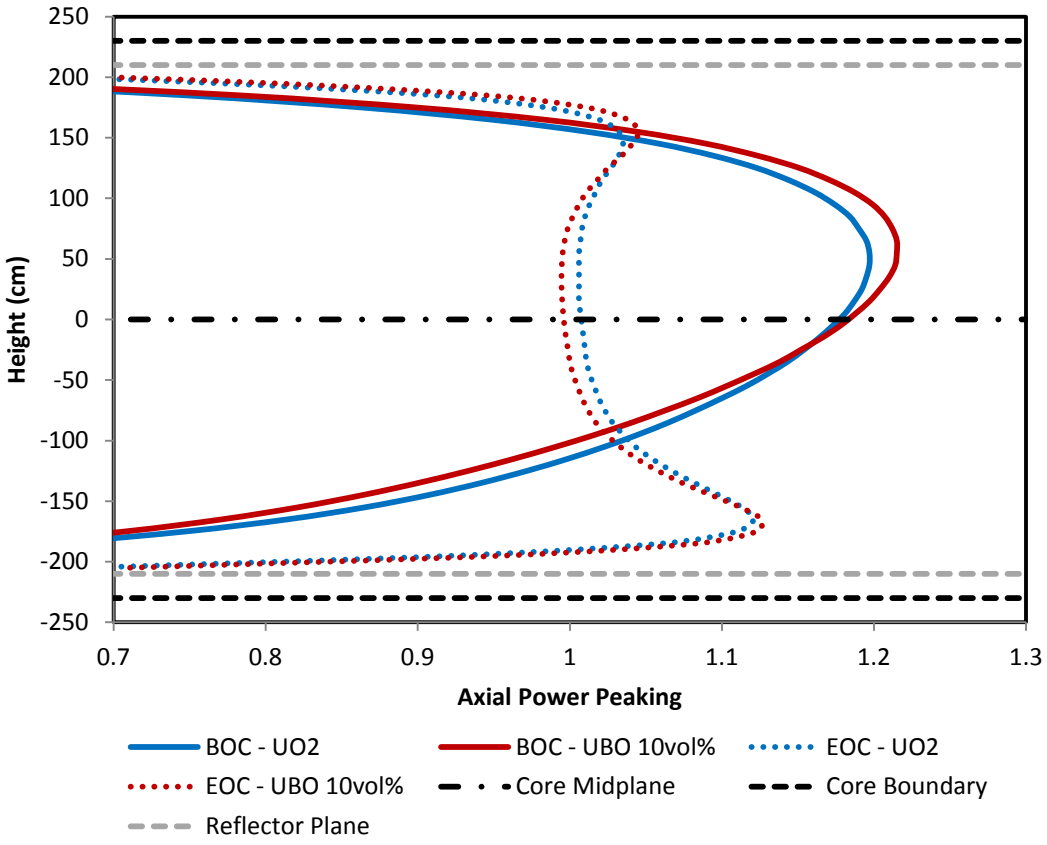

Figure 6.21 Axial power distribution comparison of UO_2 and UBO 10vol% fuel type at BOC and EOC for the 18-month equilibrium cycle.

Figure 6.21 illustrates how the axial power distribution evolves with cycle depletion. At BOC, the axial power peaked and slightly above the core mid-plane. At EOC, the axial power becomes flattened and is peaked at the bottom of the core. In addition, Figure 6.21 shows the effect of the UBO fuel. The axial power is slightly increased for the UBO 10vol% at BOC. At EOC the axial power distribution is nearly equivalent for both UO_2 and UBO 10vol% fuel types.

The radial power distribution is more difficult to visualize when comparing the UO_2 and UBO fuels. A coordinate (spatial) map comparison of the radial power peaking is complex. Therefore, only the radial power magnitudes are compared. The radial power distribution for UO_2 was subtracted from the UBO 10vol% at both BOC and EOC, as

shown in Figure 6.22. All 241 assemblies were analyzed. Figure 6.22 is additionally grouped for the 72 reload assemblies and their respective shuffling (fresh, once, twice, and thrice burnt).

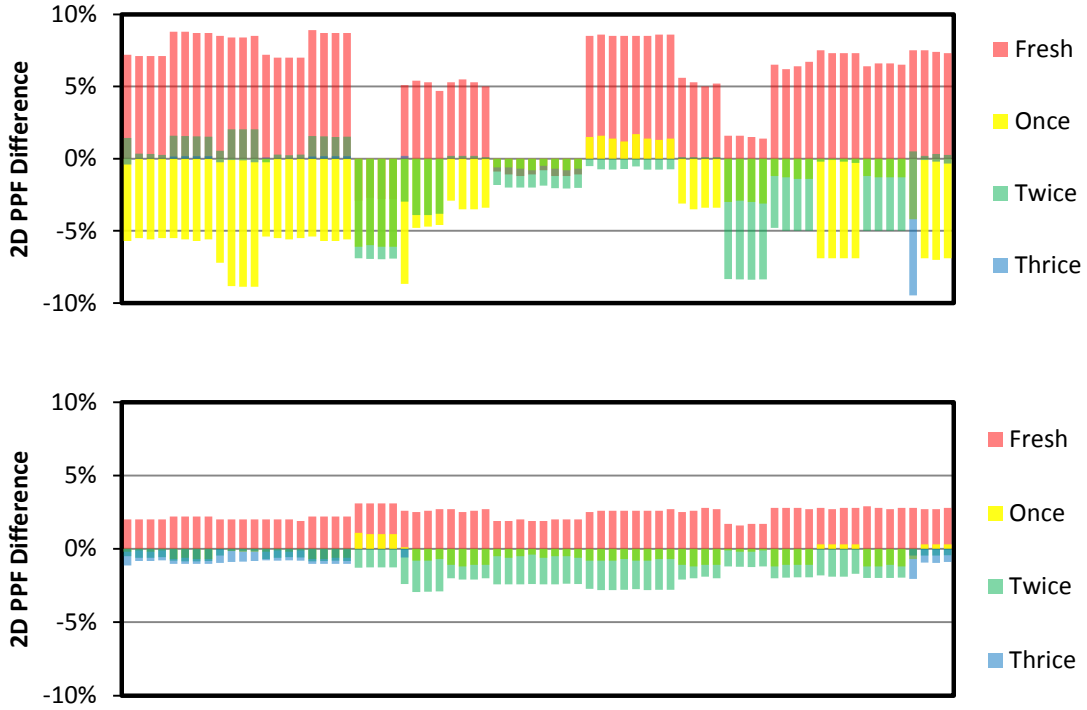

Figure 6.22 BOC (top) and EOC (bottom) radial power difference between UBO 10vol% and UO_2 for the 18-month equilibrium cycle.

As shown in Figure 6.22, the UBO 10 vol% fuel exhibits a greater 2D power peaking in the fresh fuel assemblies as compared to the UO_2 fuel. At BOC, the power peaking difference is the greatest. The power in the UBO 10vol% fresh fuel assemblies are nearly 10% greater than the UO_2 fresh fuel assemblies. At EOC, the power peaking difference is less noticeable. Approximately a 2-4% difference exists between the UO_2 and UBO 10vol% 2D radial power distributions.

6.1.2.3 3D Power Peaking

Comparison of the 3D PPF for UO_2 and UBO fuels is important because the UBO fuel will have a higher power density. The higher power density may increase the 3D PPF. As shown previously, the 2D power distributions were greater for the UBO fuel. Figure 6.23 shows the 3D PPF as a function of cycle depletion for the UO_2 and UBO fuel. A transient LOCA analysis limits the maximum allowable 3D PPF to 2.82 [9].

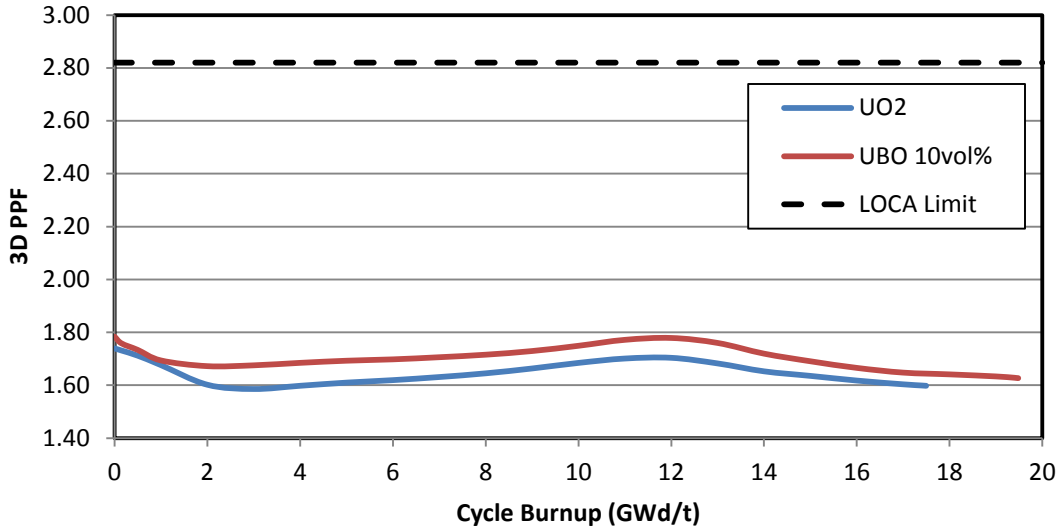

Figure 6.23 3D power peaking factor for the 18-month cycle depletion for UO_2 and UBO 10vol% fuels. A maximum power peaking factor of 2.82 is allowed.

Figure 6.23 confirms that the magnitude of 3D PPF for UBO fuels is higher than UO_2 fuel. In relation to the LOCA limit, the UBO 3D PPF is a relatively small increase compared to UO_2. There is significant margin available. Special placement of the UBO fuel assemblies could reduce the power peaking. Axial location of the 3D PPF is shown in Figure 6.24.

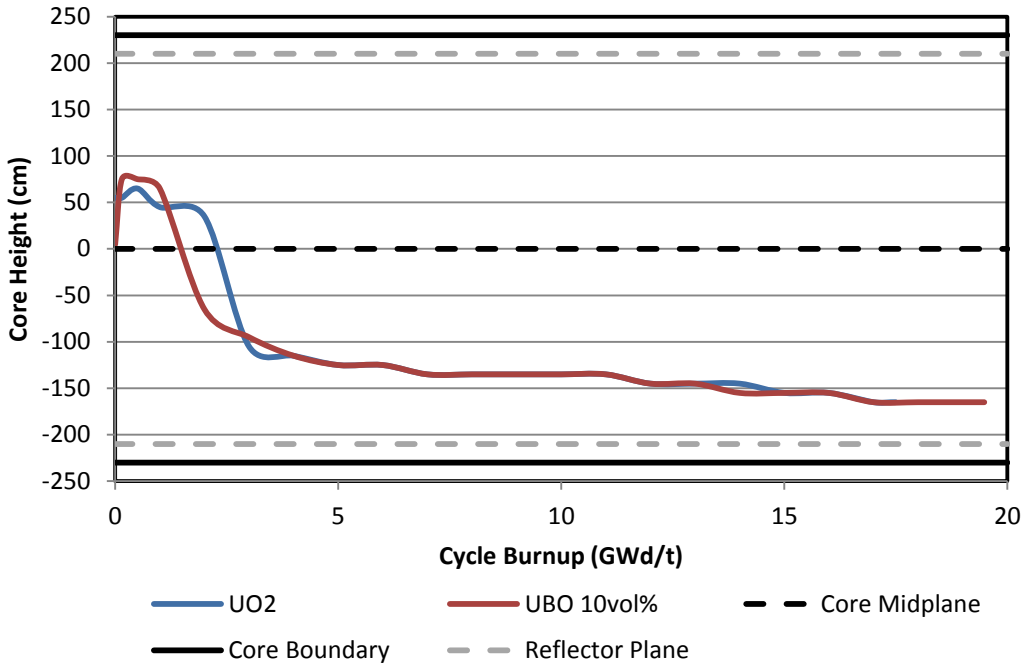

Figure 6.24 Axial location of the 3D power peaking factor during the 18-month cycle depletion.

Axial location of the 3D PPF follows a similar pattern as the axial offset except at EOC. The difference in axial location of the 3D PPF between the UO_2 and UBO fuels is minimal. As shown previously in Figure 6.21, the axial power distribution exhibits peaking in the bottom half of the core at EOC. Therefore the 3D PPF is expected to be located below the core midplane at EOC.

6.1.2.4 Enthalpy Peaking

The magnitude of the enthalpy rise peaking is shown in Figure 6.25. Similar to the 3D power peaking, the enthalpy peaking is greater for the UBO 10vol% fuel. The maximum allowable enthalpy rise peaking as determined from a LOCA analysis is 1.80 [9].

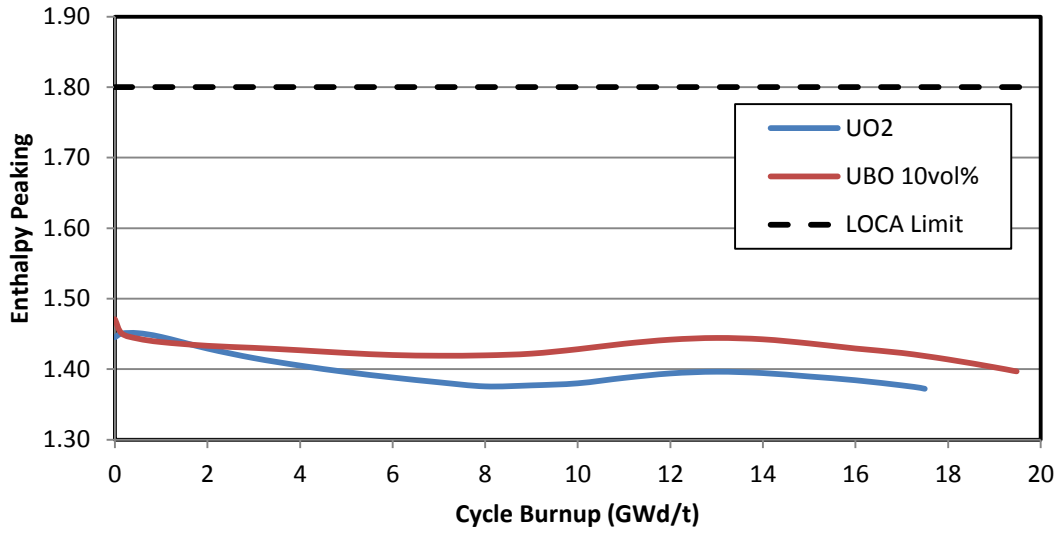

Figure 6.25 Enthalpy rise hot channel factor for the 18-month cycle depletion. A maximum peaking of 1.80 is allowed.

Figure 6.25 reveals that the enthalpy peaking is the greatest at BOC and generally decreases with cycle depletion. A small peaking increase occurs at 13 GWd/t, but it does not exceed the BOC value. The UBO fuel follows a similar pattern as the UO_2 fuel but with a slightly higher peaking. Late in the cycle, the UBO fuel loses some enthalpy peaking margin compared to the UO_2 fuel. The higher peaking is a result of the higher power density of UBO fuel. Overall the maximum peaking at BOC is nearly equivalent for both the UO_2 and UBO 10vol% fuel. An additional transient analysis would be needed to assess the impact of the higher enthalpy peaking of UBO fuels near EOC.

6.1.2.5 Fuel Temperature

The fuel temperature distribution is similar to the power and enthalpy distributions. Since the fuel temperature is a function of both the enthalpy and power, only minor differences exist. A comparison of the axial fuel temperature distribution is shown in Figure 6.26 for BOC and EOC.

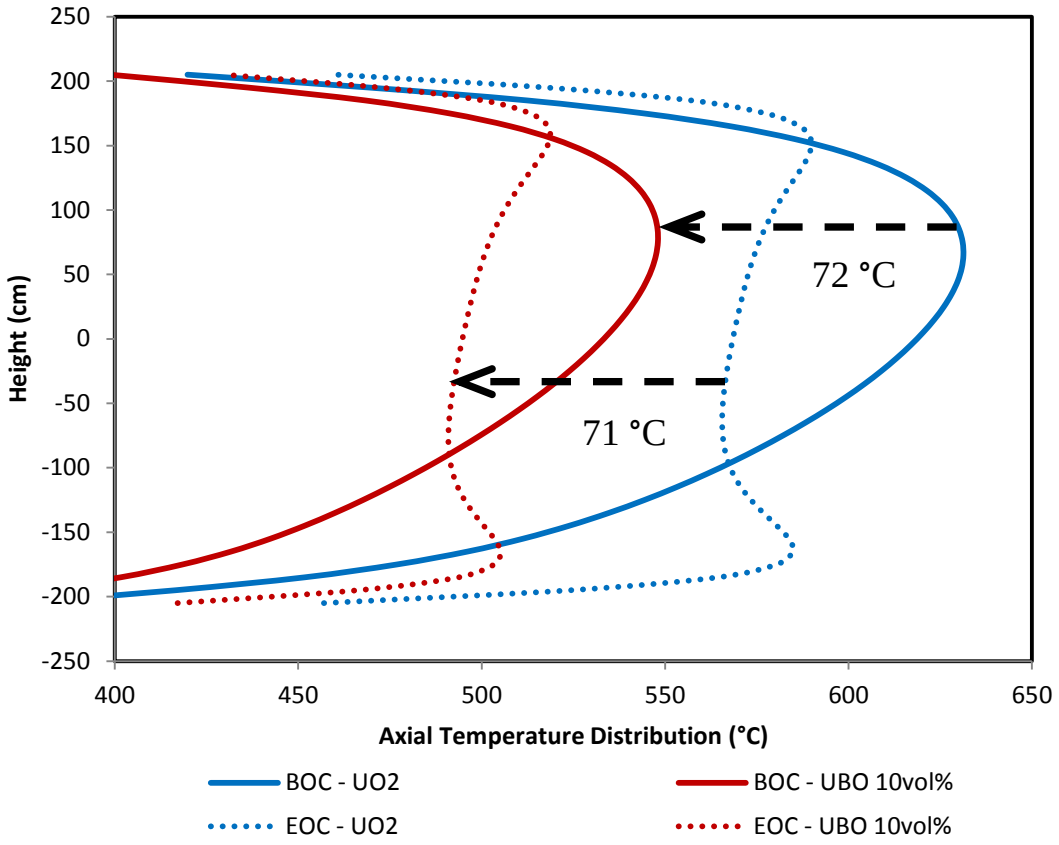

Figure 6.26 18-month cycle axial fuel temperature distribution at BOC and EOC for UO_2 and UBO 10vol% fuel type.

Figure 6.26 shows that the temperature difference between UO_2 and UBO fuel is relatively independent of cycle depletion. Approximately a 72 °C decrease in core average fuel temperature occurs for the UBO 10vol% at both BOC and EOC. However, the shape of the temperature distribution varies between BOC and EOC. The radial temperature distribution is shown in Figure 6.27. A spatial coordinate map comparison is complicated to visualize and so only the temperature magnitudes of the 241 assemblies are shown.

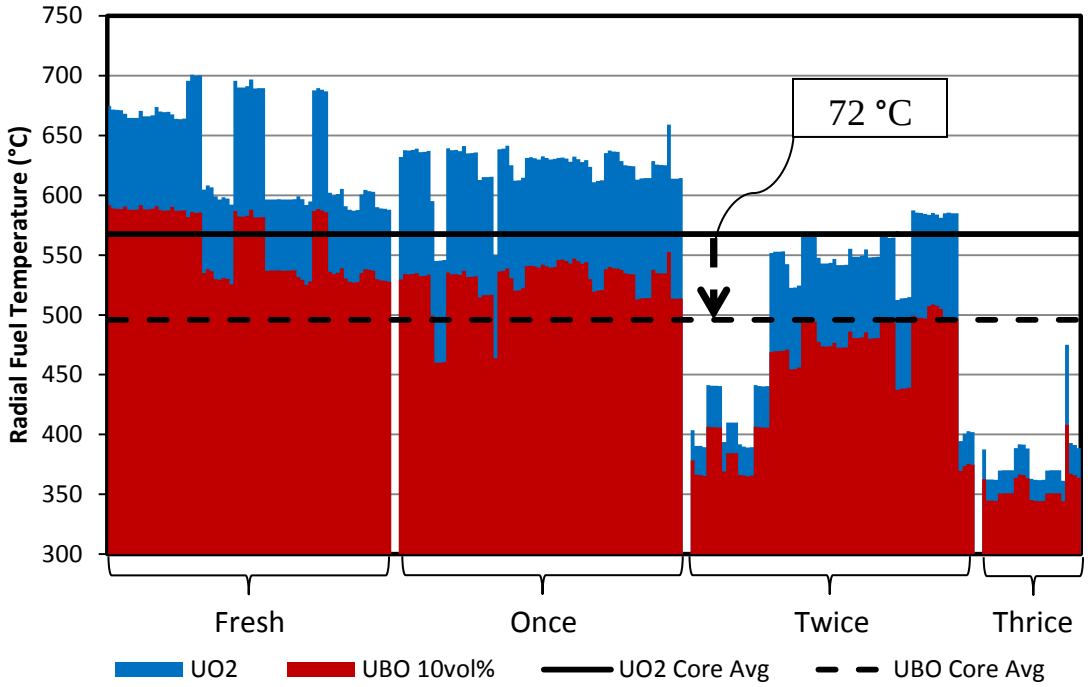

Figure 6.27 18-month cycle radial fuel temperature distribution at BOC for UO_2 and UBO 10vol% fuel type.

Figure 6.27 shows only the radial fuel temperature at BOC, but the EOC cycle results are nearly identical. On average the core temperature is reduced 72 °C for the UBO 10vol% fuel. Temperature results from the 3D core simulation are in good agreement with the 2D heat conduction analysis in a single fuel pin. At an average LHGR of 163.4 W/cm, the effective pin temperature drop using UBO 10vol% fuel is 73 °C. This close agreement verifies the UBO heat conduction in the 3D core simulations is correctly modeled.

In addition, Figure 6.27 shows the temperature difference during each stage of assembly burnup. The fresh and once burnt assemblies operate at high linear powers and therefore the temperature difference between UO_2 and UBO 10vol% fuels are greater. For the twice and thrice burnt assemblies that experience a lower linear power, the temperature difference is much smaller. A summary of the fuel temperature parameters is given in Table 6.6.

Table 6.6 Fuel temperature comparison for 18-month equilibrium cycle.

	Temperature (°C)	**UO_2**	**UBO 10vol%**	**Difference**
BOC	Core Average	568	496	-72
	Peak	786	668	-118
EOC	Core Average	566	495	-71
	Peak	710	613	-97

6.1.2.6 Reactivity Coefficients

Reactivity coefficients are used to assess cycle safety parameters. The reactivity coefficients are expressed as a change in reactivity per change in a given parameter. For example, the moderator density coefficient design limit is less than 5.15 $x10^5$ pcm g^{-1} cm^{-3} [9]. EPR design calculations for the moderator temperature coefficient (MTC) were performed at nominal power, all rods out, and at the critical boron concentration. Results for EPR MTC calculation at BOC and EOC were -24.1 and -82.6 pcm/C, respectively [9]. Values obtained from the CRONOS analysis for the moderator density coefficient and moderator temperature coefficient are shown in Figure 6.28 and Figure 6.29, respectively.

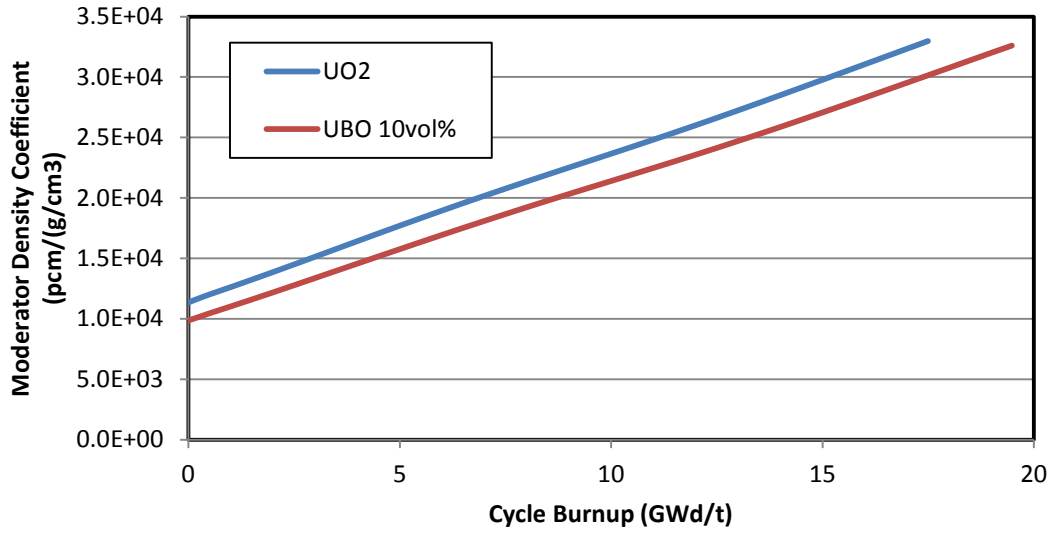

Figure 6.28 Moderator density coefficient for the 18-month cycle depletion.

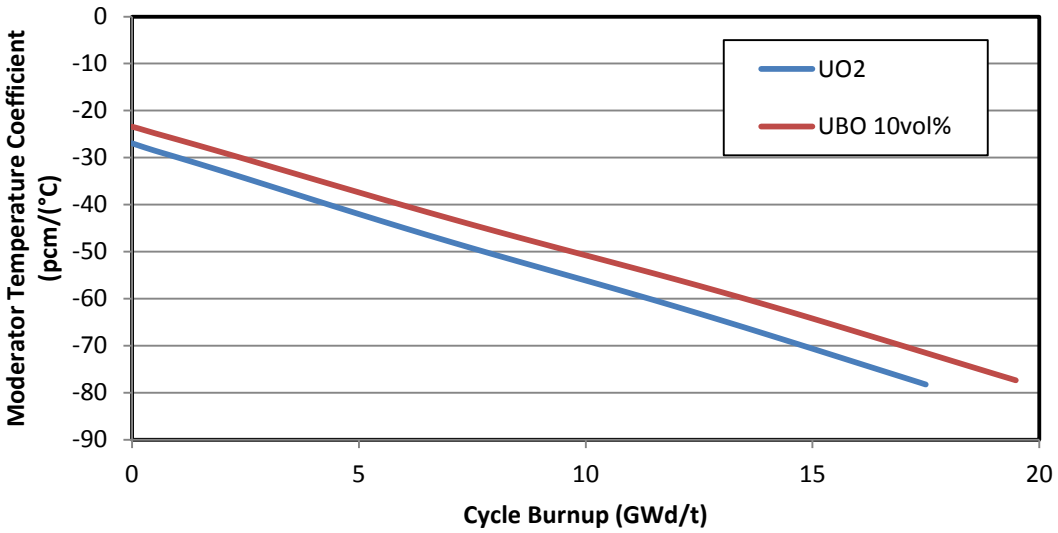

Figure 6.29 Moderator temperature coefficient for the 18-month cycle depletion.

As shown in Figure 6.29, the MTC values are similar to the reference EPR design values for the UO_2 fuel. At BOC and EOC the MTC was -26.8 and -79.5 pcm/C, respectively. In general, the MTC becomes more negative as the cycle progresses. The UBO fuel

exhibits a slightly decreased (less negative) MTC compared to the UO_2 fuel. The MTC difference of UBO 10vol% fuel is minor with a 3.5 pcm/°C decrease at BOC and a 7.1 pcm/°C decrease at EOC compared to UO_2 fuel. A 5vol% UBO fuel has an MTC nearly identical to UO_2 fuel. Therefore, the BeO addition does not have a significant impact on the negative MTC.

Another important safety coefficient is the fuel temperature coefficient (FTC). At an average fuel temperature of 550 °C, EPR design values for FTC were -2.9 and -3.1 pcm/C at BOC and EOC, respectively [9]. CRONOS results for FTC are shown in Figure 6.30. At BOC and EOC, the FTC was -2.47 and -2.72 pcm/C, respectively. Values obtained from EPR and CRONOS for the FTC are in good agreement. The UBO fuel shows an increased FTC (more negative) compared to the UO_2 fuel. However the differences are minor with a 0.073 and 0.033 pcm/°C increase for the UBO 10vol% fuel at BOC and EOC, respectively.

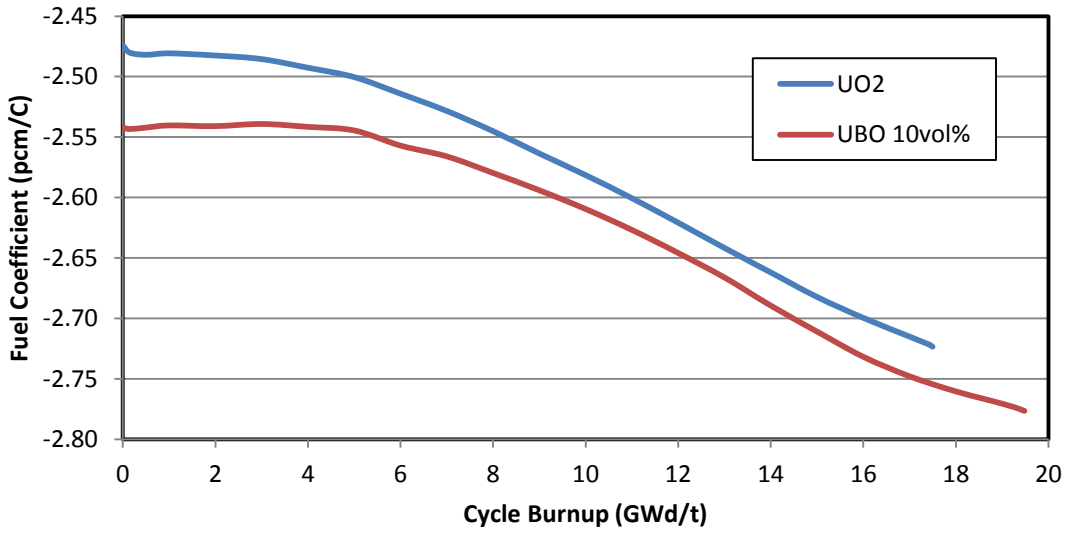

Figure 6.30 Fuel temperature coefficient for the 18-month cycle depletion. Core average fuel temperature for UO_2 and UBO 10vol% were 568 and 496 °C, respectively.

Lastly, the boron coefficient was analyzed for the UO_2 and UBO fuel. The UO_2 boron coefficient EPR design value at BOC and EOC is -6.1 and -7.1 pcm/ppm, respectively [9]. CRONOS results are similar with a -5.6 and -6.8 pcm/ppm at BOC and EOC, respectively, as shown in Figure 6.31. UBO 10vol% fuel shows an increased (more negative) boron worth coefficient compared to the UO_2 fuel. Overall, the addition of BeO does not significantly impact the boron reactivity coefficient. A 5vol% UBO fuel has a negligible difference in the boron worth coefficient.

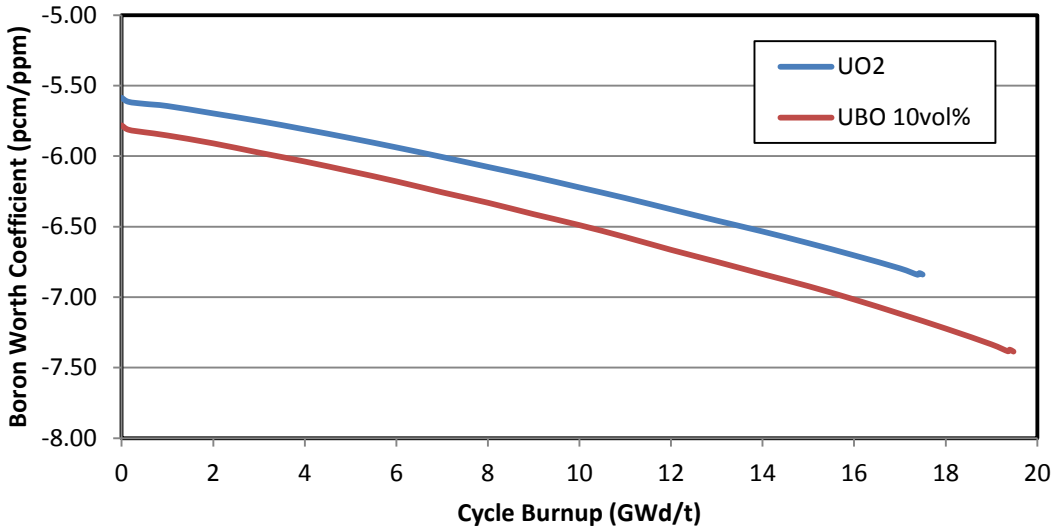

Figure 6.31 Boron worth coefficient for the 18-month cycle depletion.

6.2 Abridged 22-Month Equilibrium Cycle

6.2.1 Initial Cycle Optimization

6.2.1.1 Burnup Analysis

Similar to the previous 18-month cycle optimization, an initial equilibrium cycle was performed using the original EPR shuffle map design. As before, no assembly rotation was assumed so as to establish a baseline case for optimization. The initial incremental analysis for all 241 core assemblies with quadrant burnup is shown in Figure 6.32.

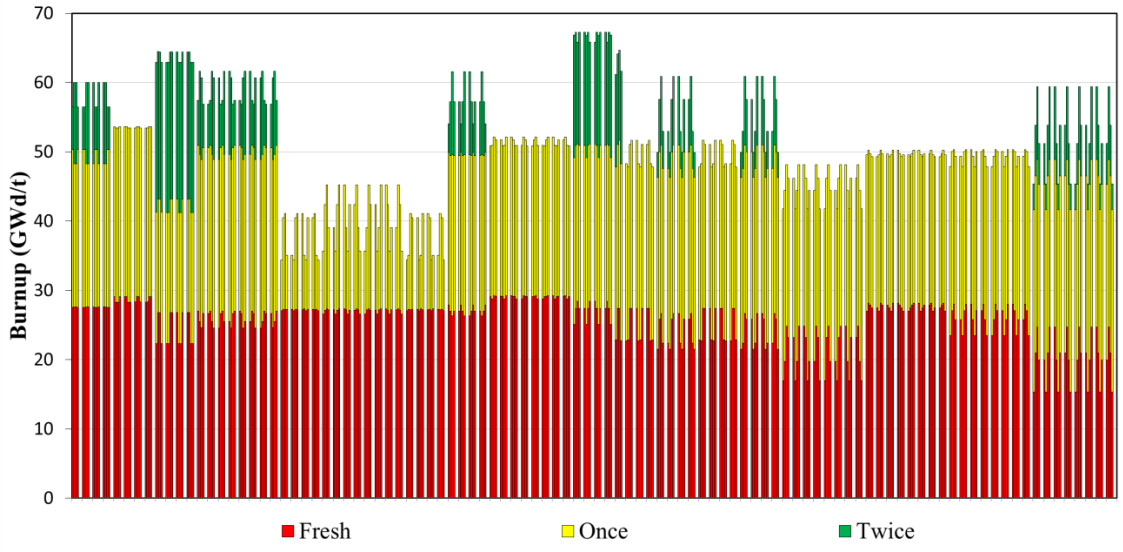

Figure 6.32 Initial incremental burnup analysis for all 241 assemblies, including the four assembly quadrants. The original EPR 22-month shuffle map with no assembly rotation was used for the UO_2 fuel.

The incremental assembly burnup for the 22-month cycle exhibits significant differences compared to the 18-month cycle. Some assemblies are removed early from the core with a relatively low burnup while other assemblies experience a relatively high burnup. This causes the average burnup of an assembly to deviate significantly from the core average burnup. The individual assembly quadrant peaking can be easily corrected with a proper assembly rotation. However, the uneven assembly burnup with respect to the core average burnup requires significant changes to the original shuffle map.

6.2.1.2 New Shuffle Map

Addition cycle requirements may have influenced the choice of the initial EPR 22-month shuffle map. The uneven assembly burnup with respect to the core average burnup may have been a compromise with other cycle constraints not documented in the EPR reference. Therefore, the goal of the 22-month cycle optimization was to make as few shuffle map changes as possible while minimizing the maximum assembly burnup. This was accomplished by moving the high burned assemblies to lower burned areas of the core. An iterative process was used until a final shuffle map was determined, as shown

in Figure 6.33. The main objective of the new cycle optimization was to reduce the maximum 3D burnup.

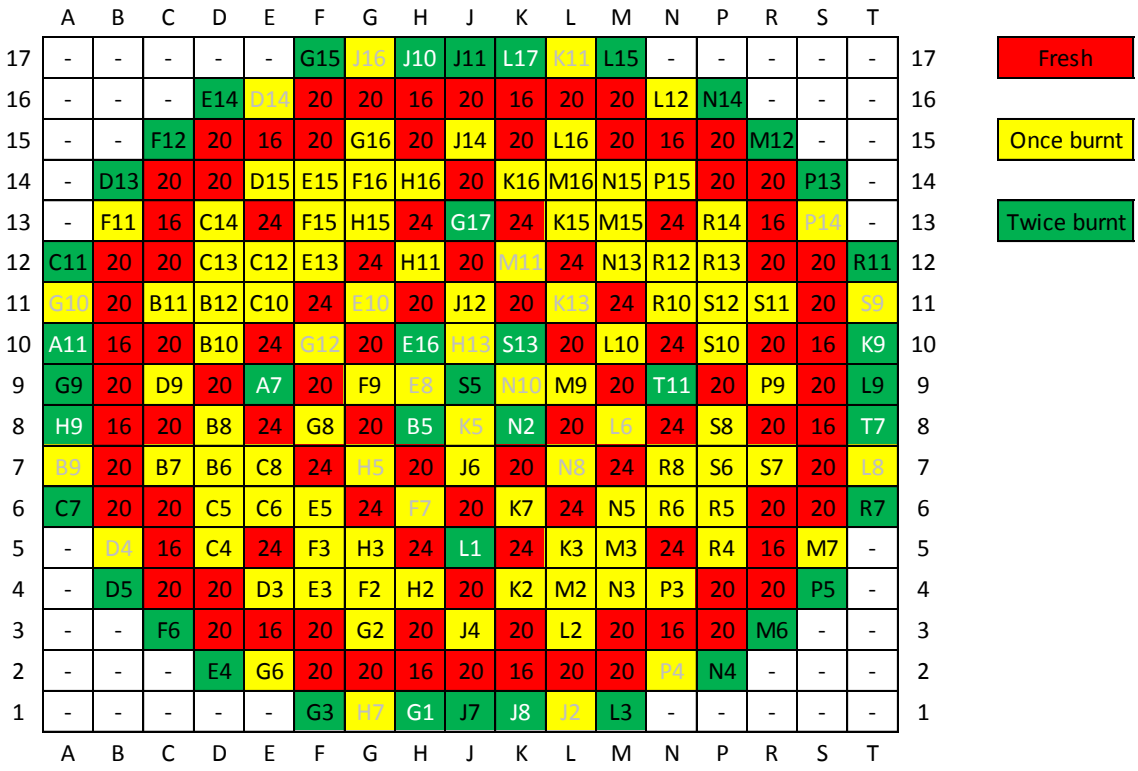

Figure 6.33 Final shuffle map chosen for the 22-month equilibrium cycle. White/grey highlighted locations represent a change from the original shuffle map.

The number of reload and in-core assemblies for the 22-month cycle is summarized in Table 6.7. Table 6.8 shows the core average power density for the three different fuel types studied. The core average power density is weighted by the number of in-core assemblies and their respective assembly type power density. Power density for each assembly type is different depending on the number of Gadolinium rods and BeO addition.

Table 6.7 Number of assemblies in a 22-month equilibrium cycle

	Number of Assemblies	
Assembly Type	**Reload**	**In-core**
Gd-16	16	32
Gd-20	64	160
Gd-24	20	49
Total	100	241

Table 6.8 Power densities for the 22-month equilibrium cycle

Fuel Type	**Core Avg Power Density (kW/kgU)**
UO_2	34.773
UBO 5vol%	36.472
UBO 10vol%	38.342

6.2.1.3 Assembly Rotation

After the final shuffle map was set, the assembly rotation map was determined. Quarter-core symmetry reduced the number of rotations to evaluate. A few iterations were required to obtain uniform assembly burnup. An efficient assembly rotation was determined using best engineering judgment. Figure 6.34 shows the final assembly rotation map for the 22-month cycle.

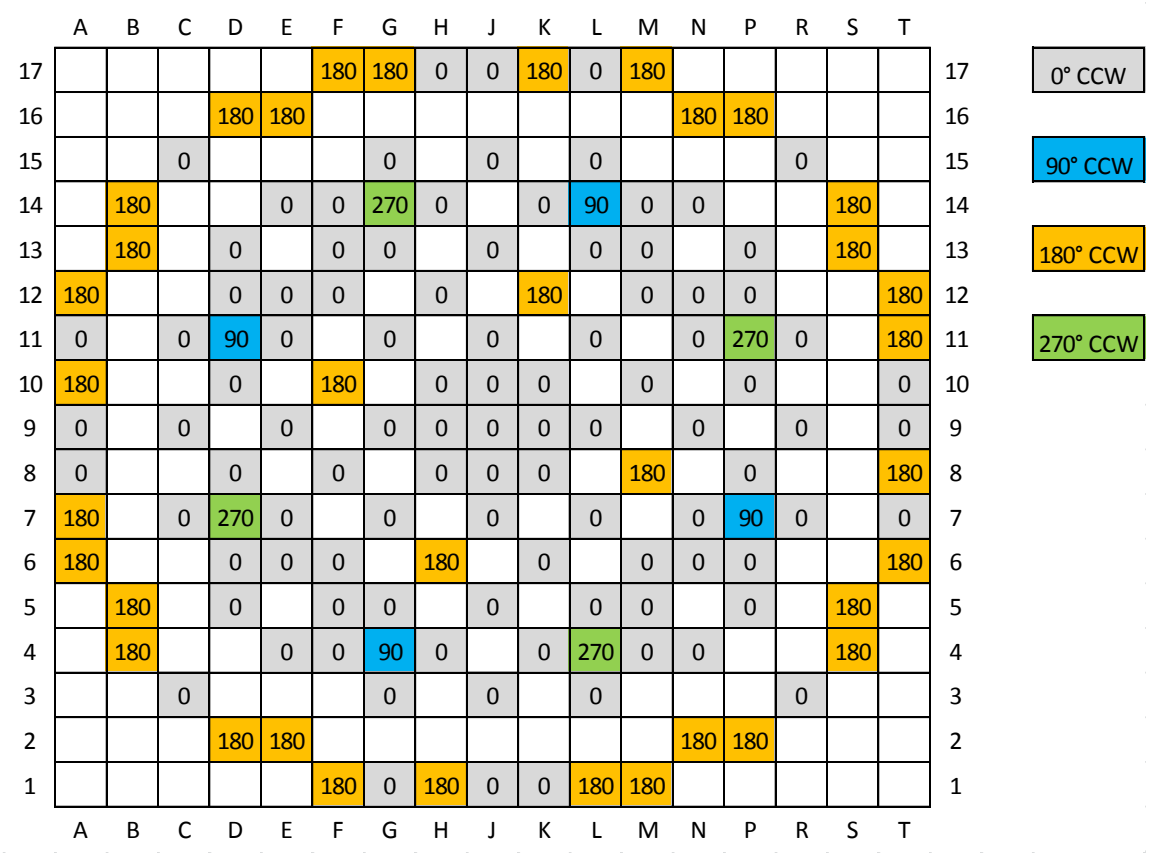

Figure 6.34 Rotation map for the final 22-month shuffle pattern.

6.2.1.4 Optimized Cycle Parameters

Optimizing the 22-month cycle was more challenging because there were more shuffling options available. The 18-month cycle had a relatively uniform core burnup so that the numbers of shuffling options were limited. Since the 22-month cycle had many possible variations, the main goal was to reduce the maximum 3D burnup rather than find the most efficient cycle burnup. Obtaining a low assembly burnup was important because the UBO fuel would certainly increase the maximum 3D burnup value. Similar to the previous cycle optimization, assemblies with a high burnup were moved to lower burnup areas of the core. An incremental burnup analysis using the final shuffle map and rotation is shown in Figure 6.35. A summary of the key cycle parameters is given in Table 6.9.

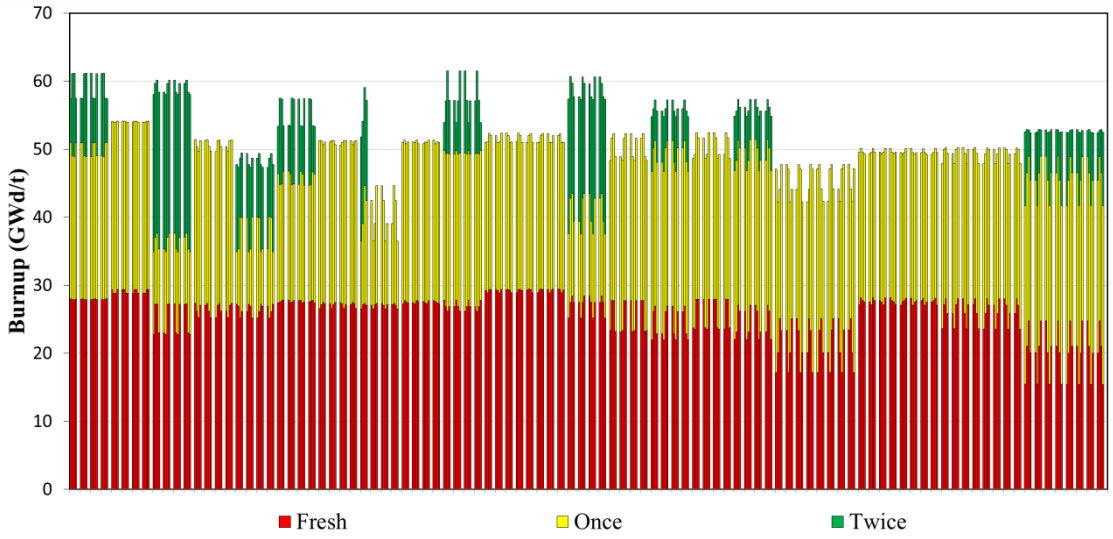

Figure 6.35 Final incremental burnup analysis for all 241 assemblies, including the four assembly quadrants. The updated 22-month shuffle map and assembly rotation was used for the UO_2 fuel.

Table 6.9 Optimized 22-month cycle parameters

Cycle Parameter	Original Shuffle Map with no Rotation	New Shuffle Map with Rotation
Core Avg Burnup (MWd/t)	40,171	39,963
EOC Burnup (MWd/t)	21,494	21,741
Cycle Length (days)	618.1	625.2
Max 3D Burnup (MWd/t)	73,928	67,417
Max 3D PPF	1.74997	1.74872
Max 3D Enthalpy Rise	1.4118	1.41422
BOL Boron (ppm)	1628.0	1648.5
BOL AO (%)	0.93653	1.26775
EOL AO (%)	-2.21181	-2.36791

A substantial cycle length increase of 7.1 days occurs due to the final optimized shuffle map and assembly rotation. In addition, the maximum 3D burnup was reduced by 6511 MWd/t to 67,417 MWd/t. Other key cycle parameters show minor changes after the

optimization. Therefore the cycle optimization results in significant improvements without a reduction in safety parameters.

6.2.2 UBO-UO_2 Comparisons

6.2.2.1 Cycle Length

The UBO fuel cycles were performed using the same optimized shuffle map and assembly rotation as the UO_2 fuel to provide an accurate comparison. In addition, there were no changes in assembly design or the number of Gadolinium rods for the UBO fuel cycles. The entire UO_2 fuel core was replaced with UBO fuel. Figure 6.36 compares the cycle burnup for UO_2 and UBO 10vol% fuels. UBO 5vol% fuel is omitted for clarity as it follows a similar cycle depletion as the 10vol% fuel.

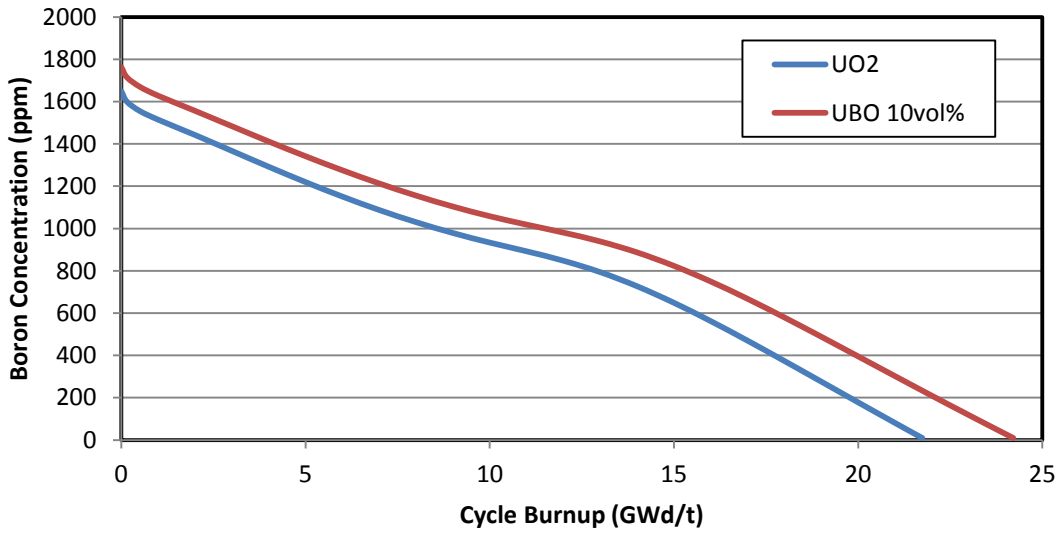

Figure 6.36 Boron concentration for the 22-month cycle depletion for UO_2 and UBO 10vol% fuels.

Initially the UO_2 cycle burnup was verified against the UK-EPR reference. The EPR reference shows an EOC burnup value of approximately 22,000 MWd/t [9]. Results in Figure 6.36 are in good agreement with the EPR design value. Table 6.10 summarizes important 22-month cycle information.

Table 6.10 22-month cycle length comparison between UO_2 and UBO fuels

Fuel Type	Core Avg Burnup (MWd/t)	Max 3D Burnup (MWd/t)	EOC Burnup (MWd/t)	Cycle Length (days)	Δ Cycle Length (days)
UO_2	39,962	67,417	21,741	625.2	-
UBO 5vol%	42,300	70,439	22,941	629.0	3.8
UBO 10vol%	44,784	74,036	24,210	631.4	6.2

The UBO 5vol% and 10vol% fuels have an increased core average burnup of 2338 and 4822 MWd/t, respectively. These results are similar to the 2D DRAGON cycle analysis. The corresponding cycle length increase is 3.8 and 6.2 days, respectively. However the maximum 3D burnup has a significant increase of 3022 and 6619 MWd/t, respectively. Reduction of the maximum 3D burnup could be achieved with selective radial and/or axial placement of the UBO fuel.

7 ECONOMICS

The economics of the nuclear fuel cycle can be split into front-end and back-end costs. Front-end costs are any costs associated with the production of the fuel prior to operation. Front-end fuel costs include the uranium purchase, conversion, enrichment, and fabrication. For UBO fuel, the BeO purchase and fabrication would also be considered a front-end cost.

Back-end costs are incurred after the fuel is removed from the reactor. The back-end costs may vary depending the on the disposal option. Two prominent disposal options are direct disposal and recycling. There is a potential benefit for UBO fuel if recycling is considered. Since BeO is relatively expensive, there is a potential credit for recycling BeO as opposed to direct disposal. However since the back-end costs are more difficult to estimate and the time scales are considerably longer, no back-end costs were calculated.

7.1 Levelized Fuel Cost

A levelized fuel cost is a useful metric for comparing different fuel options. The net present value (NPV) of the fuel costs is computed at a chosen reference date. Similarly, the net present value of the energy production is computed at the same reference date. The levelized fuel cost can then be simply calculated using Eq. (7-1). Graphically, the levelized fuel cost (LFC) calculation is shown in Figure 7.1.

$$LFC = \frac{net\ present\ value\ fuel\ cost}{net\ present\ value\ energy\ cost} \qquad (7\text{-}1)$$

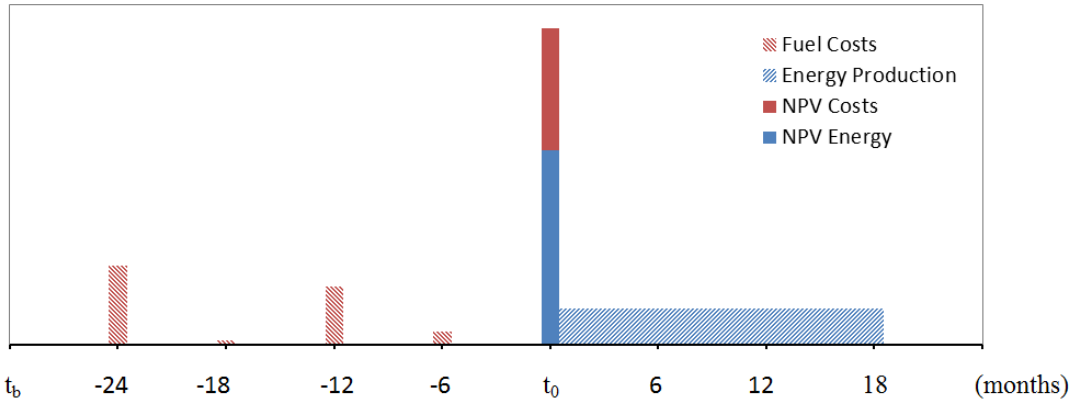

Figure 7.1 Net present value of the fuel costs and energy production for a levelized cost calculation. UBO fuel costs are not shown. Vertical axis not to scale.

Individual component fuel costs are calculated according to Nuclear Energy Agency report concerning the economics of the nuclear fuel cycle [14]. Fuel costs generally have a mass component, loss factors, applicable conversion factors, a unit cost escalation rate, and a time conversion factor back to a specified reference date. The cost of Uranium purchase is shown in Eq. (7-2) [14].

$$C_U = m_f a f_U P_U (1 + s_U)^{t - t_b} \qquad (7\text{-}2)$$

C_U is the cost of uranium purchase (\$), m_f is the mass of uranium feed (kg), a is a conversion factor from kg U to lb U_3O_8, f_U is the total uranium loss factor, P_U is the price of uranium (\$/lb U_3O_8), s_U is the escalation rate of uranium prices, t is time and t_b is the reference date of the unit price. The mass of uranium feed can be calculated using Eq. (7-3) [14].

$$m_f = \frac{(e_p - e_t)}{(e_f - e_t)} m_p \qquad (7\text{-}3)$$

m_p is the mass of uranium product desired (kg), e_p is the enrichment of the desired uranium product, e_t is the enrichment of the uranium tails (~0.25%), and e_f is the

enrichment of the feed uranium (~0.711%). Any applicable uranium loss factors are calculated using Eq. (7-4) [14].

$$f_U = (1 + l_C)(1 + l_E)(1 + l_F) \tag{7-4}$$

l_C represents losses in the conversion stage, l_E is losses in the enrichment stage, and l_F is losses in fabrication. The cost of Uranium conversion is calculated using Eq. (7-5) [14].

$$C_C = m_f f_C P_C (1 + s_C)^{t - t_b} \tag{7-5}$$

C_C is the cost of conversion ($), f_C is total loss factor during conversion, P_C is the price of conversion ($/kgU), and s_C is the escalation rate for the price of conversion. Total conversion loss factor can be calculated using Eq. (7-6) [14].

$$f_C = (1 + l_C)(1 + l_E)(1 + l_F) \tag{7-6}$$

Cost of enrichment depends on an additional factor known as the SWU (Separation Working Units) costs. Calculation of the enrichment costs is performed with Eq. (7-7) and the SWU calculation is performed with Eq. (7-8) [14].

$$C_E = S f_E P_E (1 + s_E)^{t - t_b} \tag{7-7}$$

C_E is the cost of enrichment ($), S is the SWU factor, f_E is the total enrichment loss factor, P_E is the price of enrichment ($/SWU), and s_E is the price escalation rate of enrichment.

$$S = m_p V_p + (m_f - m_p) V_t - m_f V_f \tag{7-8}$$

Calculation of the SWU factor also requires separation potentials. Calculation of the separation potentials are shown in Eq. (7-9) [14].

$$V_x = (2e_x - 1) ln\left(\frac{e_x}{1 - e_x}\right) \tag{7-9}$$

The subscript x can represent f, p, or t. Total loss factor during enrichment is calculated with Eq. (7-10) [14].

$$f_E = (1 + l_E)(1 + l_F) \tag{7-10}$$

Equation (7-11) shows the cost of fabrication. The total loss factor for fabrication is shown in Eq. (7-12) [14].

$$C_F = m_p f_F P_F (1 + s_F)^{t-t_b} \tag{7-11}$$

C_F is the cost of fabrication ($), f_F is the total fabrication loss factor, P_F is the price of fabrication ($/kgU), and s_F is the escalation rate for the price of fabrication.

$$f_F = (1 + l_F) \tag{7-12}$$

Since the cost of BeO is a new consideration, the calculation was assumed to follow a similar pattern as the previous calculations. The BeO cost and fabrication costs were calculation using Eq. (7-13) and Eq. (7-14), respectively.

$$C_B = m_B f_B P_B (1 + s_B)^{t-t_b} \tag{7-13}$$

C_B is the cost of BeO purchased ($), m_B is the mass of BeO (kg), f_B is the total loss factor for BeO, P_B is the price of BeO ($/kg BeO), and s_B is the escalation rate of BeO prices.

$$C_{B,F} = m_B f_{B,F} P_{B,F} \left(1 + s_{B,F}\right)^{t-t_b} \tag{7-14}$$

$C_{B,F}$ is the cost of BeO fabrication ($), $f_{B,F}$ is the total BeO loss factor during fabrication, $P_{B,F}$ is the price of BeO fabrication ($/kg BeO), and $s_{B,F}$ is the escalation rate of BeO fabrication prices.

The net present value for a discrete purchase can be calculated using Eq. (7-15). A discrete purchase would be a fuel cost that is purchased at a single point in time. However, energy is produced continuously. Therefore a continuous discounting method is applied for the energy production calculation, as given in Eq. (7-16).

$$NPV = \frac{NFV}{(1+r)^{t-t_0}} \tag{7-15}$$

NPV is the net present value, NFV is the net future value, r is the discount rate (or interest rate), and t_0 is the reference date at which the net present value is calculated.

$$NPV = NFV e^{-r'(t-t_0)} \tag{7-16}$$

An effective interest rate (r') must be used for continuous compounding. Calculating the effective interest rate is given in Eq. (7-17).

$$r' = ln(1+r) \tag{7-17}$$

Finally, the levelized fuel cost (LFC) can be calculated by equating the net present value of all the individual component costs to the energy produced over a given time period. Dividing the NPV of all the components costs by the energy production gives the LFC ($/MWh), as shown in Eq. (7-18) [14]. The NPV must be calculated because the individual component costs occur at different future times during the fuel cycle.

$$LFC = \frac{\sum_i \sum_t \frac{C_i(t)}{(1+r)^{(t-t_0)}}}{\sum_t \frac{E(t)}{e^{r'(t-t_0)}}} \tag{7-18}$$

7.2 Economic Parameters

Economic parameters used for the UO_2 and UBO fuel comparisons are summarized in Table 7.1. The analysis was simplified by assuming the escalation rate and loss factors were zero. Lead times were assumed from the Nuclear Energy Agency report [14]. Unit

prices were obtained from Ux Consulting [15]. The price of BeO and BeO fabrication were assumed using a best estimate.

Table 7.1 Parameters for economic calculations

Component	Annual Escalation Rate	Material Losses	Lead Time (months)	Unit Price	Unit Basis
Uranium purchase	0.00%	0.00%	24	52	\$/lb U_3O_8
Conversion	0.00%	0.00%	18	7	\$/kgU
Enrichment	0.00%	0.00%	12	138	\$/SWU
Fabrication	0.00%	0.00%	6	250	\$/kgU
BeO cost	0.00%	0.00%	24	350	\$/kg BeO
BeO fabrication	0.00%	0.00%	6	250	\$/kg BeO

7.3 Reload Requirements

Cycle reload requirements are important for economic calculations. The amount of enriched uranium is determined by the fuel density, enrichment, assembly design, and number of reload assemblies. Since the Gadolinium pins contained a different enrichment and fuel density, the reload requirements were calculated separately for both the fuel pins and Gadolinium pins. In addition, the SWU requirements were different due to the different Uranium enrichments. The reload requirements for the fuel pins and Gadolinium pins were combined for a single total. A summary of the reload requirements for the 18- and 22-month equilibrium cycle can be found in Table 7.2 and Table 7.3, respectively.

Table 7.2 Reload requirements for an 18-month equilibrium cycle (72 Assemblies)

Component (metric tons)	UO_2	UBO 5vol%	UBO 10vol%
Feed Uranium	390.5	391.5	392.5
SWU/MTU	299.1	304.0	309.1
Enriched Uranium	38.554	36.705	34.855
U-235	1.896	1.896	1.896
U-238	36.658	34.808	32.958
BeO	0.000	0.607	1.213
Gd_2O_3	0.154	0.154	0.154

Table 7.3 Reload requirements for a 22-month equilibrium cycle (100 Assemblies)

Component (metric tons)	UO_2	UBO 5vol%	UBO 10vol%
Feed Uranium	534.1	535.4	536.7
SWU/MTU	407.8	414.5	421.3
Enriched Uranium	53.366	50.880	48.394
U-235	2.595	2.595	2.595
U-238	50.771	48.285	45.799
BeO	0.000	0.815	1.631
Gd_2O_3	0.360	0.360	0.360

As shown in Table 7.2 and Table 7.3, the amount of ^{235}U required is constant because of the assumption of mass equivalence. Overall the enriched uranium requirement decreases because of the ^{238}U displaced by the BeO addition. However, the feed uranium must be increased to meet the mass equivalent enrichment of the UBO fuel. From Eq. (7-3), a higher enrichment increases the feed requirement.

The UBO fuel has higher SWU requirements than the nominal UO_2 fuel. Eq. (7-8) shows the SWU requirement increases with increased enrichment and feed requirements. Although BeO occupies a large volume of the fuel, the mass of BeO required is low due to the low density. Lastly, the Gadolinium requirement is constant because there were no assembly design changes and no BeO was added to the Gadolinium pins.

7.4 18-Month Equilibrium Cycle

Calculation of the LFC for the 18-month cycle was performed using Eq. (7-18), the economic parameters in Table 7.1, and the reload requirements in Table 7.2. Initially the LFC was computed for each fuel type without assuming any cycle extension. These calculations indicate whether the UBO fuel was more economical based on the material requirements alone. All the economic calculations were performed assuming a nominal discount rate of 5%. The discount rate, or interest rate, is a per annum rate. A summary of the 18-month cycle results is shown in Table 7.4.

Table 7.4 18-month cycle results at nominal discount 5% with no cycle extension.

	Levelized Fuel Cost ($/MWh)		
Component	**UO_2**	**UBO 5vol%**	**UBO 10vol%**
Uranium purchase	3.237	3.246	3.254
Conversion	0.163	0.163	0.164
Enrichment	2.398	2.438	2.479
Fabrication	0.547	0.520	0.494
BeO cost	0.000	0.013	0.026
BeO fabrication	0.000	0.009	0.017
Total	6.345	6.389	6.434

Results in Table 7.4 show that the UBO fuel is more expensive due to the increased component costs. The largest component increase is from the enrichment cost. Figure 7.2 shows the costs difference of the various fuel components.

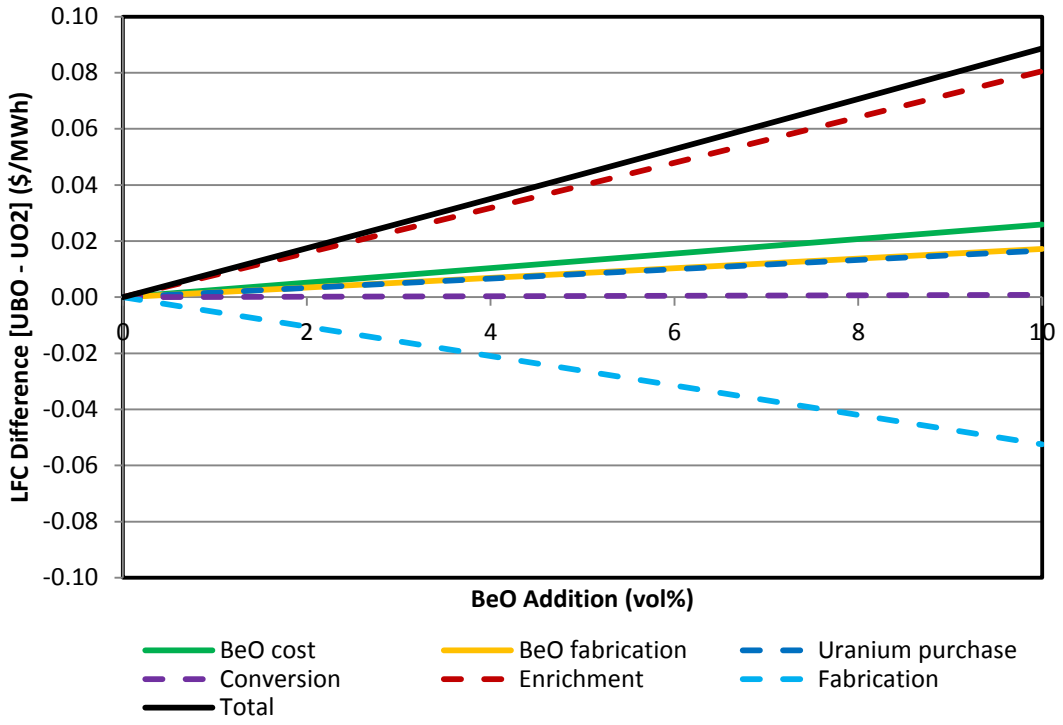

Figure 7.2 Component cost difference between UO_2 and UBO fuel at nominal discount 5% for the 18-month cycle with no cycle extension.

As shown in Figure 7.2, all fuel component costs are higher for the UBO fuel with the exception of the fabrication. However, the fabrication price of UBO fuel is only positive because of the reduced enriched uranium requirement of UBO fuel. Equation (7-11) is dependent on the mass of enriched uranium only. The fabrication cost may not be realistic because the number of reload assemblies remains the same for both UO_2 and UBO fuels.

Since UBO fuel is more expensive, a cycle increase is required to offset the higher component costs. An increased cycle length reduces the LFC because of the longer operational time. Figure 7.3 shows the LFC as a function of increased cycle length. The break-even LFC occurs when the UO_2 LFC is equivalent to the UBO LFC.

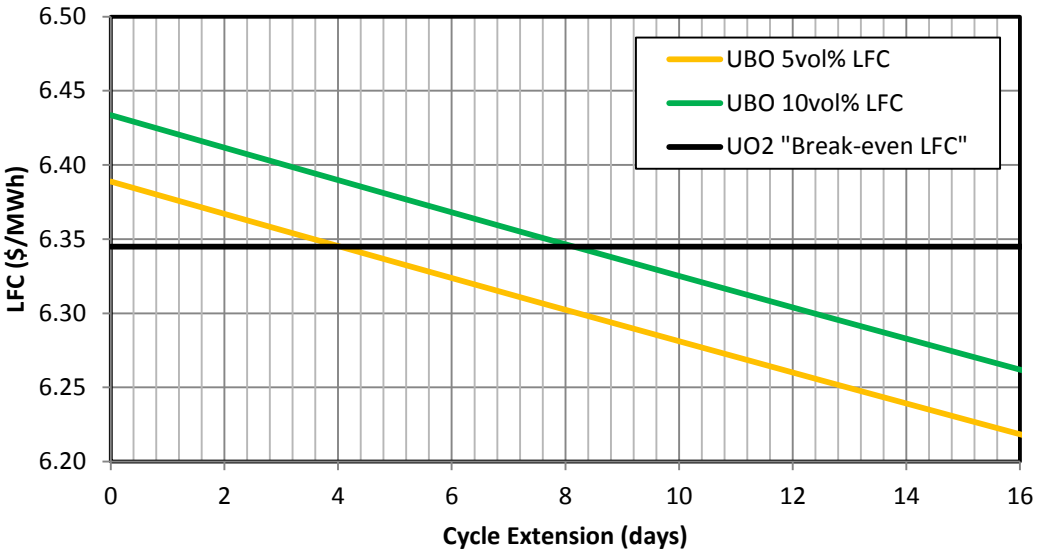

Figure 7.3 Effect of cycle extension on the total levelized fuel cost of UBO fuel for 18-month cycle at nominal discount of 5%.

The break-even LFC occurs at a cycle extension of approximately 4 and 8 days for the UBO 5vol% and UBO 10vol% fuels, respectively. A UBO cycle length less than the break-even point would not be able to recover the extra component costs. Table 7.5 summarizes the economic difference between UO_2 and UBO fuels. The actual UBO cycle extension was determined from the 3D core simulation results in Table 6.5. It is convenient to compare the LFC difference by adjusting to a reload assembly basis. Using the cycle length and number of reload assemblies, the LFC is converted to dollars per reload assembly.

Table 7.5 18-month economic comparison

Fuel Comparison	Break-even Extension (days)	Cycle Extension (days)	LFC ($/MWh)	LFC ($/reload assembly)
(UO_2 - UBO 5vol)	4.03	2.20	-0.020	-$12,365
(UO_2 - UBO 10vol%)	8.15	3.30	-0.052	-$24,712

As shown in Table 7.5, the cycle extension provided from the UBO fuel is less than the economic break-even point. Therefore the UBO fuel has a negative LFC. A nominal UO_2 reload with 72 assemblies would cost $123.3 million. The UBO 5vol% and UBO 10vol% reload would cost an additional $890,275 and $1,779,287 respectively. This is an increase in reload cost of 0.722% and 1.44%, respectively.

7.5 22-Month Equilibrium Cycle

Calculation of the LFC for the 22-month cycle was performed using Eq. (7-18), the economic parameters in Table 7.1, and the reload requirements in Table 7.3. All the economic calculations were performed assuming a nominal discount rate of 5%. A summary of the 22-month cycle results is shown in Table 7.6.

Table 7.6 22-month cycle results at nominal discount 5% with no cycle extension.

	Levelized Fuel Cost ($/MWh)		
Component	**UO_2**	**UBO 5vol%**	**UBO 10vol%**
Uranium purchase	3.682	3.691	3.701
Conversion	0.185	0.186	0.186
Enrichment	2.720	2.765	2.810
Fabrication	0.629	0.600	0.571
BeO cost	0.000	0.014	0.029
BeO fabrication	0.000	0.010	0.019
Total	7.216	7.265	7.315

Results of the 22-month cycle are similar to the 18-month cycle. The LFC is greater for the UBO fuels. Overall the LFC is higher for the 22-month cycle because of the increased number of reload assemblies. The effect of an increased cycle length on the LFC is shown in Figure 7.4. A summary of the 22-month economic comparison can be found in Table 7.7.

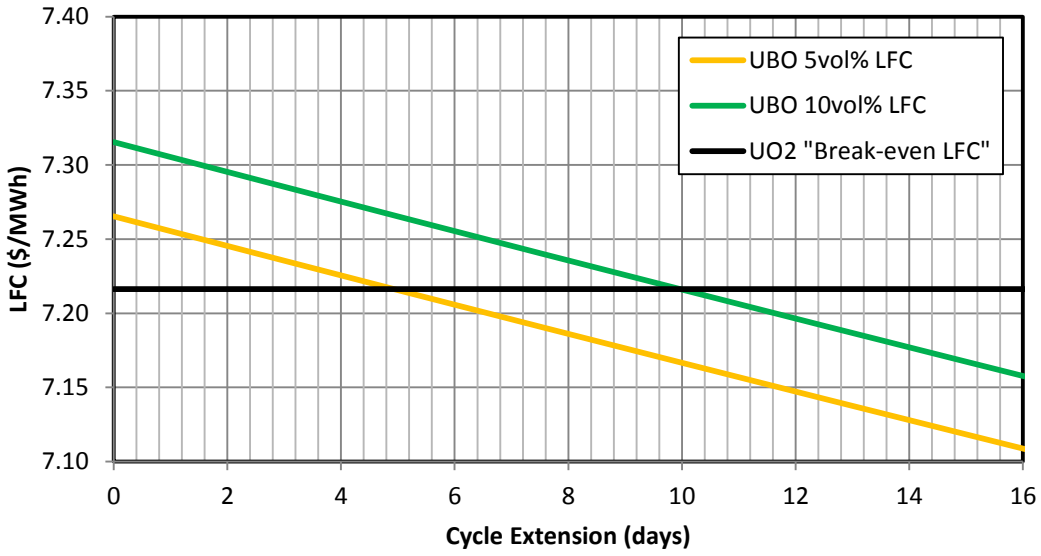

Figure 7.4 Effect of cycle extension on the total levelized fuel cost of UBO fuel for 22-month cycle at nominal discount of 5%.

Table 7.7 22-month economic comparison

Fuel Comparison	Break-even Extension (days)	Cycle Extension (days)	LFC ($/MWh)	LFC ($/reload assembly)
(UO_2 - UBO 5vol%)	4.93	3.80	-0.011	-$12,546
(UO_2 - UBO 10vol%)	9.97	6.20	-0.037	-$25,004

Similar to the 18-month cycle, the cycle extension provided from the UBO fuel is less than the economic break-even point. Therefore the UBO fuel has a negative LFC. A nominal UO2 reload with 100 assemblies would cost $171.5 million. The UBO 5vol% and UBO 10vol% reload would cost an additional $1.255 and $2.500 million, respectively. This is an increase in reload cost of 0.732% and 1.46%, respectively.

8 CONCLUSIONS

8.1 Summary

The addition of Beryllium oxide to conventional Uranium oxide fuels has been extensively studied. Many research areas have been explored in this M.S. thesis concerning the neutronic and fuel performance aspects of UBO fuel. UBO fuel is promising because of the increased thermal conductivity provided by the BeO addition. The main disadvantage of the current and widely used UO_2 fuel is the low thermal conductivity. Low thermal conductivity results in a high operating fuel temperature, which ultimately causes poor fuel performance. A UBO fuel is also beneficial as reactivity gains and cycle extensions are possible due to the favorable neutronic properties of BeO.

From the pellet heat conduction analysis, the increased thermal conductivity of UBO fuel provided a decreased fuel temperature. The centerline temperature is significantly reduced depending on the amount of amount of BeO added. However, the reactivity effect due to the reduced temperature is marginal compared to other lattice physics effects. Therefore the reduced temperature may be a more significant benefit for fuel performance rather than neutronic effects. An important concern of UBO fuel is the eutectic melting point. At peak linear powers, the UBO fuel has less fuel melting margin than standard UO_2 fuel.

The 2D lattice physics calculations revealed important results about the neutronic properties of UBO fuel. Analysis of the four factor formula showed that the resonance escape probability was greatly influenced by the BeO addition. With the assumption of ^{235}U mass equivalence, the BeO addition primarily displaces ^{238}U. The reduction of the strong resonant absorber ^{238}U caused the resonance escape probability to increase, resulting in a positive 1440 pcm reactivity addition. The BeO material addition itself provided little neutronic benefit. A -146 pcm penalty was incurred due to the BeO addition, but this was nearly compensated by the positive 137 pcm temperature effect. The BeO addition caused a slight reactivity penalty because of the homogeneous versus

heterogeneous lattice physics effect. Overall, the UBO fuel exhibits a positive reactivity gain.

Using the linear reactivity model provided many important cycle length results. A significant result is that the enrichment in ^{235}U of UBO fuels must increase to meet the cycle length of standard UO_2 fuel. The positive neutronic effects of UBO fuel does not compensate for the displaced uranium. Therefore, an increased mass of ^{235}U is required. Cycle length comparisons using the linear reactivity model must include the correct LRM multiplier. The LRM multiplier can include unequal batch sizes, assembly type weighting, and leakage models. Early cycle length comparisons were performed without including the LRM multiplier, leading to overestimation of the cycle increase of UBO fuels. The error was located after comparing results to the 3D core simulations.

The 3D core simulations provided cycle length results, peaking factors, and reactivity coefficients for the UBO fuels. Using a mass equivalent basis, the UBO fuels showed increased burnup and cycle length compared to the standard UO_2 fuel. One potential issue with UBO fuel is that the maximum 3D burnup peaking is significantly increased. Regulatory burnup limitations may result in selective radial and axial BeO placement. The power peaking factors for UBO fuels are highest at BOC. At EOC, the power peaking for UBO and UO_2 fuels are similar. Reactivity coefficients for UBO fuels are marginally different from UO_2 fuel. Since the BeO addition is small, UBO fuel has similar neutronic properties as UO_2 fuel.

Economic comparisons of UO_2 and UBO fuel were performed using a levelized fuel cost method. The analysis was simplified by only considering the front-end costs of manufacturing fuel. If one considers only the Uranium displaced by the BeO addition, the amount of uranium feed required for each fuel assembly would decrease. However, a mass equivalent UBO fuel actually requires more uranium feed due to the increased enrichment, resulting in increased fuel costs. In addition, the extra cost due to BeO purchase and BeO fabrication increases the fuel costs slightly more. From an analysis of each fuel cost component, the largest fuel cost was due to the increased enrichment

requirement. The extra fuel cost of UBO fuel could be compensated by a cycle length extension. However, results from the neutronic and economic analysis showed that UBO fuel does not meet the break-even fuel cost of standard UO_2 fuel.

8.2 Future Work

The 3D core simulations can be expanded to include radial and axial placement of UBO fuel. Replacing the entire core with UBO fuel is a coarse, base-line case. Additional loading patterns could be developed considering only select assembly locations and axial locations. In addition, the assembly design could be modified to include only BeO in select hot pins rather than all of the pins. The reduced temperature effect could be beneficial for the hot pin locations.

Future work should focus on smaller additions of BeO. The 10vol% BeO case is important for identifying and distinguishing neutronic properties, but may not be practical to fabricate. The increased ^{235}U enrichment requirement results in a significant fuel cost increase. Therefore, the amount of BeO added should be balanced with the positive fuel performance benefits. Increases in fuel performance or safety may justify the increased fuel costs.

REFERENCES

[1] Fink, J. K. (1999). Thermophysical Properties of Uranium Dioxide. *Journal of Nuclear Materials, 279*, 1-18.

[2] Ishimoto, S., Hirai, M., Ito, K., & Korei, Y. (1996). Thermal Conductivity of UO2-BeO Pellet. *Journal of Nuclear Science and Technology, 33*(2), 134-140.

[3] Sarma, K. H., Fourcade, J., Lee, S., & Solomon, A. A. (2006). New Processing Methods to Produce Silicon Carbide and Beryllium Oxide Inert Matrix and Enhanced Thermal Conductivity Oxide Fuels. *Journal of Nuclear Materials, 352*(1-3), 324-333.

[4] Latta, R., Revankar, S. T., & Solomon, A. A. (2008). Modeling and Measurement of Thermal Properties of Ceramic Composite Fuel for Light Water Reactors. *Heat Transfer Engineering, 29*(4), 357-365.

[5] McCoy, K., & Mays, C. (2008). Enhanced Thermal Conductivity Oxide Nuclear Fuels by Co-sintering with BeO: II. Fuel Performance and Neutronics. *Journal of Nuclear Materials, 375*(2), 157-167.

[6] Naramore, M. J. (2010). *High Thermal Conductivity UO2-BeO Nuclear Fuel: Neutronic Performance Assessments and Overview of Fabrication.* (Master's Thesis, Texas A&M University).

[7] Brookhaven National Laboratory. (2011). *National Nuclear Data Center.* Retrieved December, 2011, from www.nndc.bnl.gov/endf/

[8] Levin, E. M., Robbins, C. R., & McMurdie, H. F. (1989). *Phase Diagrams for Ceramists*. Columbus, Ohio: American Ceramic Society.

[9] AREVA NP & EDF SA. (2011). *UK EPR Generic Design Assessment*. Paris: AREVA.

[10] Driscoll, M. J., Downar, T. J., & Pilat, E. E. (1990). *The Linear Reactivity Model for Nuclear Fuel Management*. La Grange Park: American Nuclear Society.

[11] Stacey, W. M. (2007). *Nuclear Reactor Physics*. Weinheim: Verlag GmbH & Co, KGaA.

[12] Marleau, G., Herbert, A., & Roy, R. (2009). *A User Guide for DRAGON Version4* Institut de genie nucleaire, Department de genie mecanique, Ecole Polytechnique de Montreal.

[13] Todreas, N. E., & Kazimi, M. S. (1990). *Nuclear Systems I* New York: Taylor & Francis Group.

[14] Nuclear Energy Agency. (1994). *The Economics of the Nuclear Fuel Cycle*. Danvers: Organisation for Economic Co-operation and Development.

[15] The Ux Consulting Company, LLC. (2010). *UxC: Ux Consulting - The Nuclear Fuel Price Reporter*. Retrieved October 15, 2011, from www.uxc.com

APPENDIX A

A 22-MONTH CYCLE PARAMETERS

A.1 2D Radial and Axial Power Peaking

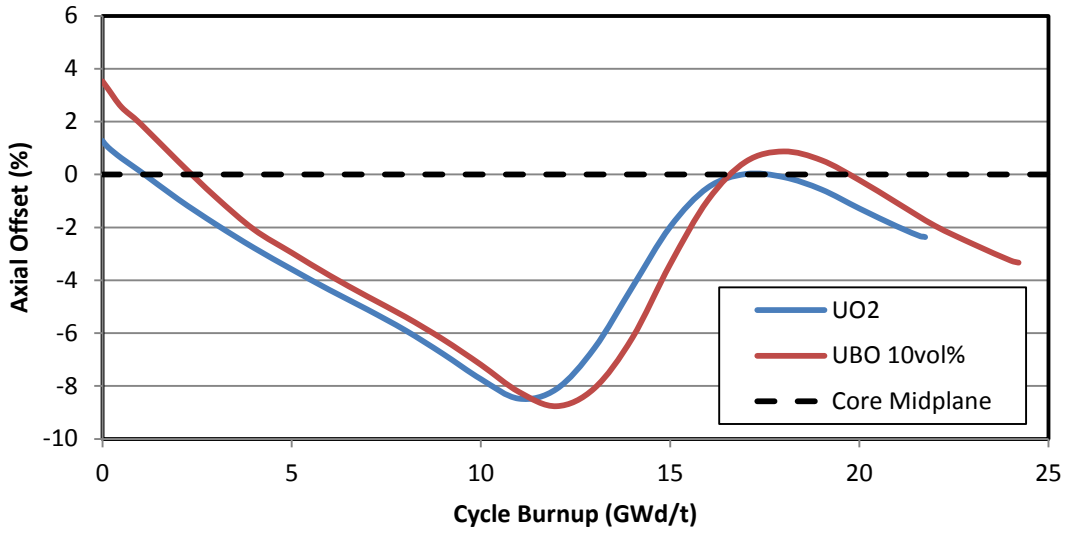

Figure A.1 Axial offset for the 22-month cycle depletion.

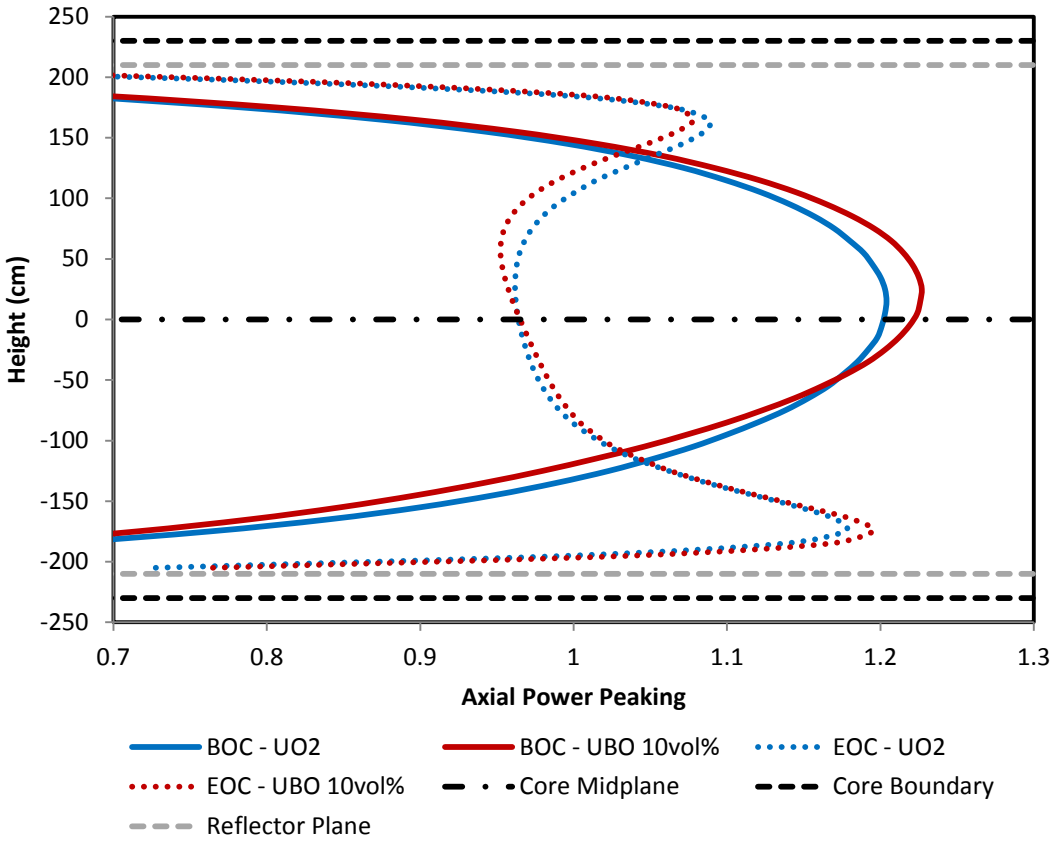

Figure A.2 Axial power distribution comparison of UO_2 and UBO 10vol% fuel type at BOC and EOC for the 22-month equilibrium cycle.

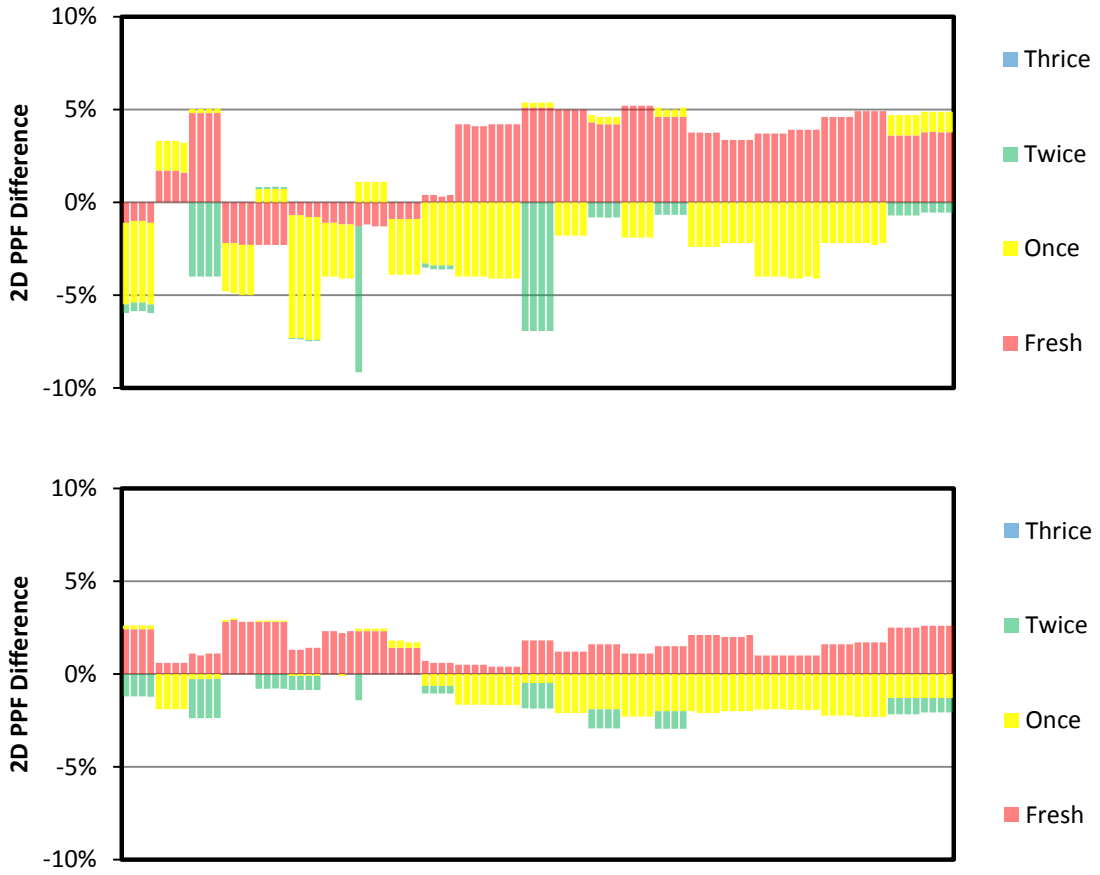

Figure A.3 BOC (top) and EOC (bottom) radial power difference between UBO 10vol% and UO_2 for the 22-month equilibrium cycle.

A.2 3D Power Peaking

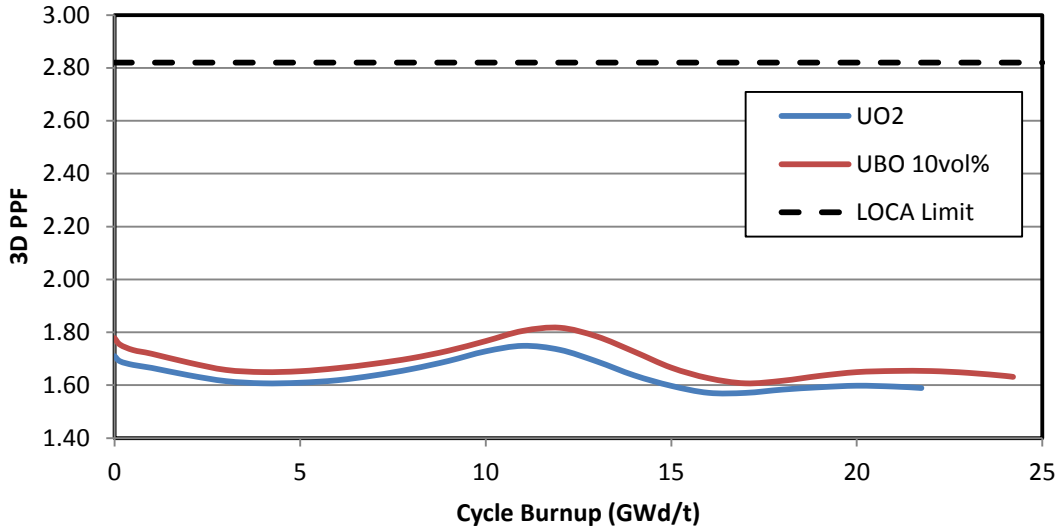

Figure A.4 3D power peaking factor for the 22-month cycle depletion for UO_2 and UBO 10vol% fuels. A maximum power peaking factor of 2.82 is allowed.

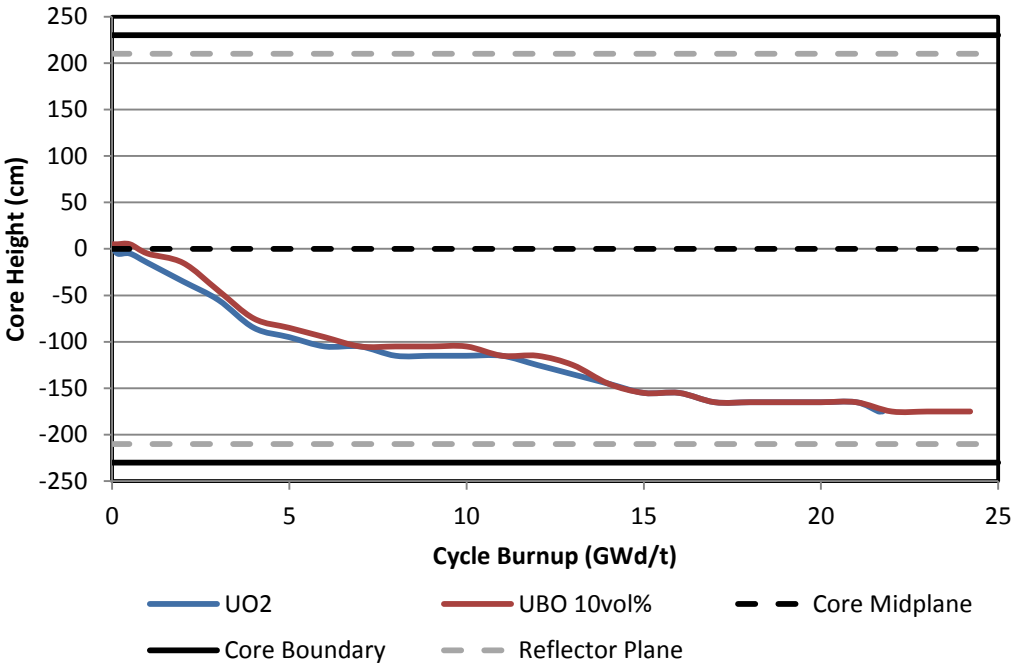

Figure A.5 Axial location of the 3D power peaking factor during the 22-month cycle depletion.

A.3 Enthalpy Peaking

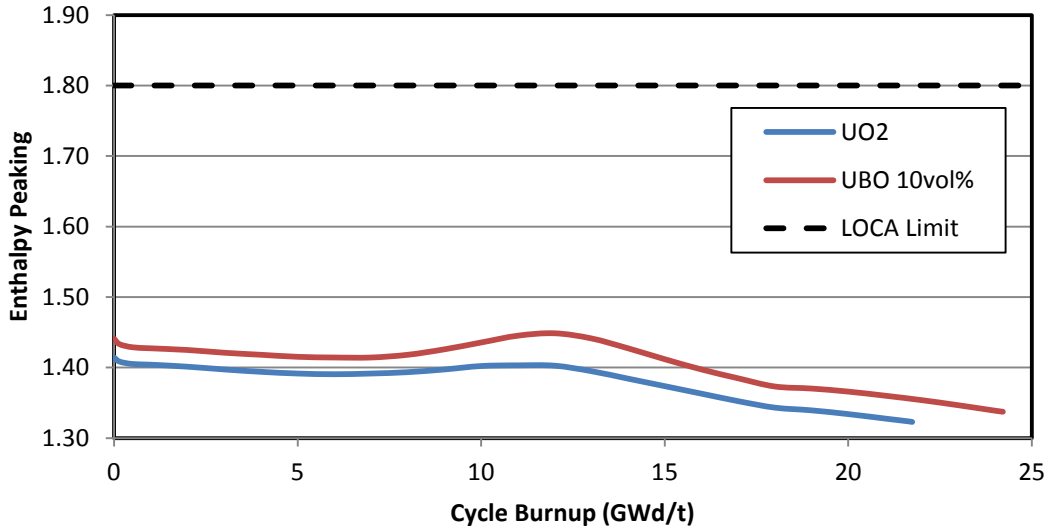

Figure A.6 Enthalpy rise hot channel factor for the 22-month cycle depletion. A maximum peaking of 1.80 is allowed.

A.4 Fuel Temperature

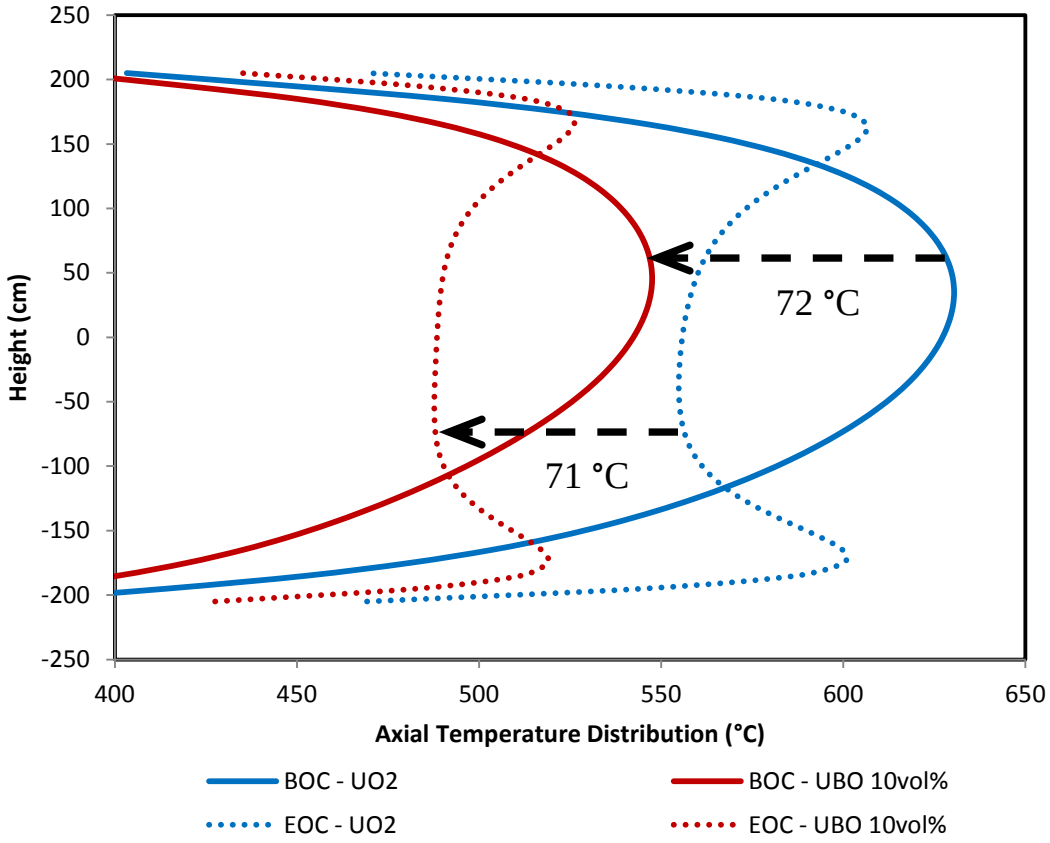

Figure A.7 22-month cycle axial fuel temperature distribution at BOC and EOC for UO_2 and UBO 10vol% fuel type.

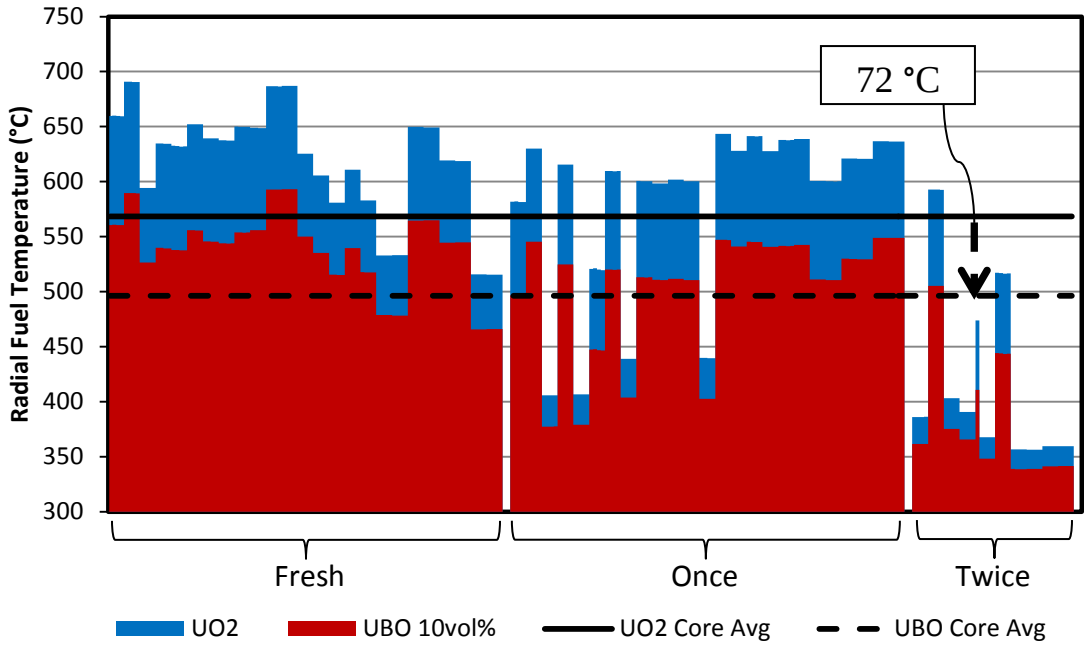

Figure A.8 22-month cycle radial fuel temperature distribution at BOC for UO_2 and UBO 10vol% fuel type.

Table A.1 Fuel temperature comparison for 22-month equilibrium cycle.

	Temperature (°C)	UO_2	UBO 10vol%	Difference
BOC	Core Average	568	496	-72
	Peak	774	659	-115
EOC	Core Average	566	495	-71
	Peak	713	607	-106

A.5 Reactivity Coefficients

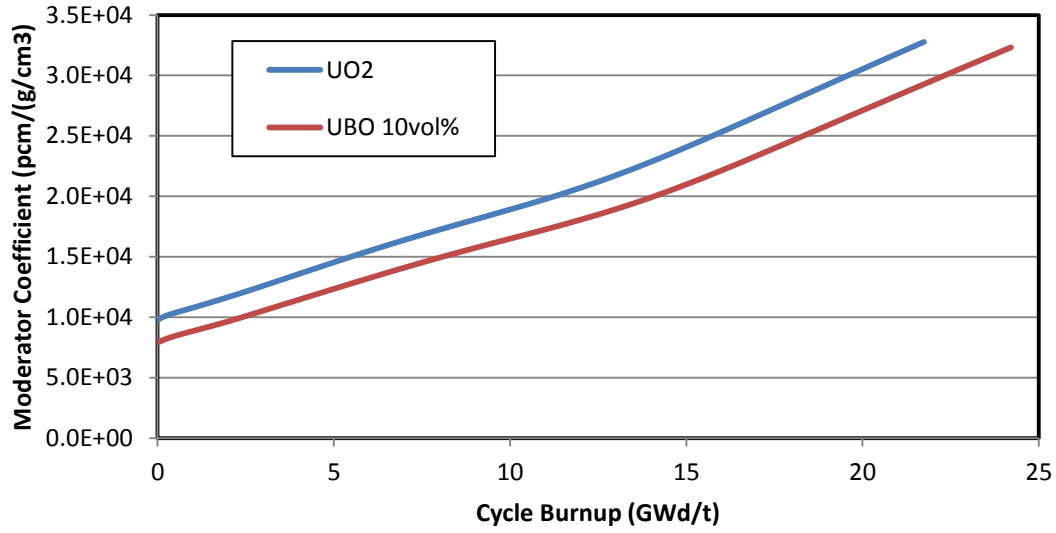

Figure A.9 Moderator density coefficient for the 22-month cycle depletion.

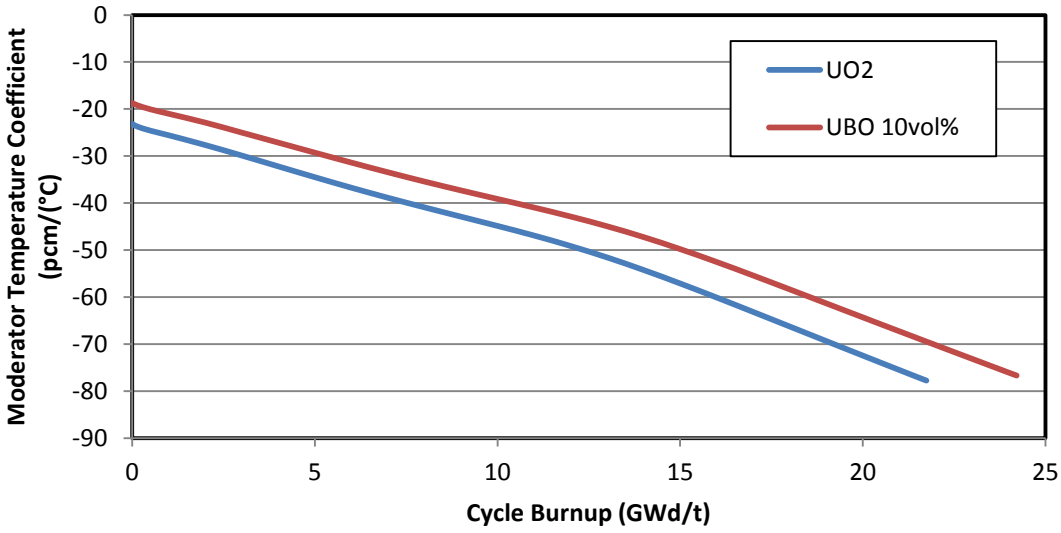

Figure A.10 Moderator temperature coefficient for the 22-month cycle depletion.

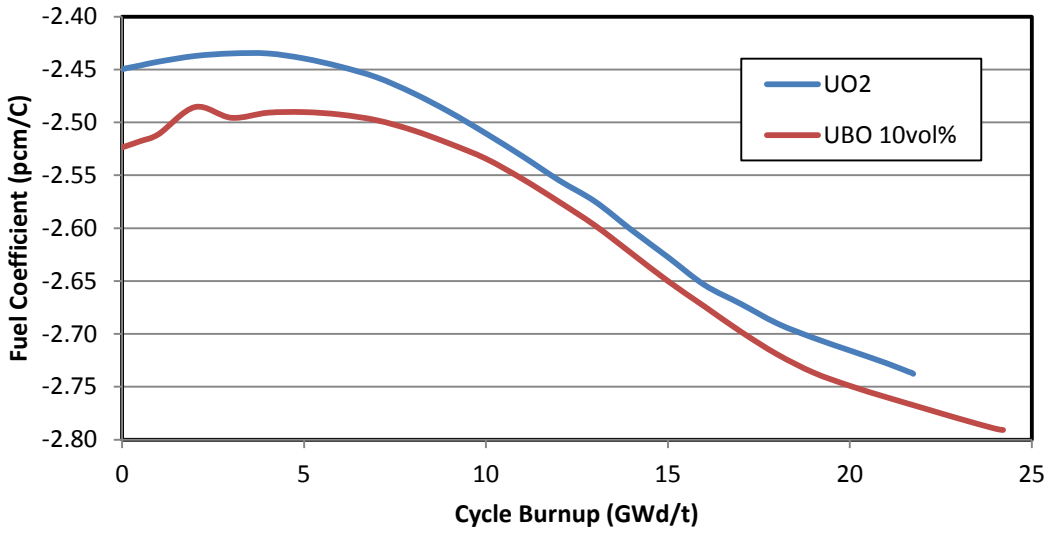

Figure A.11 Fuel temperature coefficient for the 22-month cycle depletion.

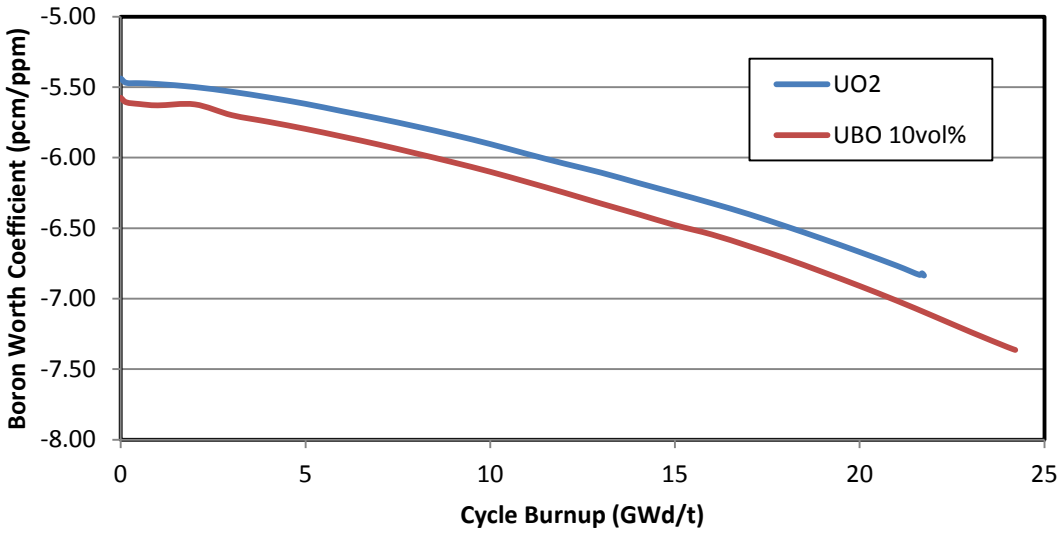

Figure A.12 Boron worth coefficient for the 22-month cycle depletion.

APPENDIX B

Perl script to grep the important cycle results and perform any conversions.

```
#!/Perl/bin/perl

# Joshua Smith, Texas A&M University
# 3/15/2012

$file     = $ARGV[0];
print "The input is  : $file\n";
$file =~s/listing/DATA/;
$file_out = $file.'.txt' ;
$file =~ s/DATA/listing/;
print "The output is : $file_out\n";

open ( INPUT , "<$file" );
open ( OUT   , ">$file_out" );

while (<INPUT>) {
    @file = <INPUT>;
}
# total number of lines in file
$tot = @file;

# find the title line when an equilibrium cycle is run in Cronos
for ($n=0;$n<$tot;$n++) {
    if ($file[$n]=~/Perform EQUILIBRIUM CYCLE/) {
        push @eqlib_line,$n ;
    }
}
$num_cycles = @eqlib_line ;
# need to add the last line in the file as well
# for the final converged eqlib cycle
push @eqlib_line,$tot ;

# MAIN PROGRAM: loop over the number of cycles ====================
for ($k=0;$k<$num_cycles;$k++) {

    print "$file[$eqlib_line[($k)]]";
    print "\n" ;
    print OUT "$file[$eqlib_line[($k)]]";
    print OUT "\n" ;
    # titles, must match the data printout below
    print OUT "MWd/t \t ppm \t AO% \t 3DPPF \t loc3D \t BScoord \t
distance_CL (cm) \t Gdtype \t pcm/(g/cm3) \t pcm/C \t pcm/ppm" ;
    print OUT "\n" ;

    for ($n=0;$n<$tot;$n++) {

        # looks at all lines that are between the cycles
        if ( ($n>$eqlib_line[$k])&&($n<$eqlib_line[$k+1]) ) {
```

```
# Moderator Coeff ---------------------------------------
if ($file[$n]=~/Moderator Density       Coefficient/) {
    @split = split(/\s+/,$file[$n+1]) ;
    @grep = grep(/[0-9]/,@split);
    #print "$grep[1] \n " ;
    push @mod,$grep[1] ;
}

# Doppler Coeff -----------------------------------------
if ($file[$n]=~/Doppler Tempereature  Coefficient/) {
    @split = split(/\s+/,$file[$n+1]) ;
    @grep = grep(/\d{2}/,@split);
    #print "$grep[0] \n " ;
    push @doppler,$grep[0] ;
}

# Boron Coeff -------------------------------------------
if ($file[$n]=~/Boron worth  Coefficient/) {
    @split = split(/\s+/,$file[$n+1]) ;
    @grep = grep(/\d{2}/,@split);
    #print "$grep[0] \n " ;
    push @boroncoeff,$grep[0] ;
}

    # find burnup steps -------------------------------
if ( $file[$n]=~ /Starting at Burnup/ ) {
    @split = split(/\s+/,$file[$n]) ;
    # the assumption is only one number in this line
    @grep = grep(/[0-9]/,@split);
    #print "$grep[0] \n" ;
    push @BU,$grep[0] ;
}

# grep lines relative to a hardcoded match
if ( $file[$n]=~ /Summary after a converged/) {

    # Axial Offset ------------------------------------
    #print $file[$n+3] ;
    @split = split(/\s+/,$file[$n+3]) ;
    # the assumption is at least two digits
    @grep = grep(/\d{2}/,@split);
    #print "$grep[0] \n" ;
    push @AO,$grep[0] ;

    # 3D power peaking factor -------------------------
    @split = split(/\s+/,$file[$n+4]) ;
    # the assumption is at least two digits
    @grep = grep(/\d{2}/,@split);
    #print "$grep[0] \n" ;
    push @PPF3D,$grep[0] ;

    # 3D power peaking factor location ----------------
```

```
                @split = split(/\*/,$file[$n+5]) ;
                #print $split[1] ;
                #split again on :
                @split2 = split(/:/,$split[1]) ;
                #print "$split2[1] \n" ;
                push @loc3D,$split2[1] ;

                @split3 = split(/\s+/,$split2[1]) ;
                #print @split3 ;
                @grep2 = grep(/[0-9]+/,@split3) ;

                # now send the coordinates to a subfunction that will
                # convert to battleship coordinates
                @BSconvert = battleship(@grep2);
                push @BS, $BSconvert[0] ;
                push @Gdtype, $BSconvert[1] ;
                push @CL, $BSconvert[2] ;

                # boron concentration ------------------------------
                #print $file[$n+10] ;
                @split = split(/\s+/,$file[$n+10]) ;
                @grep = grep(/[0-9]+/,@split);
                #print map { "$_ \n" } @grep;
                #print $grep[1] ;
                push @ppm,$grep[0] ;

            }

        }

    }

    $count = @BU ;
    #print $count ;
    # printout settings -----------------------------------------------
    for ($i = 0; $i <= $count ; $i++) {

        print     "$BU[$i] \t $ppm[$i] \t $AO[$i] \t $PPF3D[$i] \t
$loc3D[$i] \t $BS[$i] \t $CL[$i]  ";
        print     "\n" ;
        print OUT "$BU[$i] \t $ppm[$i] \t $AO[$i] \t $PPF3D[$i] \t
$loc3D[$i] \t $BS[$i] \t $CL[$i] \t $Gdtype[$i] \t $mod[$i] \t
$doppler[$i] \t $boroncoeff[$i] ";
        print OUT "\n" ;
    }

    # reset variables that you pushed ------------------------------
    # so they are clear for next cycle
    @mod = () ;
    @doppler = ();
    @boroncoeff = ();
    @BU = () ;
    @AO = () ;
```

```
    @PPF3D = () ;
    @loc3D = () ;
    @ppm = () ;
    @radialBU = () ;
    @array = () ;
    @BS = () ;
    @Gdtype = () ;
    @CL = () ;
}
# End of MAIN PROGRAM ========================================

sub battleship {

    @coordinates = @_;
    $x = $coordinates[0];
    $y = $coordinates[1];
    $z = $coordinates[2];

    # this map is non-specific to a cycle BUT specific to a 17x17 core
    @map = ("3 36 -",   "4 36 -",   "5 36 -",   "6 36 -",   "7 36 -",
"8 36 -",   "9 36 -",   "10 36 -",  "11 36 -",  "12 36 -",  "13 36
F17",    "14 36 F17",    "15 36 G17",    "16 36 G17",    "17 36 H17",
"18 36 H17",    "19 36 J17",    "20 36 J17",    "21 36 K17",    "22 36
K17",    "23 36 L17",    "24 36 L17",    "25 36 M17",    "26 36 M17",
"27 36 -",  "28 36 -",  "29 36 -",  "30 36 -",  "31 36 -",  "32 36 -",
"33 36 -",  "34 36 -",  "35 36 -",  "36 36 -",
"3 35 -",   "4 35 -",   "5 35 -",   "6 35 -",   "7 35 -",   "8 35 -",
"9 35 -",   ...
    ) ;
    $mapsize = @map ;
    for ($i=0; $i<=$mapsize; $i++) {
        @split = split(/\s+/,$map[$i]) ;
        #print @split ;
        @grep = grep(/[0-9]+/,@split) ;
        $xBS = $grep[0];
        $yBS = $grep[1];
        $zBS = $grep[2];
        # use the map to convert to battleship coord
        if( ($xBS==$x)&&($yBS==$y) ) {
            $return = $zBS ;
        }
    }
    # ---------------------------------------------------------------
    # this map is specific to a cycle
    # it returns the # Gd rods for the FRESH assemblies only
    @Gdmap = (
"U12      M3","U12      R12","U12      F15","U12      C6",
"U8       N3","U8       R13","U8       E15","U8       C5",
"U12      P4","U12      P14","U12      D14","U12      D4",
"U12      R6","U12      M15","U12      C12","U12      F3",
"U8       R5","U8       N15","U8       C13","U8       E3",
"U16      J6","U16      M9","U16      J12","U16      F9",
"U12      J2","U12      S9","U12      J16","U12      B9",
```

```
"U16      K2","U16      S10","U16      H16","U16      B8",
"U16      L5","U16      N11","U16      G13","U16      E7",
"U16      N7","U16      L13","U16      E11","U16      G5",
"U8       P3","U8       R14","U8       D15","U8       C4",
"U8       R4","U8       P15","U8       C14","U8       D3",
"U16      S8","U16      K16","U16      B10","U16      H2",
"U16      J4","U16      P9","U16      J14","U16      D9",
"U12      L16","U12      B11","U12      G2","U12      S7",
"U8       S6","U8       M16","U8       B12","U8       F2",
"U12      B7","U12      L2","U12      S11","U12      G16",
"U8       M2","U8       S12","U8       F16","U8       B6"
) ;
    $Gdmapsize = @Gdmap ;
    for ($i=0; $i<=$Gdmapsize; $i++) {
        @split = split(/\s+/,$Gdmap[$i]) ;
        if( $return=~$split[1] )  {
            $return2 = $split[0] ;
            #print "$return2 \t" ;
        }
    }
    # ---------------------------------------------------------------------
    # this takes the zth node and return the distance to the centerline
plane
    # the distance is from the midpoint of the (i) and (i+1) node to
centerline plane
    # this is specific to EPR core geometry chosen by user
    @dist_CL = (
"1 -225","2 -215","3 -205","4 -195","5 -185","6 -175","7 -165","8 -
155",
"9 -145","10 -135","11 -125","12 -115","13 -105","14 -95","15 -85","16
-75","17 -65","18 -55",
"19 -45","20 -35","21 -25","22 -15","23 -5","24 5","25 15","26 25","27
35","28 45",
"29 55","30 65","31 75","32 85","33 95","34 105","35 115","36 125","37
135","38 145",
"39 155","40 165","41 175","42 185","43 195","44 205","45 215","46 225"
) ;
    $dist_CL_size = @dist_CL ;
    for ($i=0; $i<=$dist_CL_size; $i++) {
        @split = split(/\s+/,$dist_CL[$i]) ;
        if( $z==$split[0] )  {
            $return3 = $split[1] ;
            #print "$return3 \n" ;
        }
    }
    return ($return,$return2,$return3);
}
exit 0;
```

APPENDIX C

Perl script to grep the enthalpy results following an equilibrium cycle.

```
#!/usr/bin/perl

# Joshua Smith, Texas A&M University
# 4/20/2012
# #!/Perl/bin/perl

$file     = $ARGV[0];
print "The input is  : $file\n";
$file =~s/listing/ENTHALPY/;
$file_out = $file.'.txt' ;
$file =~ s/ENTHALPY/listing/;
print "The output is : $file_out\n";

open ( INPUT , "<$file" );
open ( OUT   , ">$file_out" );

while (<INPUT>) {
    @file = <INPUT>;
}
# total number of lines in file
$tot=@file;

# EPR core specific value
$inlet_enthalpy = 1294.6 ;

# ================================================================
# MAIN PROGRAM:
# go through all lines in the file
for ($n=0;$n<$tot;$n++) {

    if($file[$n]=~ /Summary after a converged/) {

        # boron concentration --------------------
        #print $file[$n+10] ;
        @split = split(/\s+/,$file[$n+10]) ;
        @grep = grep(/[0-9]+/,@split);
        $boron = $grep[0] ;
        print OUT "\n $grep[0] ppm \n" ;

        # enthalpy map --------------------------
        # pick which lines you want to get
        # hardcoded
        foreach $_ ( @file[($n-181)..($n-16)]) {
            push @array,$_ ;
        }
        print OUT "@array \n";
        @fields = grep(/\|/,@array);
        $N_lines = @fields ;
```

```
print OUT "@fields \n";

for ($i=0;$i<$N_lines;$i++) {
    @split2 = split(/\s/,$fields[$i]) ;
    @grep = grep(/\|/,@split2) ;
    @split3 = split(/\|/,$grep[0]) ;
    $line = join(" ",@split3) ;
    push @array2,$line ;
}

# ---------------------------------------
# sum the enthalpies
print OUT map { "$_ \n" } @array2;
$count = @array2;
for ($i=0;$i<$count;$i++) {
    # sum enthalpy
    @temp = split(/\s/,$array2[$i]) ;
    $sum_line = eval(join("+", @temp));
    push @sum_tot,$sum_line ;
    # find maximum in line
    @ret = min_and_max(@temp) ;
    push @max_line,$ret[1] ;
}
$total = eval(join("+", @sum_tot));
print OUT "\n Total sum of enthalpies: $total \n " ;
@ret = min_and_max(@max_line) ;
$max_enth = $ret[1] ;
print OUT "\n Absolute maximum enthalpy: $max_enth \n\n" ;

# -------------------------------------
# take the difference between inlet enthalpy
for ($i=0;$i<$count;$i++) {
    @temp = split(/\s/,$array2[$i]) ;
    $temp_count = @temp ;
    for ($j=1;$j<$temp_count;$j++) {
        $temp[$j] = $temp[$j] - $inlet_enthalpy ;
    }
    $sum_line = eval(join("+", @temp));
    push @sum_tot_diff,$sum_line ;
    $join = join(" ",@temp) ;
    push @array3,$join ;
}

print OUT map { "$_ \n" } @array3;
$total_diff = eval(join("+", @sum_tot_diff));
print OUT "\n Sum of enthalpy diff: $total_diff \n " ;
# division specific to 241 assemblies in quarter divisions
$avg_delta_h = $total_diff / (241*4) ;
print OUT "\n Avg delta enthlapy: $avg_delta_h \n\n" ;

# -----------------------------------
# now make the enthalpy peaking map
for ($i=0;$i<$count;$i++) {
```

```
            @temp = split(/\s/,$array3[$i]) ;
            $temp_count = @temp ;
            for ($j=1;$j<$temp_count;$j++) {
                $temp[$j] = $temp[$j] / $avg_delta_h ;
            }
            # find maximum enthalpy factor in line
            @ret = min_and_max(@temp) ;
            push @max_peaking,$ret[1] ;
            $join = join(" ",@temp) ;
            push @array4,$join ;
        }

        print OUT map { "$_ \n" } @array4;
        @ret = min_and_max(@max_peaking) ;
        $max_peaking = $ret[1] ;
        print OUT "\n Max enthalpy peaking factor : $max_peaking \n" ;

        # -------------------------------------
        # now determine location of peaking and convert to battleship
coord.
        # very hardcoded so always double check results
        push @coord,":" ;
        for ($i=0;$i<38;$i++) {
            @temp = split(/\s/,$array2[$i]) ;
            $temp_count = @temp ;
            for ($j=1;$j<$temp_count;$j++) {
                if($temp[$j] =~ $max_enth) {
                    $adj_row = (38-$i) ;
                    push @coord,$adj_row ;
                    push @coord, "," ;
                    push @coord,$j ;
                    push @coord, ":" ;
                }
            }
        }
        #--------------------------------------
        # map overruns to next lines, must make adjustments
        for ($i=39;$i<=76;$i++) {
            @temp = split(/\s/,$array2[$i]) ;
            $temp_count = @temp ;
            for ($j=1;$j<$temp_count;$j++) {
                if($temp[$j] =~ $max_enth) {
                    $adj_col = $j + 20 ;
                    $adj_row = (76-$i) ;
                    push @coord,$adj_row ;
                    push @coord, "," ;
                    push @coord,$adj_col ;
                    push @coord, ":" ;
                }
            }
        }

        $coord_str = join("",@coord) ;
```

```
        push @store_boron,$boron ;
        push @store_peaking,$max_peaking ;
        push @store_coord,$coord_str ;
        # ---------------------------
        # reset pushed variables for next BU step
        @array = () ;
        @enthalpy = () ;
        @max_line = () ;
        @sum_tot = () ;
        @array2 = () ;
        @array3 = () ;
        @sum_tot_diff = () ;
        @array4 = () ;
        @max_peaking = () ;
        @coord = () ;
        @BS = () ;
        print OUT " ======================================== \n\n" ;
    }
}
        print "\n" ;
    # now finish up with formating and conversion ------------
    $coord_count = @store_coord ;
    # 3 entries + spaces = 6
    for ($m=0 ; $m<$coord_count ; $m++) {
        @temp = split(/:/,$store_coord[$m]) ;
        @grep = grep(/,/,@temp) ;
        $grep_count = @grep ;
        @temp2 = @grep ;
        for ($j=0;$j<($grep_count);$j++) {
            @temp3 = split(/,/,$temp2[$j]) ;
            @BSconvert = battleship(@temp3);
            push @BS, $BSconvert[0] ;
        }
        $BS_str = join(" ",@BS) ;
        push @store_BS,$BS_str;
        @BS = () ;
    }

    $count = @store_boron ;
    # final printout
        print OUT "
============================================================\n" ;
        print OUT " SUMMARY OF RESULTS \n\n" ;
    for ($i = 0; $i <= $count ; $i++) {
        print     "$store_boron[$i] \t $store_peaking[$i] \t
$store_coord[$i] \t $store_BS[$i] \t ";
        print     "\n" ;
        print OUT "$store_boron[$i] \t $store_peaking[$i] \t
$store_coord[$i] \t $store_BS[$i] \t ";
        print OUT "\n" ;
    }
        print OUT "
============================================================" ;
```

```perl
# max and min subroutine
sub min_and_max
{
    @numbers = @_;
    $min = $numbers[0];
    $max = $numbers[0];
    foreach $i (@numbers)
    {
        if ($i > $max)
        {
            $max = $i;
        }
        elsif ($i < $min)
        {
            $min = $i;
        }
    }
    return ($min, $max);
}

exit 0;
```